KFA

GA GENERAL ATOMIC

Jül-1502

GA-A14759
UC-77

LOW-ENRICHED FUEL PARTICLE PERFORMANCE REVIEW

by

F. HOMAN (Oak Ridge National Laboratory)
H. NABIELEK (Kernforschungsanlage Jülich GmbH)
L. YANG (General Atomic Company)

Prepared under the Umbrella Agreement for Cooperation in Gas-Cooled Reactor Development between the United States and the Federal Republic of Germany.

Work supported in part by
Contract EY-76-C-03-0167
Project Agreement No. 65
for the San Francisco Operations Office
Department of Energy

AUGUST 1978

NOTICE

Printed in the United States of America
Available from
National Technical Information Service
U.S. Department of Commerce
5285 Port Royal Road
Springfield, Virginia 22161
Price: Printed Copy $9.25; Microfiche $3.00

KFA

GENERAL ATOMIC

Jül-1502

GA-A14759
UC-77

LOW-ENRICHED FUEL PARTICLE PERFORMANCE REVIEW

by

F. HOMAN (Oak Ridge National Laboratory)
H. NABIELEK (Kernforschungsanlage Jülich GmbH)
L. YANG (General Atomic Company)

Prepared under the Umbrella Agreement for Cooperation in Gas-Cooled Reactor Development between the United States and the Federal Republic of Germany.

Work supported in part by
Contract EY-76-C-03-0167
Project Agreement No. 65
for the San Francisco Operations Office
Department of Energy

GENERAL ATOMIC PROJECT 3273
AUGUST 1978

FOREWORD

This report presents the results of a cooperative effort between the General Atomic Company (GA), Kernforschungsanlage (KFA), and the Oak Ridge National Laboratory (ORNL) under the United States-Federal Republic of Germany Umbrella Agreement for Cooperation in Gas-Cooled Reactor Development. The objective of this task is to evaluate existing low-enriched (LEU)* fuel particle information to support the development and licensing of LEU or medium-enriched (MEU)* fuel particles for use in high-temperature gas-cooled reactors to meet safeguard and nonproliferation requirements. The evaluation results will also be used to plan a developmental program for providing additional information needed and for improving the irradiation performance of LEU/MEU fuel particles. This report completes the work scope described in Project Work Statement FD1, "Critical Evaluation of LEU Fuel Performance Data."

Two major guidelines were followed in the preparation of this report. First, the review is strictly material-oriented; no reference is made to the design requirements of specific reactor systems. Secondly, the review is confined primarily to information related to the irradiation performance of LEU uranium-oxide-based fuel systems. Data from other fuel materials are included only if they are applicable to the LEU fuel systems. Information on LEU fuel fabrication is excluded.

The main part of this report contains a condensed version of the information related to the four important areas that control the irradiation performance of LEU fuel particles:

*In this review, LEU, MEU, and HEU refer to fuels of different enrichment in U-235. Generally speaking, LEU refers to fuels of less than 10% enrichment, HEU refers to fuels of about 93% enrichment, while MEU refers to fuels of intermediate enrichment (20% to 40%).

1. Plutonium transport
2. Fission product transport
3. Mechanical performance
4. Chemical performance

Details are contained in the references noted throughout. The LEU fuel programs of various laboratories and information too detailed to be included in the main part of the report are described in Appendixes A, B, C, and D.

In view of the short time span during which this report was prepared, and the continuous evolution of LEU/MEU fuel particle technology, the authors of this report do not claim that the information gathered is complete and current. However, they hope that this report can serve as the basis for continuous updating of LEU/MEU fuel particle performance information.

ABSTRACT

The available data on low-enriched (LEU) fuel particles were reviewed under the United States-Federal Republic of Germany Agreement. The most influential factors controlling the irradiation performance of LEU fuel particles were found to be plutonium transport, fission product transport, fuel particle mechanical performance, and fuel particle chemical performance.

PLUTONIUM TRANSPORT

Pu-238, which is derived from U-235, represents the dominant radiological hazard. Since the U-235 inventory in an LEU core is approximately the same as that in an HEU core, plutonium transport is therefore of importance to both LEU and HEU systems.

The diffusion coefficient of plutonium in high-temperature-isotropic pyrocarbon is about an order of magnitude higher than that of uranium and two orders of magnitude higher than that of thorium. A BISO coating is not a good barrier for plutonium release, but a TRISO coating retains plutonium. Graphite appears to be an effective trap for plutonium.

The phase compositions and plutonium vapor pressures over irradiated uranium oxycarbide kernels have been deduced from thermodynamic data. It is concluded that plutonium is present in solid solution in the corresponding uranium-containing phases, and that the vapor pressure is lower than that of plutonium carbide. Experimental confirmation of these conclusions is desirable.

FISSION PRODUCT TRANSPORT

The reduced diffusion coefficients D' of cesium diffusion in oxide kernels of different compositions, enrichments, and densities have been

compared. Good agreement exists in some cases. More work is needed to establish how the structures (porosity, grain size) and burnup affect the D' values.

Silver release is higher from BISO particles than TRISO particles. Silver release is also higher from carbide fuel than oxide fuel. The retention of silver in intact TRISO particles is not as complete as the other fission products, at least at temperatures above 1450 K. High density SiC with minimum free silicon content (<0.3 weight %) is required for minimum release. A breakthrough mechanism that is activated when a certain critical silver concentration is reached at the inner SiC surface is proposed for silver transport through SiC. Silver is trapped in irradiated nuclear graphite at temperatures around 1300 K. The same is true for unirradiated graphite and matrix materials at some temperatures below 1100 K, but there is no retention in compacts, fuel rods, or spherical fuel elements at typical operating temperatures.

Strontium is retained virtually completely in UO_2 kernels surrounded by an intact coating layer, but above 1750 K strontium and barium are lost from the TRISO particles although Kr, Xe, and Cs are still retained. It appears that strontium and barium diffuse through the pyrocarbon coating at these high temperatures and attack the SiC coating. When the SiC layer is penetrated, it is no longer a barrier for the diffusion of these nuclides. The D' values for strontium and barium have been determined for $(Th,U)O_2$ in the temperature range $1760 < T < 1920$ K and in UO_2. The D' for barium is slightly higher than that of strontium.

D' values for the diffusion of short-lived gaseous fission products in UO_2 and $(Th,U)O_2$ are deduced from release data. The release of short-lived gaseous fission products from porous kernels does not seem to depend on burnup, but for the dense kernels there is a large increase with burnup. Empirical equations have been given to relate the release from failed particles with the burnup. No information, however, is available on the effect of conversion to carbide and hydrolysis on the release from failed

particles. A model to be used for reactor safety analysis has been proposed; its purpose is to make conservative estimates of fission product release from failed particles during temperature transients.

FUEL PARTICLE MECHANICAL PERFORMANCE

The present stress-strain models have been successful in describing TRISO particle failure and BISO particle dimensional changes for existing particles. For neutronic and fuel cycle cost reasons, the LEU/MEU particles are larger in diameter. There are indications that, in agreement with Weibull statistics of strength of brittle materials, coatings of larger diameter have lower strength and higher failure probability. This is, however, not substantiated by some of the experimental results available. Nevertheless, it appears that the larger LEU/MEU particles might require development work to improve their coating strength in order to survive the required service limits. Otherwise, these particles have to be designed within the range of existing technology (i.e., $\leq$800 μm diameter).

Models, diffusion equations, and empirical formulas have been given to describe the release of stable fission gases from oxide kernels. For the burnup planned for the LEU/MEU fuel systems, the release appears to be relatively high. More carefully planned experiments are needed to relate the structures of the kernels, the temperature, and the burnup with the release.

Because of the high free oxygen yield for plutonium fissioning, the CO pressure in irradiated LEU fuel particles is expected to be much higher than that in irradiated HEU fuel particles. Higher CO pressure can lead to pressure vessel failure and "amoeba" failure. The theoretical maximum and minimum values of excess oxygen per fission are calculated from the fission yields of different fissile nuclides and their oxidation state. Most of the experimentally observed values for porous UO_2, dense $(Th,U)O_2$, and dense ThO_2 fall below the theoretical minimum value.

The use of oxygen getters or buffers (SiC, UC, ZrC, and Ce_2O_3) for lowering the CO pressure has shown promise in a number of irradiation experiments, although a small increase in the release of barium and rare earths has been observed.

FUEL PARTICLE CHEMICAL PERFORMANCE

The existing results obtained by studying kernel migration coefficients have been compared. It appears that the HEU oxide fuel particle results can be used to establish the LEU/MEU oxide fuel particle design. However, some discrepancies exist among the available kernel migration coefficients of UO_2, and an understanding of the oxide kernel migration mechanism is still lacking.

Oxygen getters and buffers (SiC, UC, ZrC, and Ce_2O_3) have been tested for reduction of amoeba migration in oxide particles. The results are encouraging.

Localized attack of the SiC coating by the noble metal fission product Pd has been observed in a number of irradiation experiments involving LEU and plutonium fuels. Controlled experiments are needed to define the temperature and burnup for the Pd-SiC reaction to occur. Development of improved coatings that can resist Pd attack is necessary in order to prevent the Pd-SiC reaction from limiting LEU/MEU fuel particle performance.

Available LEU fuel particle performance information has provided a broad data base for the development of LEU/MEU fuel systems. With confirmation and refinement of these data, and a carefully planned program for improving the LEU/MEU fuel particle performance, it should not be difficult to develop a licensable fuel system to meet the demand of LEU/MEU high-temperature gas-cooled reactor systems.

CONTENTS

FIGURES

TABLES

1. PLUTONIUM TRANSPORT

During its in-pile operation, the LEU fissile particle breeds more plutonium than the HEU fissile particle. The higher plutonium yield is of concern for two reasons: (1) plutonium is a potential health hazard, and the release of plutonium isotopes from fuel particles can lead to serious consequences from the standpoint of reactor safety, and (2) the fissioning of Pu-239 produces more noble metal fission products (e.g., Pd) and less stable oxide-forming fission products than the fissioning of U-235; such differences in fission product yields are detrimental to the irradiation performance of the fuel particle.

Since Pu-239 is derived from U-238, which is more abundant in LEU fuel, the fuel particle performance problem is much more important to the LEU fuel particle than to the HEU fuel particle. This will be addressed in more detail in Sections 3 and 4. The health hazard problem, however, is not unique with LEU fuel. As pointed out by Bell (1977), among all the plutonium isotopes Pu-238 (half life = 87.4 years) is the dominant plutonium nuclide of radiological concern. Since Pu-238 is derived mainly from U-235, and since the LEU and HEU cores contain about the same amount of U-235, the Pu-238 inventory in the LEU core does not differ significantly from that in the HEU core. An understanding of plutonium's transport behavior is thus of importance in the design of both LEU and HEU gas-cooled reactor systems.

1.1. PLUTONIUM TRANSPORT THROUGH INTACT PARTICLE

At a given temperature, the plutonium pressure in an irradiated oxide particle depends upon the nature of the phases present and the plutonium concentration in these phases. These are, in turn, controlled by the initial kernel composition, the U-235 enrichment, and the burnup. To

reach outside the intact particle, the plutonium atoms would have to diffuse through the pyrocarbon coating and the SiC coating.

The diffusion coefficients of plutonium in high-temperature-isotropic (HTI) methane coatings (density = 1.860 Mg/m^3, BAF* = 1.034, deposited at 2273 K at a rate of 60 μm/h) have been measured by Baldwin, Winchell, and Langer (1977) in the temperature range of 1260 to 2050 K. The results are shown in Fig. 1-1, which can be expressed by the equation

$$\log_{10} D_{Pu} \ (m^2/s) = -7.35 - \frac{12,000}{T} \quad . \qquad (1\text{-}1)$$

The D values for plutonium are about an order of magnitude higher than those of uranium in isotropic pyrolytic carbon and two orders of magnitude higher than those of thorium. It would be highly desirable to extend these measurements to low-temperature-isotropic (LTI) coatings.

Buzzelli (1977a) measured the in-pile release of plutonium and certain metallic fission products from loose, intact, BISO coated and TRISO coated $(Th,U)C_2$ particles (95% enriched) irradiated in the General Electric test reactor. The BISO coated particles were irradiated in capsules P17 at 1500 to 1700 K and P18 at 1650 to 1850 K, and the TRISO coated particles were irradiated in capsule P22 at 1550 to 1750 K. During the irradiation, each of the three particle samples was contained in a graphite thimble inserted into the graphite body of the capsule. The wall thickness of the thimble was about 0.1 cm. The irradiation times were 159 days for capsule P17, 264 days for capsule P18, and 266 days for capsule P22. The nuclide inventories in the particles, the thimbles, and the graphite bodies were determined after the irradiation. Results for Pu, U, Th, and Sr-90 are given in Table 1-1 (Buzzelli, 1977b), from which the following conclusions were drawn by Bell (1977).

1. The fractional release of plutonium from the TRISO particles was low (1.0×10^{-5}), which could be attributed to contamination. This indicates that SiC effectively retains plutonium.

*Bacon anisotropy factor.

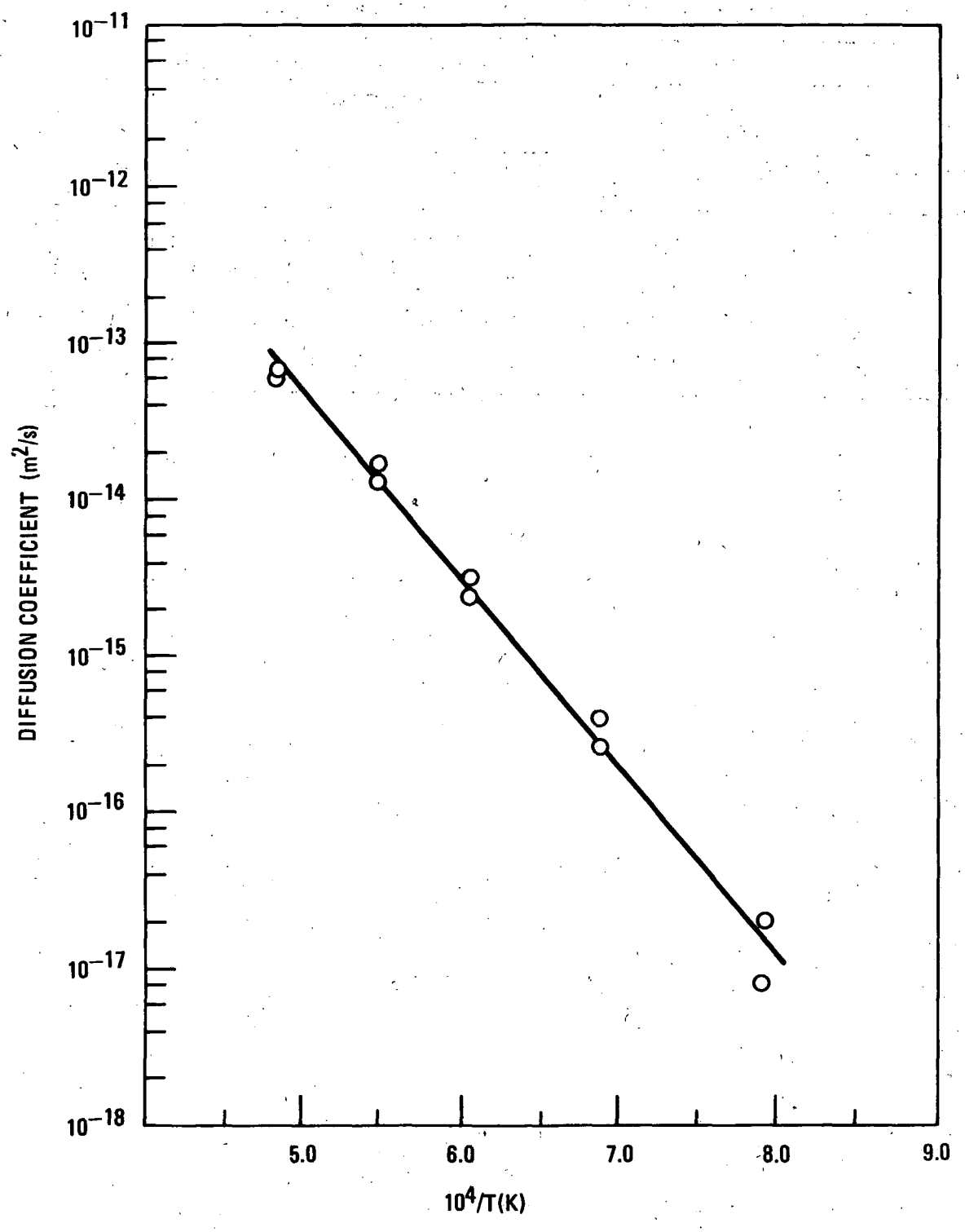

Fig. 1-1. Diffusion coefficients of plutonium in isotropic pyrolytic carbon

TABLE 1-1
RELEASE FRACTIONS AND DISTRIBUTION FOR INTACT BISO AND TRISO PARTICLES IN P17, P18, AND P22 (BUZZELLI, 1977b)

Species	Fractions Found in Thimble and Graphite Body				
	P17, BISO $(Th,U)C_2$		P18, BISO $(Th,U)C_2$		P22, TRISO $(Th, U)C_2$
	Thimble	Graphite Body	Thimble	Graphite Body	Thimble
Pu	1.3×10^{-3}	1.4×10^{-5}	2.1×10^{-2}	1.1×10^{-5}	1.0×10^{-5}
U	7.9×10^{-5}	8.9×10^{-5}	2.1×10^{-4}	1.6×10^{-4}	5.6×10^{-5}
Th	1.2×10^{-4}	1.3×10^{-4}	1.4×10^{-3}	2.1×10^{-5}	2.6×10^{-5}
Sr-90	0.09	0.01	0.35	0.41	low

2. The fractional release of plutonium from the BISO particles was relatively high (1.3×10^{-3} for P17, and 2.1×10^{-2} for P18). This indicates that a pyrocarbon coating is not an effective diffusion barrier for plutonium.

3. Essentially all the released plutonium stopped in the thin-walled graphite thimble that contained the particles. This indicates that graphite can act as an effective sink for the sorption of plutonium or an effective diffusion barrier.

4. The fractional releases of uranium and thorium were low, which could be attributed to contamination.

5. The fractional release of Sr-90 from the BISO particles was high (0.10 for capsule P17, and 0.76 for capsule P18). The thin-walled graphite thimble does not appear to be an effective barrier for strontium diffusion, and a large fraction of the Sr-90 released was found in the graphite body outside the thimble.

6. Plutonium release from BISO particles was much lower than strontium release.

The effectiveness of SiC as a diffusion barrier for plutonium has been demonstrated in other high temperature irradiation experiments. For instance, TRISO coated plutonium oxide particles (20% Pu_2O_3, 80% PuO_2, dispersed in carbon at Pu/C ratios of 1:30.5 and 1:21) were irradiated in Studsvik to 20% FIFA* at 2123 K (Barr et al., 1967). No evidence of plutonium release from the coated particles was detected during postirradiation examination by gamma-ray spectrometry.

*Fissions per initial fissile atom.

1.2. TRANSPORT FROM FAILED PARTICLE

In an intact oxide particle, the phases present in the kernel are in equilibrium with the carbon buffer and the prevailing CO pressure in the particle. When the coating fails, the CO molecules escape from the particle and the kernel reacts with the surrounding carbon until all the kernel is converted into the carbide phase in equilibrium with carbon. However, if the CO partial pressure in the helium coolant exceeds the equilibrium CO pressure for the conversion reaction, the conversion will not take place. If the CO pressure is low and the kernel is converted to carbide, and subsequently the moisture level of the helium coolant increases, then the carbide will be hydrolyzed and returned to oxide through the oxycarbide stage. Thus, depending upon the CO pressure and moisture level in the helium coolant, the fuel in the failed particles could contain oxide, carbide, oxycarbide, or a mixture of these phases, and the vaporization loss of plutonium could vary widely. Table 1-2 compares the vapor pressures of various plutonium and uranium oxides, carbides, and oxycarbides at 1500 K (Bell, 1977). It can be seen that while UC_2 has a lower vapor pressure than UO_2, PuC_2 has a higher vapor pressure than PuO_2. The vapor pressure of $PuC_{0.5}O_{0.5}$, determined by Potter (1967) using the Langmuir free evaporation method, is many orders of magnitude higher than that of both PuC_2 and PuO_2. This could be due to experimental error. Nevertheless, the vaporization loss of plutonium from failed LEU fuel particles can vary widely, depending upon the initial fuel composition, the irradiation conditions, and the environmental impurity contents in the helium coolant. To assess the plutonium vaporization loss, an evaluation should be made on the basis of the thermodynamic data and phase relationships of the U-C-O (Stoops and Hamme, 1964; Chiotti, Robinson, and Kanno, 1966; Henney, 1966; Henry et al., 1967; Steele, Javed, and Alcock, 1970) Pu-C-O (Potter, 1967) and Pu-U-C-O (Potter, 1970) systems to determine the phases present in the kernel and the equilibrium CO pressure as a function of temperature and burnup.

Recently, Besman of ORNL calculated, on the basis of thermodynamic data, the nature of the phases present in uranium oxycarbide fuels of

TABLE 1-2
VAPOR PRESSURE OF PLUTONIUM AND URANIUM FUELS AT 1500 K

System	Total Pressure (atm)	Principal Vapor Species	Reference
PuC_2+C	6.8×10^{-10}	Pu	Mulford et al., 1962
UC_2+C	6.7×10^{-15}	U	Lonsdale and Graves, 1962
PuO_2	1.0×10^{-12}	PuO, PuO_2	Cleveland, 1970
UO_2	1.1×10^{-12}	UO_2	Cordfunke, 1969
$PuC_{0.5}O_{0.5}$	3×10^{-7}	-	Potter, 1967

various carbon-to-oxygen ratios and different plutonium concentrations. Details are presented in Appendix A. The calculations assume thermodynamic equilibrium and ideal solid solution behaviors present in the phases. The calculated results indicate that the plutonium will be present in solid solutions with the corresponding uranium-containing phases, and that the plutonium partial pressure over the equilibrium phases is considerably lower than that shown in Table 1-2. The concentration of plutonium in the irradiated fuel is shown to have more effect on the plutonium partial pressure than the amount of carbide in the initial fuel. In view of the assumptions made in the calculations, the quality of the thermodynamic data available, and the effects of CO and moisture levels in the helium coolant, these conclusions need to be checked experimentally. Irradiated LEU fuel particles of various oxygen-to-uranium ratios can be laser-failed and studied for plutonium loss in helium as a function of temperature and the CO and H_2O content of the helium. The information generated will be useful in the selection of LEU kernel composition, which can lower the amoeba effect, tie up the rare earth fission products, and have tolerable plutonium loss from failed particles.

REFERENCES

Baldwin, N. L., P. Winchel, and S. Langer, 1977; "Diffusion of Plutonium in High Temperature Isotropic Pyrolytic Carbon," General Atomic Report GA-A14136.

Barr, P., et al., 1967; "High Temperature Irradiation Experiments on Plutonium-Bearing Coated Particle Fuel," Plutonium as a Reactor Fuel, International Atomic Energy Agency, Vienna.

Bell, W. E., 1977; "Plutonium Release Limitations," General Atomic Company, private communication.

Buzzelli, G., 1977a; "In-Pile Release of Plutonium from BISO and TRISO Fuel Particles," General Atomic Company, private communication.

Buzzelli, G., 1977b; General Atomic Company, private communication to W. Bell.

Chiotti, P., W. C. Robinson, and M. Kanno, 1966; "Thermodynamic Properties of Uranium Oxycarbides," J. Less-Common Metals 10, 273-289.

Cleveland, J. M., 1970; The Chemistry of Plutonium, Gordon and Breach, New York, p. 300.

Cordfunke, E. H. P., 1969; The Chemistry of Uranium, Elsevier Publishing Company, New York, p. 60.

Henney, J., 1966; UKAEA Harwell Report AERE-R 4661.

Henry, J. L., et al., 1967; U.S. Bureau of Mines Report 6968.

Lonsdale, H., and J. Graves, 1962; "Vaporization of the Dicarbides of Uranium, Thorium, and Protactinium," Proc Thermodyn of Nuc Mat, 601-23.

Mulford, R. N. R., et al., 1962; "The Volatility of Plutonium Carbide," Symposium on Thermodynamics of Reactor Materials, IAEA, Vinenna.

Potter, P. E., 1967; "The Tenary System Plutonium-Carbon-Oxygen," Symposium on Thermodynamics of Nuclear Materials, IAEA, Vienna, p. 337.

Potter, P. E., 1970; "On the U-Pu-C-O Systems, Plutonium 1970 and Other Actinides, Nuclear Metallurgy," Proceedings of the 4th International Converence on Plutonium and Other Actinides, Vol. 17, Santa Fe, New Mexico, October 5-9.

Steele, B. C. H., N. A. Javed, and C. B. Alcock, 1970; "Measurement of the Equilibrium Oxygen, Carbon, and Uranium Activities Associated with the Uranium Oxycarbide Phase," J. Nuclear Materials 35, 1-13.

Stoops, R. F., and J. V. Hamme, 1964; "Phase Relations in the System Uranium-Carbon Oxygen," J. Amer. Ceramic Soc. 47, 59.

2. FISSION PRODUCT TRANSPORT

2.1. CESIUM RELEASE

2.1.1. Cesium Release From LEU Oxide Kernels

Cs-137 is one of the most intensively studied isotopes used when investigating fission product transport behavior, and much experimental data are available. For LEU fuel, the main sources of information are the measurements of Brown and Faircloth (1976) of the United Kingdom Atomic Energy Authority (UKAEA), Harwell, on 80% dense UO_2 prepared using the powder agglomeration technique. The kernel release was determined by cracking irradiated, intact, TRISO coated particles and measuring the Cs-137 content in the kernel and the coating. Since work on the Dragon project (Voice, Walter, and York, 1973) shows that no cesium is released through intact SiC ($D < 10^{-21}$ m^2/s), the ratio of the Cs-137 content in the coating to that in the particle can be taken as the fractional release from the kernel. By applying the equivalent sphere model, the experimental data can be used to calculate the reduced diffusion coefficient D'_{Cs} of Cs-137 in the kernel. The logarithm of D' (s^{-1}) is plotted versus the inverse of the mean kernel surface temperature T (K) during irradiation (or annealing) to show an Arrhenius-type relationship (see Fig. 2-1).

Careful evaluation of the data obtained from most recent experiments with 80% dense, 18% enriched, and HTI-TRISO coated UO_2 kernels by Brown (1977a) gives the relationship

$$\log_{10} D'_{Cs} = 3.92\ (\pm 0.21)^* - 18{,}900/T \qquad (2\text{-}1)$$

*One standard deviation from mean.

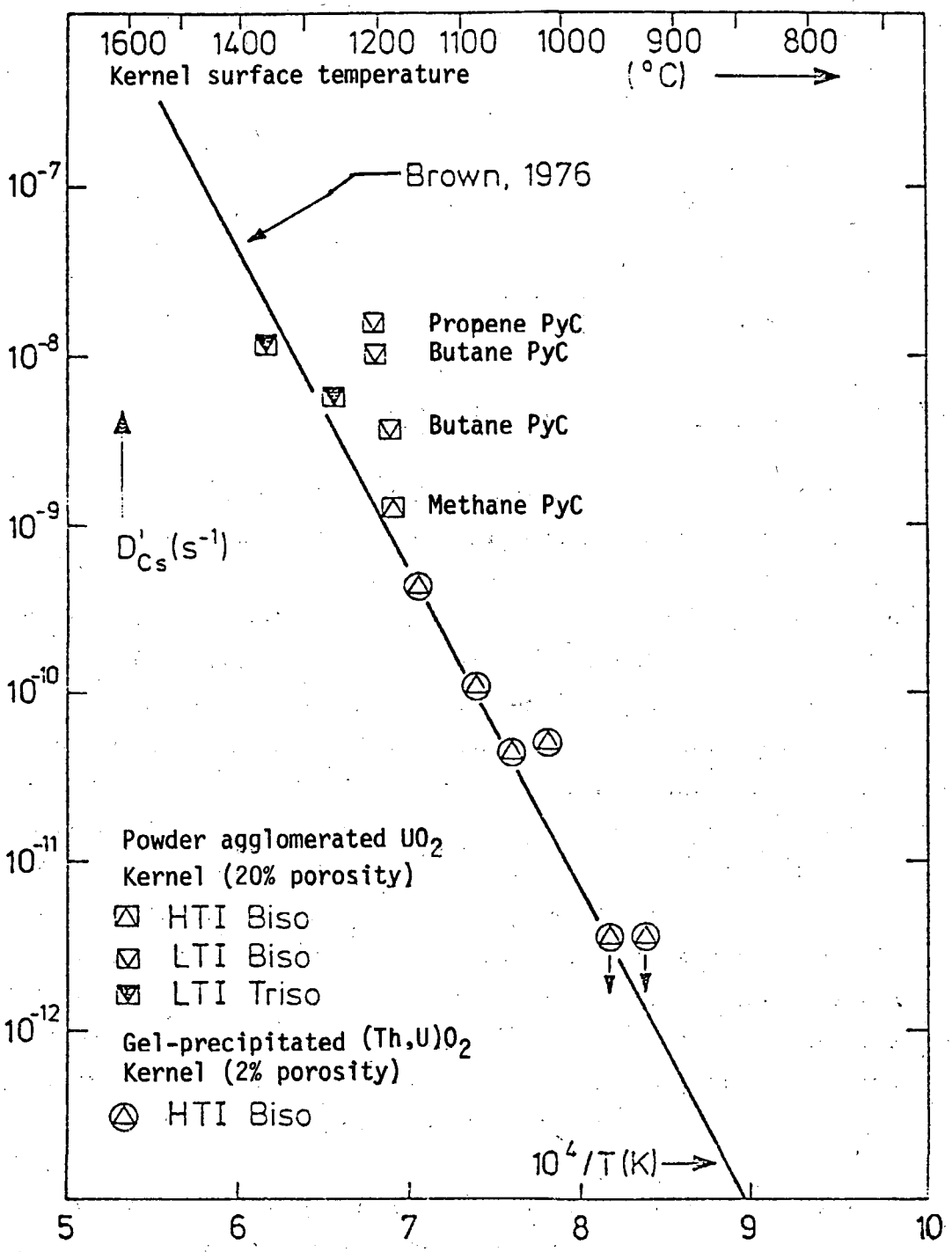

Note the deviation of LTI Biso coatings and the agreement with diffusion from (initially) dense $(Th,U)O_2$).

Square symbols: Results from the HTR 3 experiment with low-enriched fuel (4%)

Circle symbols: Results from DR-K3 and DR-K4 experiment (Ball irradiation in Dragon) with high-enriched fuel (90%)

Fig. 2-1. Reduced diffusion coefficient of Cs in UO_2 and $(Th,U)O_2$ versus mean kernel surface temperature

for the following irradiation conditions: 0.1 to 1 W per particle rating, 3% to 12% FIMA,* 70 to 700 days, 1300 to 1800 K, 0.1 to 4 x 10^{25} m^{-2} fluence (EDN†). Specifically, there is no burnup dependence and no dependence on the cesium concentration in the buffer/inner pyrocarbon layer for the D' value obtained. The results shown in Fig. 2-1 also indicate that LTI coatings result in higher cesium releases from the kernel (Brown, 1977b; Reitsamer, Falta, and Nabielek, 1978), which cannot be explained by the higher diffusivity of Cs in LTI pyrocarbon.

Friskney (1975c) determined the distribution of cesium in the kernel and the coating of UO_2 particles irradiated at a high rating (1 W per particle; Friskney and Simpson, 1975a) and at low rating (0.1 W per particle; Friskney, 1975c) for a longer time. The measured amount of cesium retained in the UO_2 kernel is in good agreement with that deduced from Eq. 2-1 up to 1700 K. However, there are indications of a temperature-independent limiting value of the effective diffusion coefficient in UO_2 at temperatures $\geq$1700 K.

2.1.2. Comparison With Other Data

Figure 2-1 shows good agreement between the data obtained on porous, powder-agglomerated UO_2 and dense, gel-precipitated, high-enriched $(Th,U)O_2$ (HTI-BISO coatings irradiated to 13% FIMA) (Reitsamer, Falta, and Nabielek, 1978). Good agreement also exists between these data and those for dense UO_2 and UC_2 particles irradiated to 50% FIMA (Zoller, 1976). However, the main reference data at GA and KFA for dense ThO_2 and high-enriched $(Th,U)O_2$ fuels differ significantly from that expressed by Eq. 2-1.

The diffusion coefficients of cesium in dense sol-gel ThO_2 and HEU $(Th,U)O_2$ kernels have been determined by GA and ORNL from postirradiation annealing results, using irradiated bare ThO_2 kernels, coated ThO_2 kernels,

*Fissions per initial heavy metal atom.
†Equivalent Dido nickel.

and coated $(Th,U)O_2$ kernels (Myers and Bell, 1978a). The results are plotted in Fig. 2-2, and the GA data can be expressed by the equation

$$\log_{10} D'_{Cs} = -2.42 - 14{,}000/T \quad . \tag{2-2}$$

While the GA data indicate no significant dependence of D' on burnup, the ORNL data do. Furthermore, the D' values of GA are significantly larger than the D' values of ORNL, particularly for FIMA values of about 1%.

When Fig. 2-1 is compared with Fig. 2-2, it can be seen that there is a difference in the D' values by over two orders of magnitude. This could be due to the difference in the grain sizes (i.e., the effective diffusion distances) in these different types of irradiated kernels, but more studies are needed to resolve this discrepancy.

Furthermore, the KFA reference figures for kernel cesium release from 400 μm diameter $(Th,U)O_2$ at burnups greater than 5% FIMA are calculated by using the equation (Stöver and Hecker, 1977)

$$\log_{10} D'_{Cs} = -5.93 - 4100/T \quad , \tag{2-3}$$

which yields D'_{Cs} values much higher than those given by Eqs. 2-1 and 2-2. Stöver and Hecker point out that at low burnups (<5% FIMA) cesium retention in the kernel is high in the temperature range of 1200 to 1400 K, and that at high burnups the data are much more scattered. No attempt has been made to explain this scatter and the difference in D'_{Cs} values obtained from Eqs. 2-1, 2-2, and 2-3.

The fission product release measurements on kernels or coated particles in general yield the reduced diffusion coefficient D' on the basis of the equivalent sphere model. The D' value is related to the in-grain diffusion coefficient D, which is an inherent material property, and the effective diffusion distance (or grain size) "a" by the equation $D' = D/a^2$. The D' value can also be related to the effective diffusion coefficient D_{eff} and

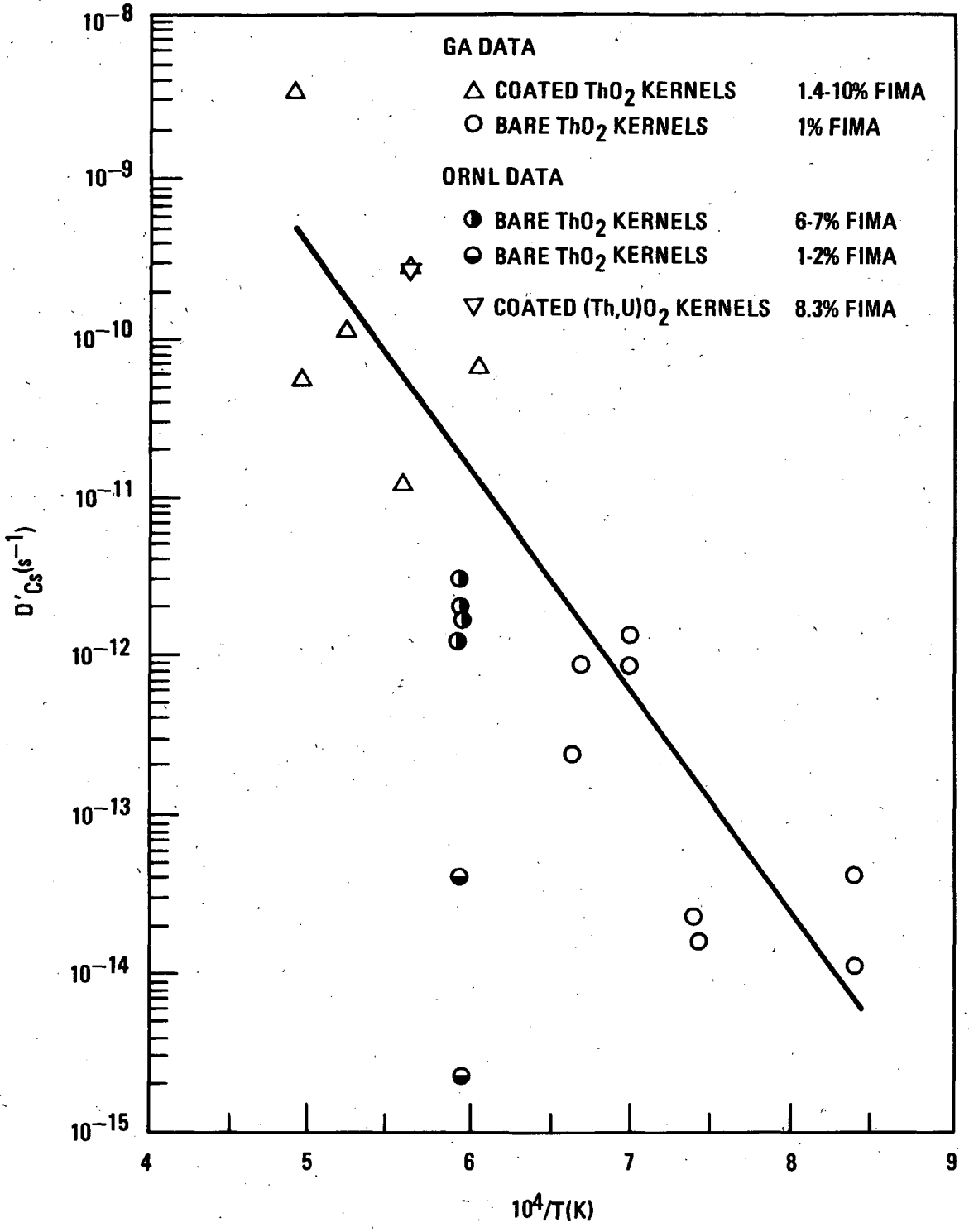

Fig. 2-2. Reduced diffusion coefficients for cesium diffusion in ThO_2 kernels

the kernel radius r by the equation $D' = D_{eff}/r^2$. In reviewing the fission product release data obtained from kernels and coated particles in this report, we shall give the D' values deduced directly from experimental release data instead of the D or the D_{eff} values. This is because (1) we do not know the mean value of the grain size in the kernel or how it will change during irradiation, and (2) we do not think the whole kernel structure can remain unchanged during irradiation. Therefore, caution has to be exercised in applying the D' values obtained on one type of kernel structure to calculate the fission product release from the kernel of a different structure (i.e., for a certain "a" value) unless we are sure that no matter what the initial kernel structures are the irradiated kernels have essentially the same "a" value. This is an important point to remember when literature D' values are used for calculating fission product release.

2.2. SILVER RELEASE

2.2.1. Silver Release From LEU Particles

The silver inventory is one order of magnitude higher in 20% enriched fuel irradiated to 27% FIMA than in 93% enriched fuel irradiated to 80% FIMA. Use of LEU fuel, therefore, increases the need to deal with the silver release problem.

The experimental evidence of silver kernel release from oxide fuel comes from three sources:

1. Fission product content in kernel and coating of intact TRISO particles (Brown and Faircloth, 1976; Reitsamer, Falta, and Nabielek, 1978).

2. Measurement of Ag-110m and Ag-111 (Nabielek and Brown, 1975) released from BISO particles in fuel bodies and trapped in graphite (Nabielek, Brown, and Offermann, 1977; Groos et al., 1977).

3. Annealing at 1770 K of BISO particles irradiated below 920 K (Fig. 2-3) (Brown, Brownsword, and Hooper, 1977a). The study demonstrates that only kernel retention is limiting the particle release rate and yields the reduced diffusion coefficient $D' = (9.3 \times 10^{-9})/s$. The results are identical for methane- and propene-derived pyrocarbon coatings.

The reduced diffusion coefficient D' of silver in UO_2 and $(U,Th)O_2$ can be represented by the equation (Nabielek, Brown, and Offermann, 1977; Reitsamer, Falta, and Nabielek, 1978)

$$\log_{10} D'_{Ag} = 1.26 - 11,140/T \quad , \tag{2-4}$$

where T is the irradiation or annealing temperature in K (Fig. 2-4). The results are based on the evaluation of low-enriched UO_2 in the temperature range of 1300 to 1700 K and of high-enriched $(U,Th)O_2$ of Th/U = 3 to 25 in the temperature range of 1100 to 1400 K. It is possible that more detailed studies may reveal differences due to different fabrication routes and kernel composition. The most complete and definitive evaluation of the behavior of fission product silver is contained in a recent paper by Nabielek, Brown, and Offermann (1977). The conclusions from this work are stated below:

1. Silver release from BISO particles is higher than from TRISO particles (Fig. 2-5). There is practically no retention of silver by pyrocarbon (see also Offermann, 1977) at temperatures >1100 K.

2. There is higher Ag-release from carbide fuel than from oxide fuel (Fig. 2-6).

3. The retention of silver in intact TRISO particles is not as complete as for all other fission products, at least at irradiation temperatures above 1450 K (Fig. 2-7). High density silicon carbide ($\geq$3200 kg x m^{-3}) with minimum content of free silicon (<0.3

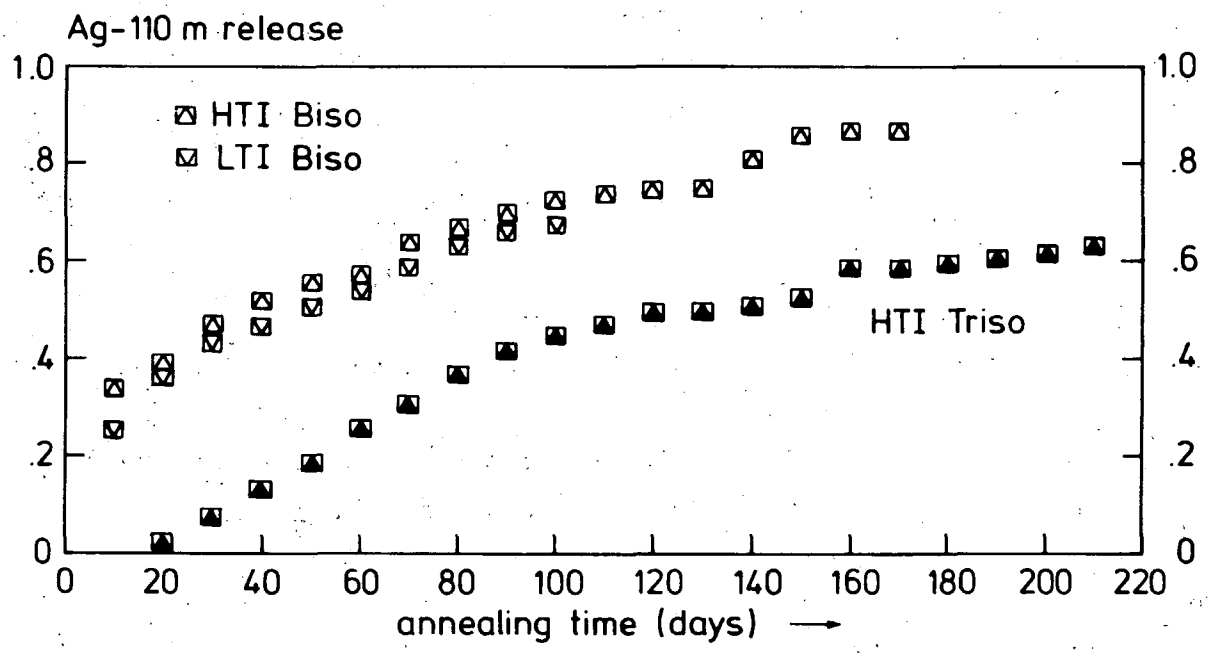

Fig. 2-3. Measured Ag-110 m release during 1770 K anneal of BISO and TRISO particles irradiated below 920 K (UKAEA Harwell 919/6 experiment)

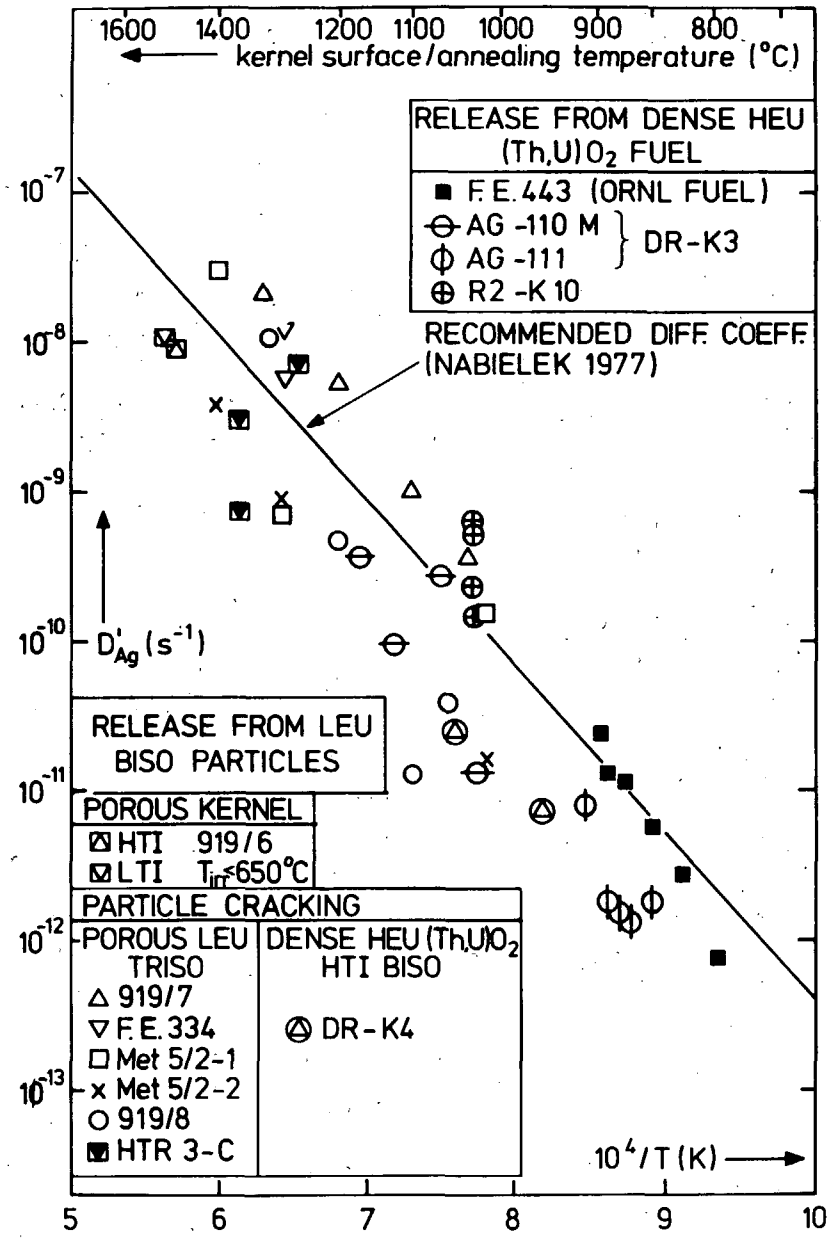

The origin of data:

Brown and Faircloth, 1976	- F.E. 334, Met 5 919/7, 919/8
Nabielek et al., 1977	- F.E. 443, DR-K3, 919/6 (from Brown, 1977a), R2-K10 (from Groos et al., 1977)
Reitsamer, Falta, and Nabielek, 1978	- DR-K4, HTR 3

Fig. 2-4. Reduced diffusion coefficients of silver in UO_2 and $(Th,U)O_2$

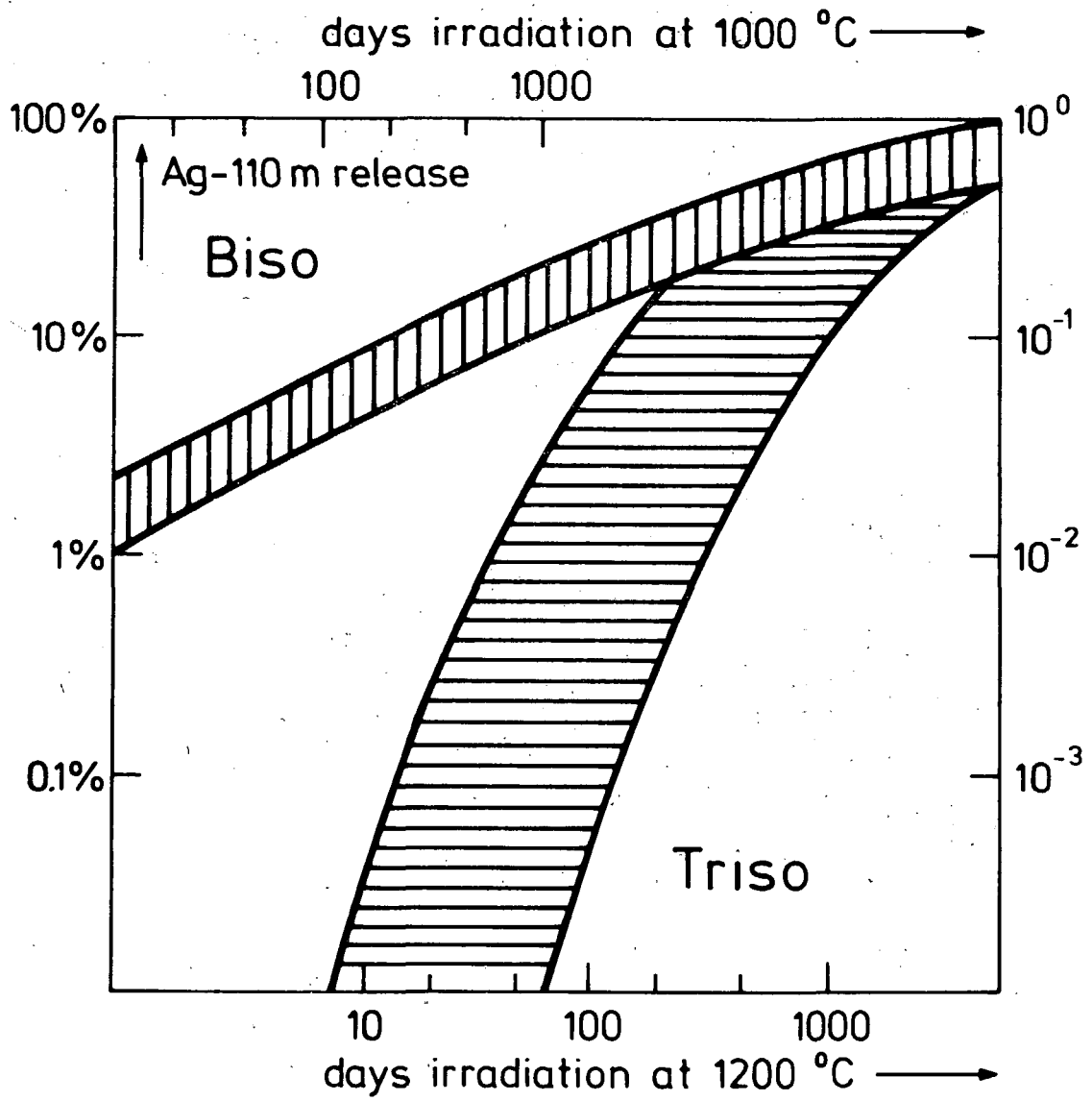

Fig. 2-5. Summary of measured silver releases from Dragon TRISO and BISO low-enriched UO_2 particles

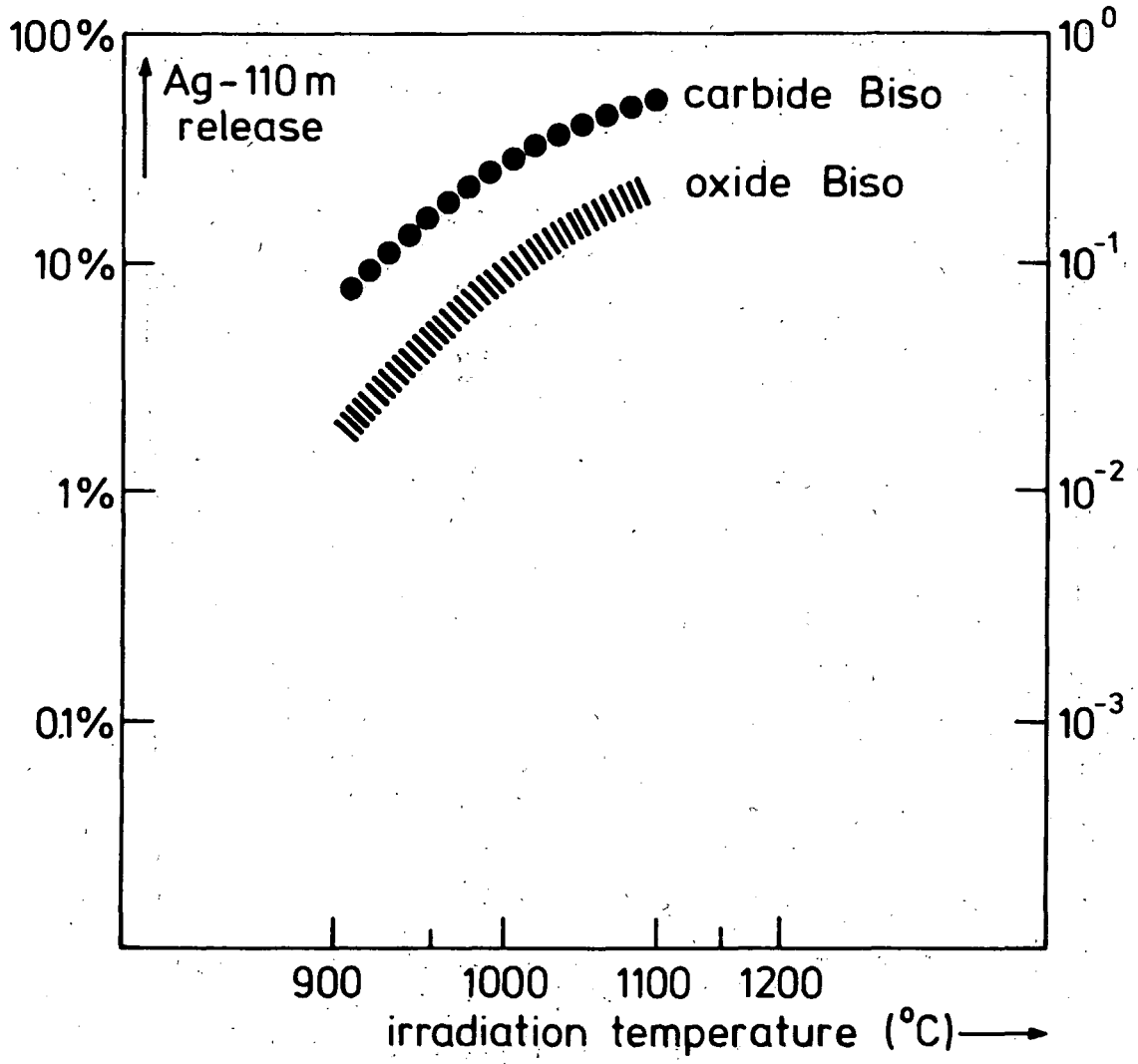

Fig. 2-6. Measured Ag-110 m release from BISO oxide and carbide fuel (Dragon FE 477/rods 1, 2, and 6; 557 full-power days irradiation)

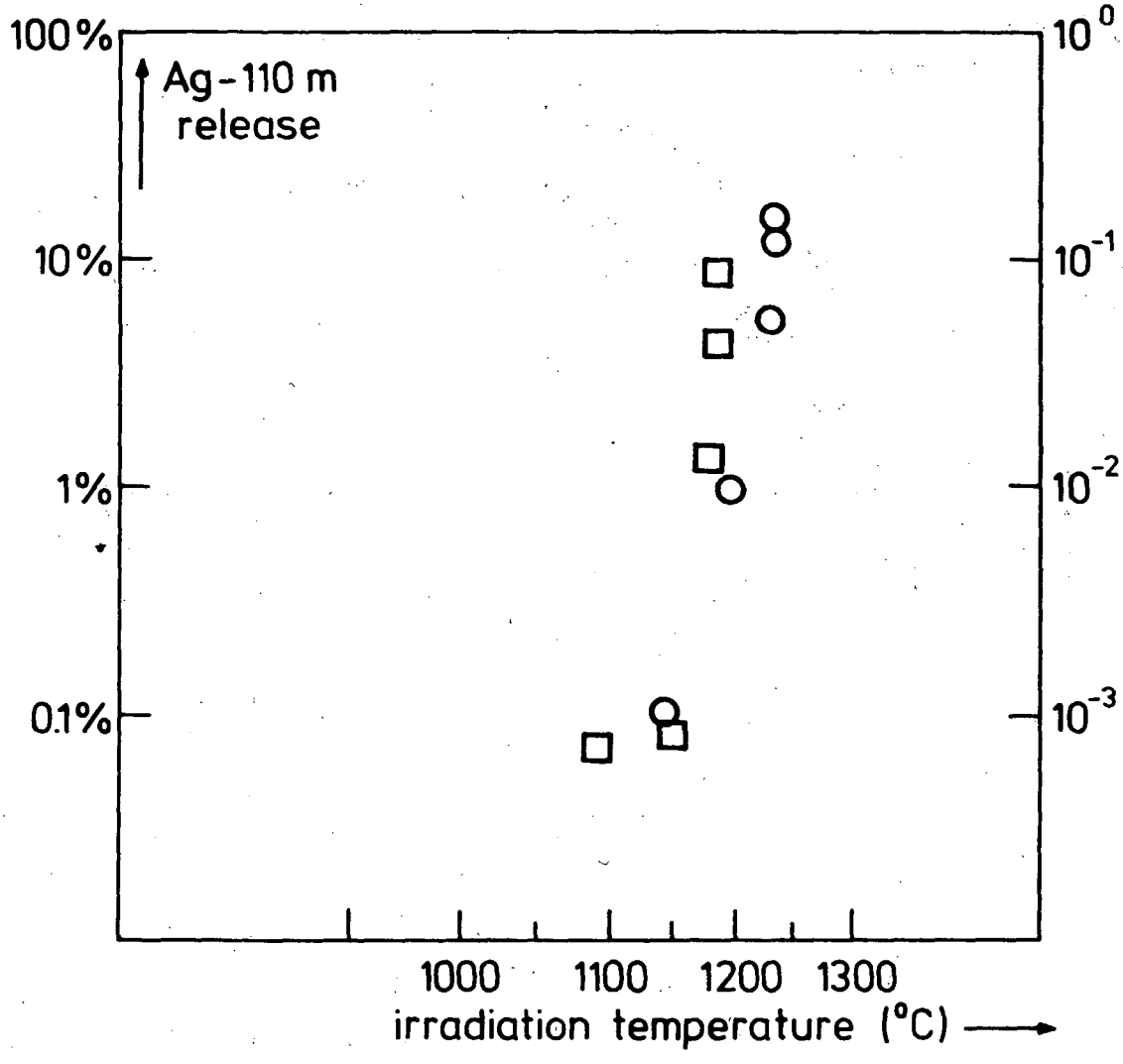

Fig. 2-7. Measured Ag-110 m release from TRISO particles with well-characterized SiC deposited under optimum conditions (Dragon MT 2; 347 full-power days)

weight %) is required for minimum release, but the SiC property responsible for Ag permeation through SiC has not been identified.

An undetectably small amount of free silicon ($\leq$0.1 weight %) is likely to be still present in grain boundaries and small pores of SiC coating. It can be argued that this leads to a breakthrough type of mechanism (Nabielek, 1976a; see also Fig. 2-8) which depends on a certain critical Ag concentration to be reached at the inner SiC surface. Silver release fractions below 10^{-3} can be achieved by either reducing the free silicon in SiC or by reducing kernel release (low irradiation temperature/SiC getter in kernel; Brown and Faircloth, 1976).

Ag moves through graphite like a gas, but is trapped in irradiated nuclear graphite at temperatures around 1300 K (Fig. 2-9; Nabielek and Brown, 1975). The same is true for unirradiated graphite and matrix materials at some temperatures below 1100 K, but there is no retention in compacts, sticks, and spherical fuel elements at typical operating temperatures.

2.2.2. Recommendations for Improving Silver Retention

As indicated earlier, the release from BISO particles is practically identical to kernel release observed in the temperature range 1100 to 1800 K. While intact silicon carbide produced under "optimum" conditions (Voice and Scott, 1972; Ford, Hibbert, and Martin, 1972) retains all other fission products completely, silver is released to a variable degree at irradiation temperatures above 1450 K* (Nabielek, Brown, and Offermann, 1977).

This necessitates the use of solely TRISO fissile particles and the development of means for improving silver retention in fuel bodies. The

*The annealing of TRISO particles at 1773 K (Fig. 2-3) showed a breakthrough time of 10 days, while cesium did not break through after 250 days (Brown, Brownsword, and Hooper, 1977a).

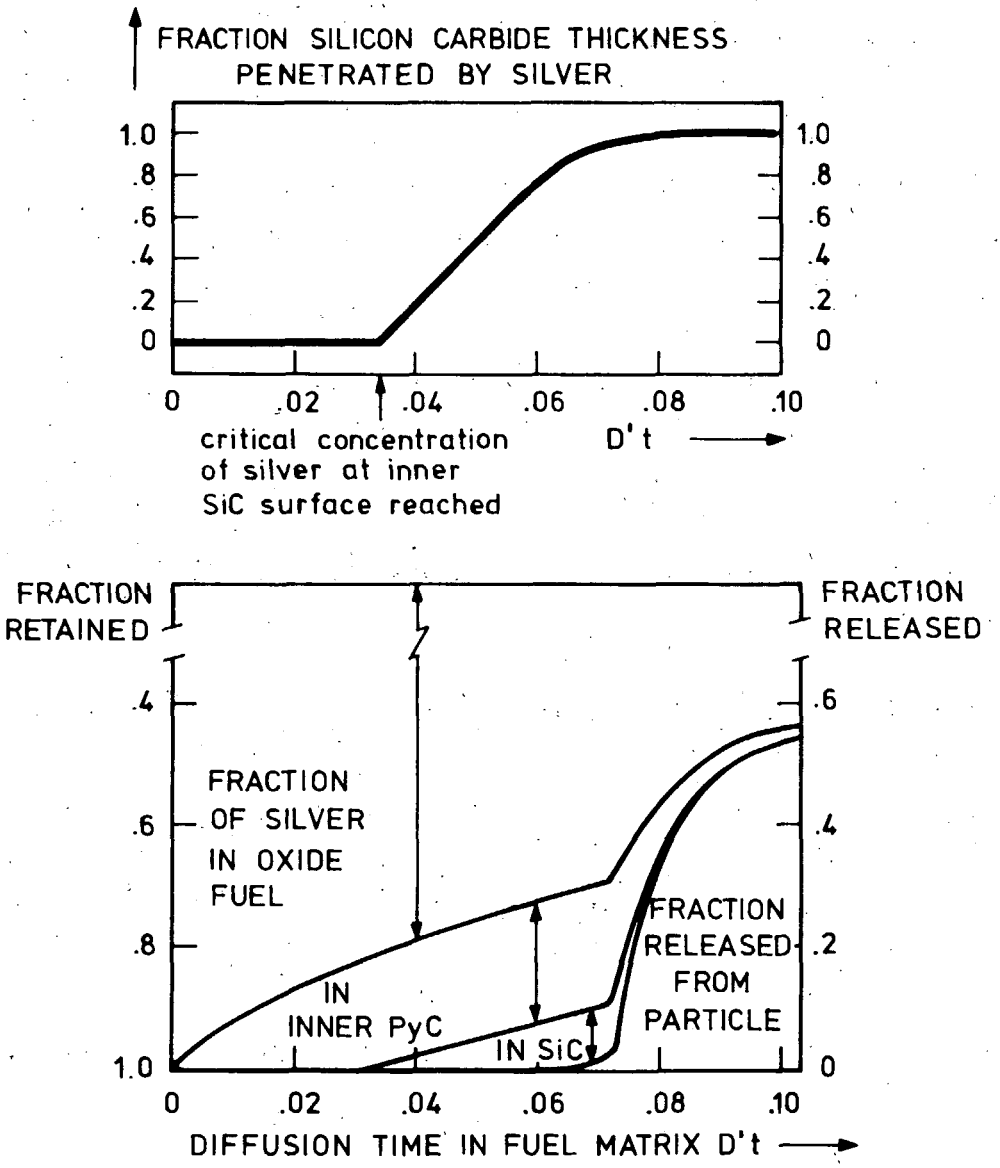

Fig. 2-8. Model description of silver penetration through silicon carbide follows in-pile (and out-of-pile) release rates

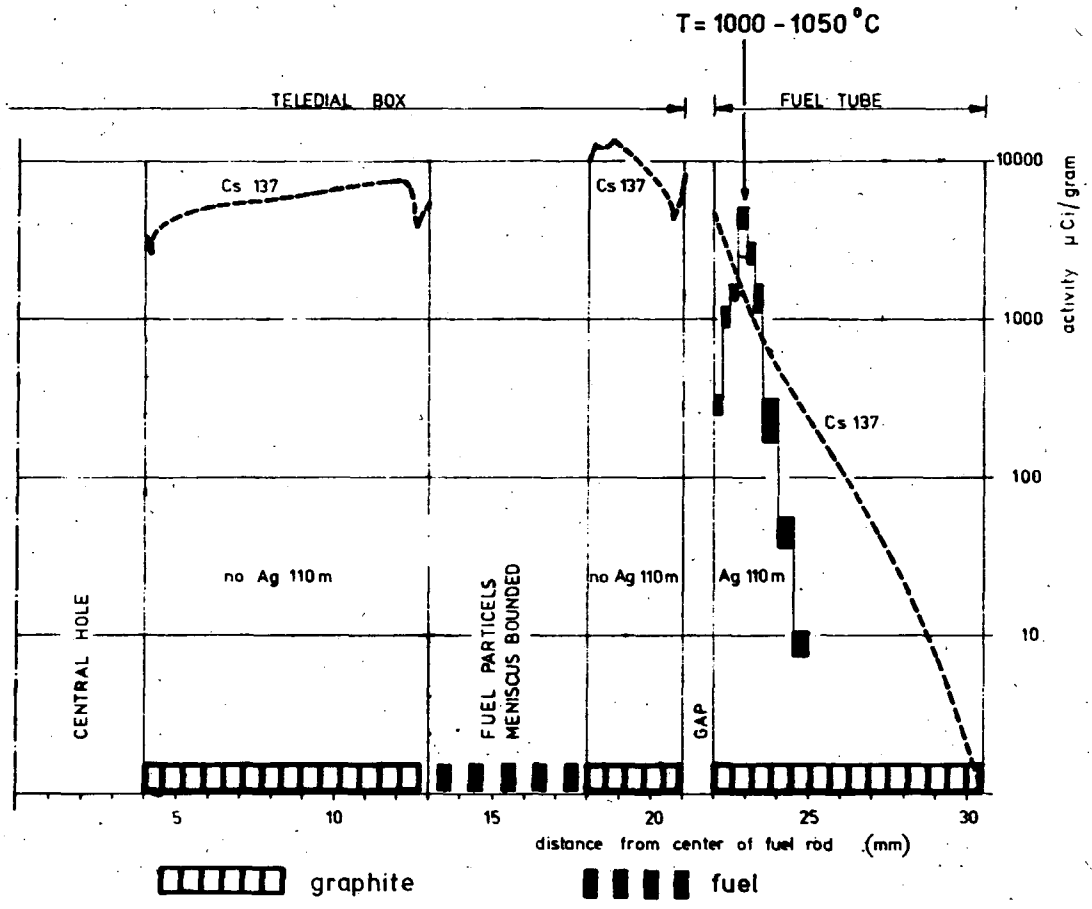

Fig. 2-9. Radial profile of Cs-137 and Ag-110 m in irradiated graphite (Dragon LE7/1400)

development program should include the careful study of silver transport in as-produced silicon carbide (irradiation plus postirradiation examination) and further investigations of the following observations:

1. SiC addition to the kernel has shown a gettering effect (Brown and Faircloth, 1976) while other additions are ineffective (Förthmann et al., 1977).

2. Improved SiC produced by depositing the outermost layers very slowly (reduction of surface flaws to give increased strength) showed some improvement in silver retention* (Brown, 1977b).

3. Thicker (90 μm) SiC gives some improvement in silver retention (Nabielek, Brown, and Offermann, 1977).

4. Nitrogen-doped SiC (reduction of free silicon) has 20% increased bursting strength (Hick, 1976) and is expected to show improvements in silver retention.

5. Silver is trapped in irradiated nuclear graphite (Nabielek and Brown, 1975) and by metallic getters in matrix materials (Förthmann, Grübmeier, and Stöver, 1977).

2.3. STRONTIUM AND BARIUM RELEASE

Dragon project measurements of Sr-90 in kernel and coating (irradiated at T < 1750 K) after the cracking of intact TRISO particles revealed that (after correction for recoil and contamination) strontium is retained virtually completely in UO_2 kernels surrounded by an intact coating layer (Nabielek et al., 1974; Brown and Faircloth, 1976). Microprobe analysis failed to detect strontium in the inner pyrocarbon coatings (Friskney and Simpson, 1975b), but showed it to be evenly distributed in the UO_2 matrix

*The improvement is probably negligible for long-term irradiation.

(Friskney and Simpson, 1976). It appears that the recoil fraction is reabsorbed in the kernel at irradiation temperatures up to 1750 K and that strontium is largely retained in the UO_2 (Förthmann et al., 1975; Friskney and Simpson, 1976).

Above 1750 K some strontium is lost from the oxide kernel. This can be described approximately by a reduced diffusion coefficient D' with (Fig. 2-10; Brown and Faircloth, 1976)

$$\log_{10}D' \text{ [Sr in } UO_2\text{, } 1770 < T < 1920 \text{ K]} = 10.5 - 36{,}100/T \quad . \quad (2\text{-}5)$$

In this temperature range, Kr, Xe, and Cs are still retained in TRISO particles, but Sr and Ba are lost from the particle. These elements (Sr and Ba) are released from the kernel in sufficient concentration to attack the SiC layer. When the SiC layer is completely penetrated, it is no longer a barrier to these nuclides or to Cs release (Brown and Faircloth, 1976).

At General Atomic Company, the diffusion coefficients for strontium (Myers and Bell, 1974) and barium (Myers, 1977b) in HEU $(Th,U)O_2$, (Th/U = 14, 17) kernels have been determined in the temperature range $1760 < T < 1920$ K (see Fig. 2-10). The results can be expressed by the equations:

$$\log_{10}D' \text{ [Sr in } (Th,U)O_2\text{, } 1670 < T < 1920 \text{ K]} = 9.29 - 31{,}030/T \quad , \quad (2\text{-}6)$$

$$\log_{10}D' \text{ [Ba in } (Th,U)O_2\text{, } 1670 < T < 1920 \text{ K]} = 8.33 - 29{,}100/T \quad . \quad (2\text{-}7)$$

Barium release has been observed to be higher than Sr release from porous UO_2 fuel by Friskney and Simpson (1975a, 1976), but it is difficult to quantify the electron microprobe observations made there.

Strontium release of 98% has been observed during the irradiation of loose, bare, carbon-diluted kernels at 1640 K (Nabielek, 1976b).

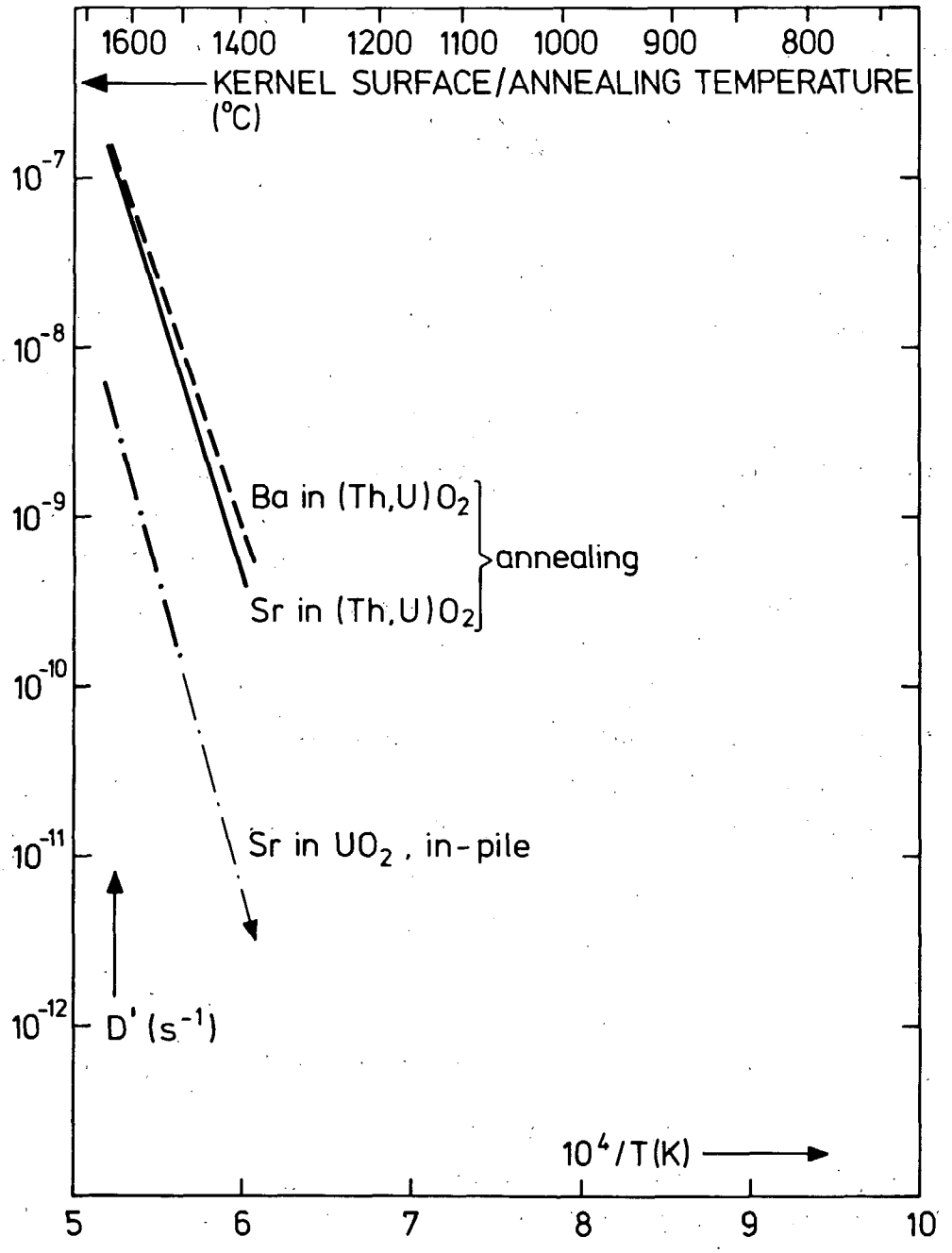

Fig. 2-10. Reduced diffusion coefficients of strontium in UO_2 (Brown and Faircloth, 1976) and of strontium (Myers and Bell, 1974) and barium (Myers, 1977b) in (Th,U)O_2

2.4. SHORT-LIVED FISSION GAS RELEASE FROM FAILED PARTICLES

The release of short-lived fission gases (Kr-88, Kr-85m, etc.) from failed fuel particles represents one of the principal contributors to the radioactivity of the circulating helium coolant and must be limited during normal operations. Furthermore, R/B measurements (R = release rate, B = birth rate) provide important information about particle breakage during irradiation tests, and they can be used to confirm the validity of stress-strain model calculations of particle failure fraction (Hick, Nabielek, and Harrison, 1973; Bongartz, 1977).

In a fundamental study, J. R. Findlay at Harwell (Brown et al., 1971) measured the fission product isotopes Kr-85m, Kr-87, Kr-88, Kr-89, Kr-90, Kr-91, I-131, I-133, Te-132, Xe-133, Xe-135, Xe-137, Xe-138, and Xe-140 (half lives from 14 s to 8 d) released in-pile from bare kernels. After producing powder route kernels with LTI and HTI TRISO coatings and sol-gel kernels with HTI TRISO coatings, the coatings were cracked off and the bare kernels, mixed with graphite powder, were irradiated to approximately 1% FIMA at temperatures of 973, 1273, 1523, and 1773 K. Purified CO was added to the helium flow to maintain the stoichiometry in the bare UO_2 kernels. The measured release rates over this temperature range can be interpreted in terms of the equivalent sphere model with the steady state release given by

$$\frac{R}{B} = 3\left(\frac{D'}{\lambda}\right)^{1/2}\left[\coth\left(\frac{\lambda}{D'}\right)^{1/2} - \left(\frac{D'}{\lambda}\right)^{1/2}\right] , \qquad (2\text{-}8)$$

where $\lambda = \ln 2/t_{1/2}$ (s^{-1}) is the decay constant, which has to include a flux correction for Xe-135. The D' values deduced from the experimental release results can be fitted by the equation

$$\log_{10} D' \ (s^{-1}) = -a - \frac{b}{T} \quad . \qquad (2\text{-}9)$$

The numerical values of a and b* obtained from the least-squares-fitted lines are given in Table 2-1. The diffusion coefficients are plotted versus 1/T in Figs. 2-11 and 2-12.

As seen in Fig. 2-11, the diffusion characteristics of short-lived fission gases are not influenced strongly by the kernel fabrication route or heat treatment during coating. Despite the limitations of this work (low burnup, no carburization of the kernel surface), these data have successfully been used to describe total core release from the Dragon reactor (Shepherd, 1971; Nabielek et al., 1974) and the out-of-pile release measurements of Dragon test fuel (Good and Giles, 1975). Furthermore, no burnup dependence was observed with porous, light-enriched UO_2 fuel.

The expressions shown in Eq. 2-9 with the constants given in Table 2-1 represent an overall fit to the release data for all isotopes over the temperature range 1000 to 1800 K. These fits imply an activation energy for diffusion in the range 80 to 120 kJ/mol. More careful treatment of the data might permit differentiation between the effects of volume diffusion, grain boundary diffusion, and recoil. It is assumed that volume diffusion [with activation energies of approximately 280 kJ/mol (Nabielek et al., 1974)] operates above 1550 K, while the release rate becomes very nearly independent of temperatures at low temperatures (Burnette, Bell, and Baldwin, 1973; Pointud and Chenebault, 1977).

Müller (1976) investigated short-lived fission-gas release rates from the THTR ball tests in R2 Studsvik (dense mixed oxide fuel). The measurements include the isotopes Kr-85m, -87, -88, -89, -90, -91; Xe-133, -135, -137, -138, -139, -140; and I-133, -135, and led to an assumption of diffusion coefficients (see Table 2-1 and Figs. 2-11 and 2-12)

$$\log_{10} D' \text{ (Kr, Xe in } (Th,U)O_2,\ 1000 < T < 1500 \text{ K}) = -7.60 - 2187/T \quad , \quad (2\text{-}10)$$

*Care must be taken not to confuse the activation energy of D', given by 19.14 x b kJ/mol, with the activation energy of R/B, which is one-half of the value above when $R/B = 3(D'/\lambda)^{1/2}$.

TABLE 2-1

CONSTANTS a, b IN THE DESCRIPTION OF THE REDUCED DIFFUSION COEFFICIENT D' (s^{-1}) OF FISSION GASES IN OXIDE FUEL AS A FUNCTION OF TEMPERATURE T (K): LOG_{10} D' = - a - b/T

State of Kernel	Kernel Composition	Burnup FIMA (%)	Isotopes	a	b	R/B (Kr-85 m) at 1000°C	
						Formula (%)	Measurement (%)
Findlay Experiment (Brown et al., 1971)							
Bare, porous (HTI)	18 % enr. UO_2	1	Kr-85 m,87,88,89,90,91	4.83	4512	3.0	4.7
Bare, porous (LTI)	18 % enr. UO_2	1	I-131,133, Te-132	3.79	6475	1.7	1.6
Bare, dense (HTI)	18 % enr. UO_2	1	Xe-133,135,137,138,140	3.31	6736	2.3	1.6
Studsvik THTR-Ball Experiments (Müller, 1976)							
In-pile broken, dense (HTI)	$(Th,U)O_2$ N = 5 - 40	10-18	Kr-85 m,87,88,89,90,91 Xe-133,135,137,138,139,140	7.60	2187	1.0	<1.0 (R2-K4/3;14% FIMA)
			I-133, 135	4.70	6560		
CEA/GA (Pointud and Chenebault, 1977; Myers, Baldwin, and Bell, 1977c)							
Laser failed, dense (LTI)	$(Th,U)O_2$ N = 4 - ∞	0	Kr-85 m, 88	5.94	5463	0.4	0.1
		7	Xe-133	4.68	5463	1.5	1.2
		14	assumed applicable to I, Te, Br, Se	4.13	5463	2.8	-

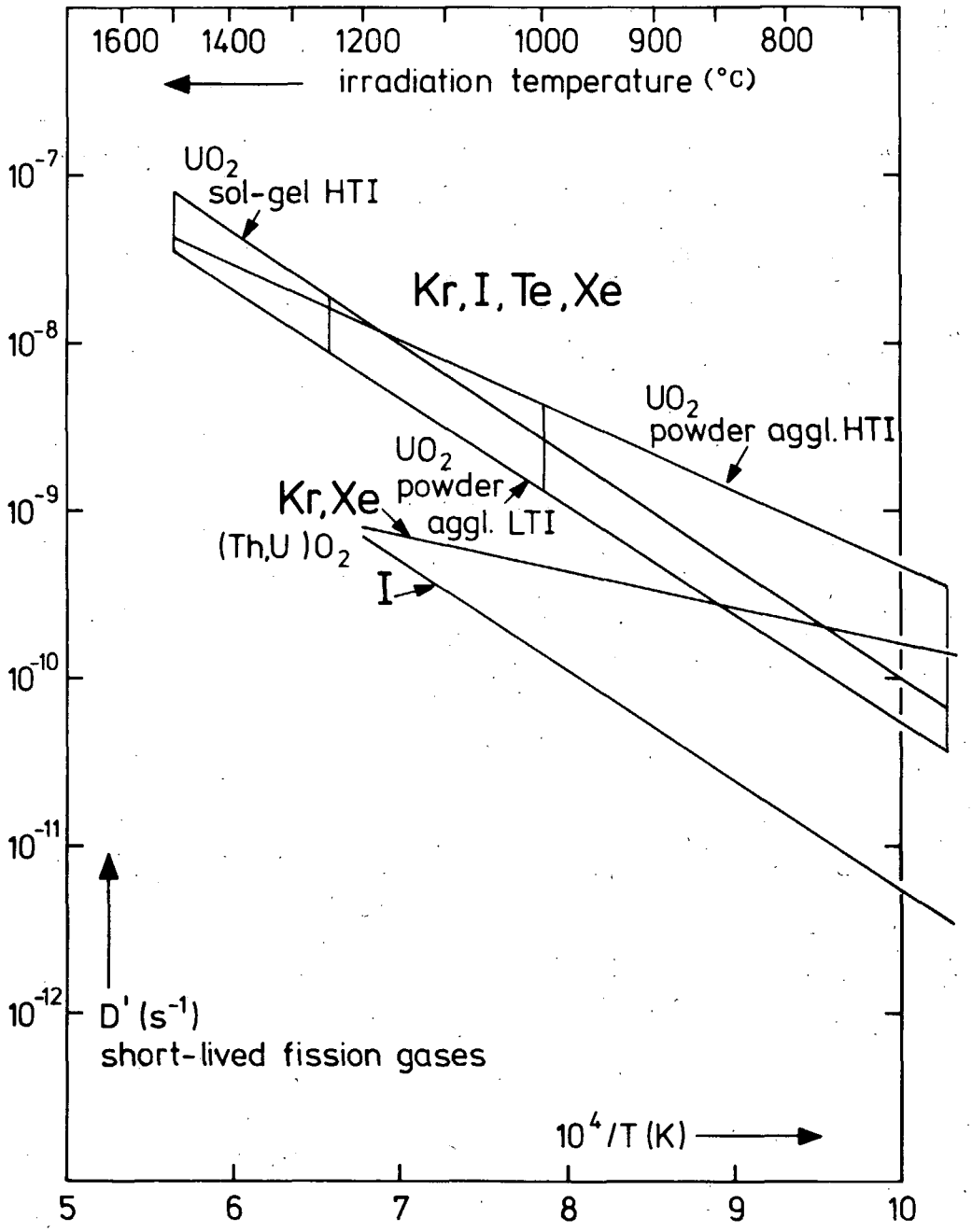

Note: UO_2 figures from in-pile release of bare kernels (Brown et al., 1971). $(Th,U)O_2$ figures from release of broken particles in spherical fuel elements (Müller, 1976).

Fig. 2-11. Reduced diffusion coefficients of Kr, I, Te, and Xe effective in the release of short-lived fission gases

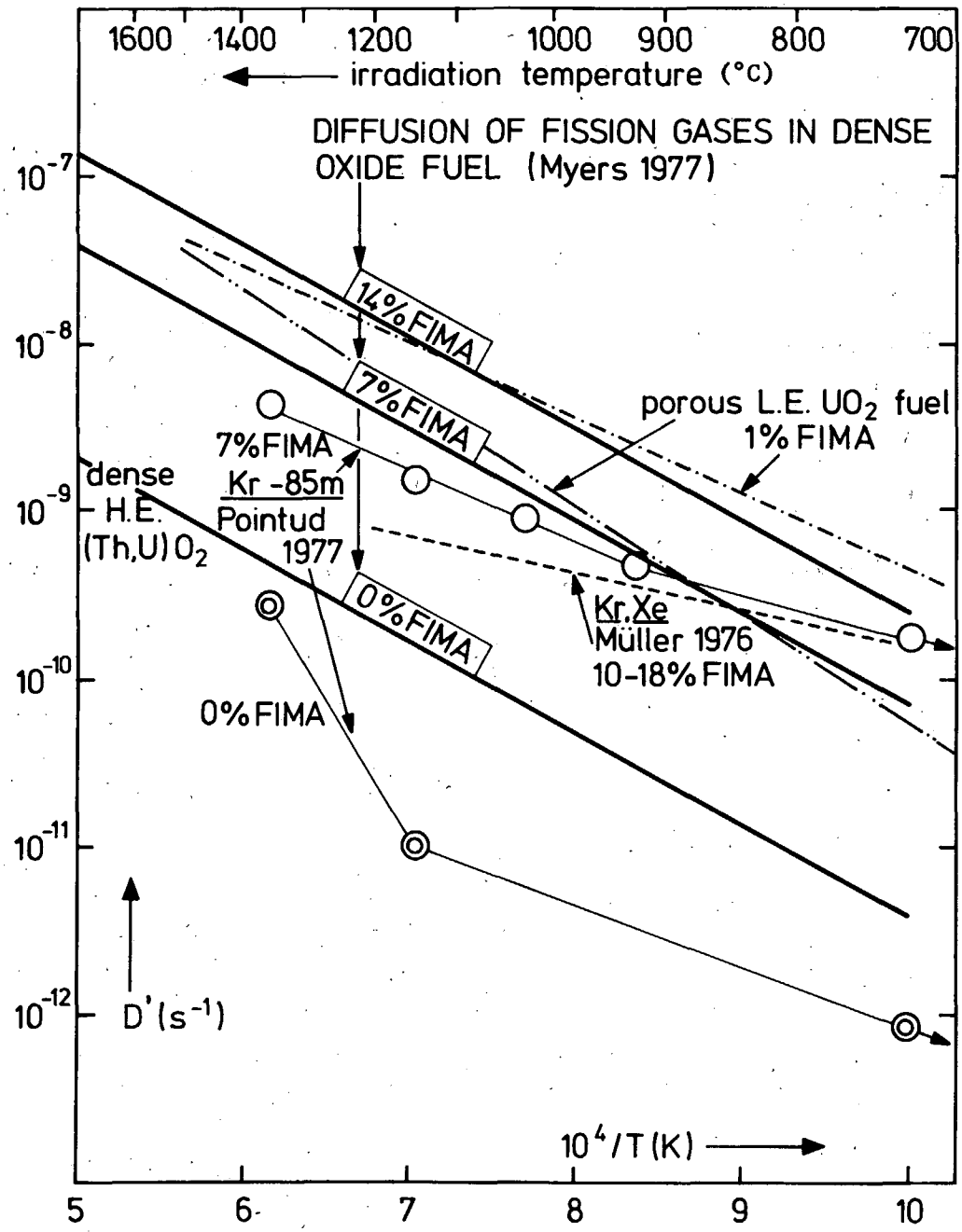

Fig. 2-12. Reduced diffusion coefficients of Kr and Xe versus irradiation temperature. Comparison of overall fit for dense oxide fuel (Myers, Baldwin, and Bell, 1977c; Müller, 1976) to measured Kr-85 m (Pointud and Chenebault, 1977), and fit for porous low-enriched oxide fuel (Brown et al., 1971)

$$\log_{10} D' \text{ (I in (Th,U)}O_2,\ 1000 < T < 1500 \text{ K)} = -4.70 - 6560/T \quad , \qquad (2\text{-}11)$$

for an overall fit to the data on 15 spherical fuel elements. It is concluded that these diffusion coefficients are relevant (if somewhat approximate) to the prediction of R/B within the equivalent sphere model formula (Eq. 2-8) for in-pile broken fuel at end-of-life burnups of 10% to 18% FIMA. Massive particle breakage >50% occurred only in one case (R2-K4, sphere 3), but end-of-life Kr-88 and Kr-85m from broken fuel remained <1% (EOL temperatures 1000° to 1150°C).

The behavior of fission gas release from failed fuel particles has been reviewed by Myers, Baldwin, and Bell (1977c). An upper limit on the release rates of Xe, I, Te, Br, and Se is given by assuming effective diffusion coefficients, which are shown for burnups 0%, 7%, and 14% FIMA in Table 2-1 and Fig. 2-12. From these, in-pile release rates for short-lived fission products can be predicted according to Eq. 2-8, and the same diffusion coefficients also apply to the calculation of the fractional release of stable gases in terms of the equivalent sphere model.

Studies on the release of short-lived fission gases (Kr-85m, Kr-88, and Xe-133) have been conducted by GA and CEA (Burnette, Bell, and Baldwin, 1973; Harmon and Scott, 1975; GA, 1975; GA, 1976; Pointud and Chenebault, 1977) on bare oxide and carbide kernels, laser-failed oxide and carbide fuel particles, and in-pile broken oxide and carbide particles. The release rates are found to be a function of the substrate surrounding the kernel, the porosity of the kernel, and burnup. The results lead to the following conclusions:

1. At temperatures greater than 1300°C, the release of short-lived fission gases from failed fuel particles in fuel rods occurs primarily by recoil and knock-out from the kernel into the porous carbon buffer layer, followed by gas phase diffusion (below 600°C) and bulk diffusion (above 900°C).

2. The activation energy for bulk diffusion in fuel rods is 33 ±8 kcal/mol for Kr and 27 ±8 kcal/mol for Xe in the temperature range 1000° to 1500°C. The activation energy for the gas phase diffusion is 0.7 kcal/mol for Kr and Xe at temperatures below 400°C. These activation energy values for bulk diffusion are in good agreement with those obtained by KFA workers (Groos et al., 1977). No activation energy measurements have been made directly on failed fuel particles.

3. The steady-state fractional release depends on a power of the nuclide half-life, with the exponent equal to 0.2 ±0.1 at temperatures between 250° and 350°C, and approaching 0.5 ±0.1 at temperatures between 850° and 1300°C.

4. For failed particles containing dense kernels in fuel rods at low burnups, the R/B value for Kr-85m at 1100°C is 0.005 ±0.003. At high burnups, the initially dense kernels become porous and the R/B value increases significantly.

For ThO_2 and 8 ThO_2 - 1 UO_2, Myers (1977f) obtained the following formula to relate the R/B with the burnup F (% FIMA) for F < 11% on the basis of data from CEA and GA:

$$(R/B)_{T,F} = [0.133 + 0.828\ F^{0.6} + 0.867\ e^{-205F}](R/B)_T \quad ,$$

where $(R/B)_{T,F}$ = R/B for temperature T and burnup F (% FIMA),

$(R/B)_T$ = R/B for temperature T and zero burnup.

This formula, however, is found not applicable to oxide fuel of higher uranium content.

In agreement with the Dragon project, Pointud and Chenebault (1977) noticed that the release rates of initially porous kernels did not change

with burnup, but that initially dense kernels showed a large increase in release rate with burnup. Similar effects can be observed with internal cesium release and the internal release of stable Xe and Kr. This is not unexpected. Initially, the releasing unit of the dense kernel is of the size of the whole kernel, while with high burnups the kernel is broken up into crystallites 3 to 30 μm in size with resulting higher releases. A unified concept describing all fission product transport within particle kernels would contain:

1. Crystallite size as a function of production route, burnup, and temperature.

2. "True" diffusion coefficient in UO_2, etc.

3. Hold-up in grain boundaries (if applicable).

The above treatment disregards the reaction between the oxide kernel and the coating in failed particles. Upon continuous operation at high temperature in the reactor core, the oxide kernels of the failed particles will be converted to carbides if the equilibrium CO pressure of the reaction is higher than the partial pressure of CO in the helium coolant, which is in turn controlled by the reaction between the graphite and the moisture in the helium coolant. The rate of conversion is temperature-dependent and the converted carbide kernel will have a much higher R/B value if exposed to helium coolant containing high moisture content. The rate of conversion of ThO_2 kernels in failed particles has been determined under various conditions at different temperatures (Burnette, 1978). The kinetics of the reduction of UO_2 by carbon was studied by Lindemer, Allen, and Leitnaker (1969). The effect of hydrolysis on the fission gas release rate of converted ThO_2 kernels is under investigation (Montgomery, 1978). Similar work should be carried out on failed fuel particles containing LEU oxide kernels in order to provide information on how the R/B value is affected by conversion to carbide and the subsequent hydrolysis by moist helium. Carburization of broken or bare oxide particles has been observed by the

Dragon project in loose particle irradiations, but neither the Dragon project nor KFA have found it within fuel bodies (compacts/spherical fuel elements).

The burst release of the inventory of short-lived fission gases upon particle failure is of interest to reactor safety analysis. At high temperatures (>850°C) measured R/B values are in general proportional to the square root of the half life ($\propto \tau_{1/2}^{0.5}$). During the in-pile burst of a significant number of particles, the sudden escape of stored fission gases (inventory $\propto \tau_{1/2}^{0.5}$) should produce a short time $\tau_{1/2}^{1.5}$ dependence. This has been observed in a Dragon project particle test in Studsvik (Nabielek, 1976b).

2.5. RELEASE OF SOLID FISSION PRODUCTS FROM IN-PILE BROKEN PARTICLES

2.5.1. Observations on Strontium

While the release of strontium and barium from UO_2 kernels remains below 1% in intact oxide particles (T_{irr} < 1700 K), about 50% loss of strontium has been observed when particles break during irradiation (T_{irr} = 1570 K; Baker, 1974). This possibly is due to a partial conversion of the oxide kernel to carbide (in loose particle irradiations).

2.5.2. Observations on Cesium

No drastic loss of cesium could be detected from in-pile broken oxide particles (Reitsamer, Falta, and Nabielek, 1978). See Table 2-2. The higher release from broken particles is assumed to be due to the loss from kernel voids.

2.6. RELEASE OF FISSION PRODUCTS FROM FAILED OXIDE PARTICLES DURING TEMPERATURE TRANSIENTS

Myers (1977e) has proposed a model for making a conservative estimation of fission product release from failed particles during temperature transients.

TABLE 2-2

Cs-137 KERNEL RELEASE FROM $(Th,U)O_2$ HTI BISO PARTICLES IN SPHERICAL FUEL ELEMENTS OF DR-K4, IRRADIATED IN DRAGON FOR 742 DAYS (SEE FIG. 2-13).

	Fast Neutron Dose 10^{21} cm^{-2} (E>0.1MeV)	Burnup FIMA (%)	Outer Fuel Zone		Centre Fuel Zone	
			Kernel Temp. (°C)	Kernel Release (%)	Kernel Temp. (°C)	Kernel Release (%)
Sphere 11[(a)]						
Intact Particles	7.2	13	924	4	1011	13
Broken Particles (Approx. 1%)				17		30
Sphere 7						
Intact Particles (No broken particles)	6.4	12	950	4	1044	12

(a) As expected with HTI BISO coated particles, particle failures in sphere 11 started at dose 7×10^{21} cm^{-2} (E > 0.1 MeV)

ThO_2 BISO particles irradiated at 1270 K to burnups of 1.5% and 15% FIMA are laser-failed and reirradiated at low temperatures for the measurement of the release rates of short-lived Xe, Kr, and I isotopes. The release rates are measured both isothermally at 1430°, 1740°, and 2030°C and for temperature ramps from 1000° to 2300°C (5 or 24 hours). The release behavior is identical for Xe and I isotopes and similar with Cs. The time-dependent released fraction consists of a slow component and a fast phase.

The contribution of the fast phase is determined experimentally as a function of annealing temperature with burnup as a parameter. The release during temperature transients is estimated by Myers (1977e) on the basis of the fast phase contribution taking into account the difference between the annealing and irradiation temperatures and the burnup. Together with data on particle breakage during temperature transients, this provides the information on fission product release needed for a safety analysis of reactor operation.

It is suspected that the apparent increase of the cesium diffusion coefficient in $(Th,U)O_2$ in the case of temperature-cycled experiments (750°C/900°C/1050°C) with burnup >10% FIMA is also related to the existence of a fast diffusion path (Reitsamer, Falta, and Nabielek, 1978; see dashed line in Fig. 2-13).

At KFA, Schenk (1978) has observed that the Kr-85 release during post-irradiation annealing of high-burnup $(Th,U)O_2$ broken particles is very sensitive to the steepness of the temperature ramp. High-burnup, dense, low-enriched UO_2 fuel shows Kr-85 release results independent of the heating procedure, and, up to 1800°C, the release fraction is less or equal to the measurement of stable gas release after crushing at the irradiation temperature (see compilation of SGAE measurements by Fessler, 1976).

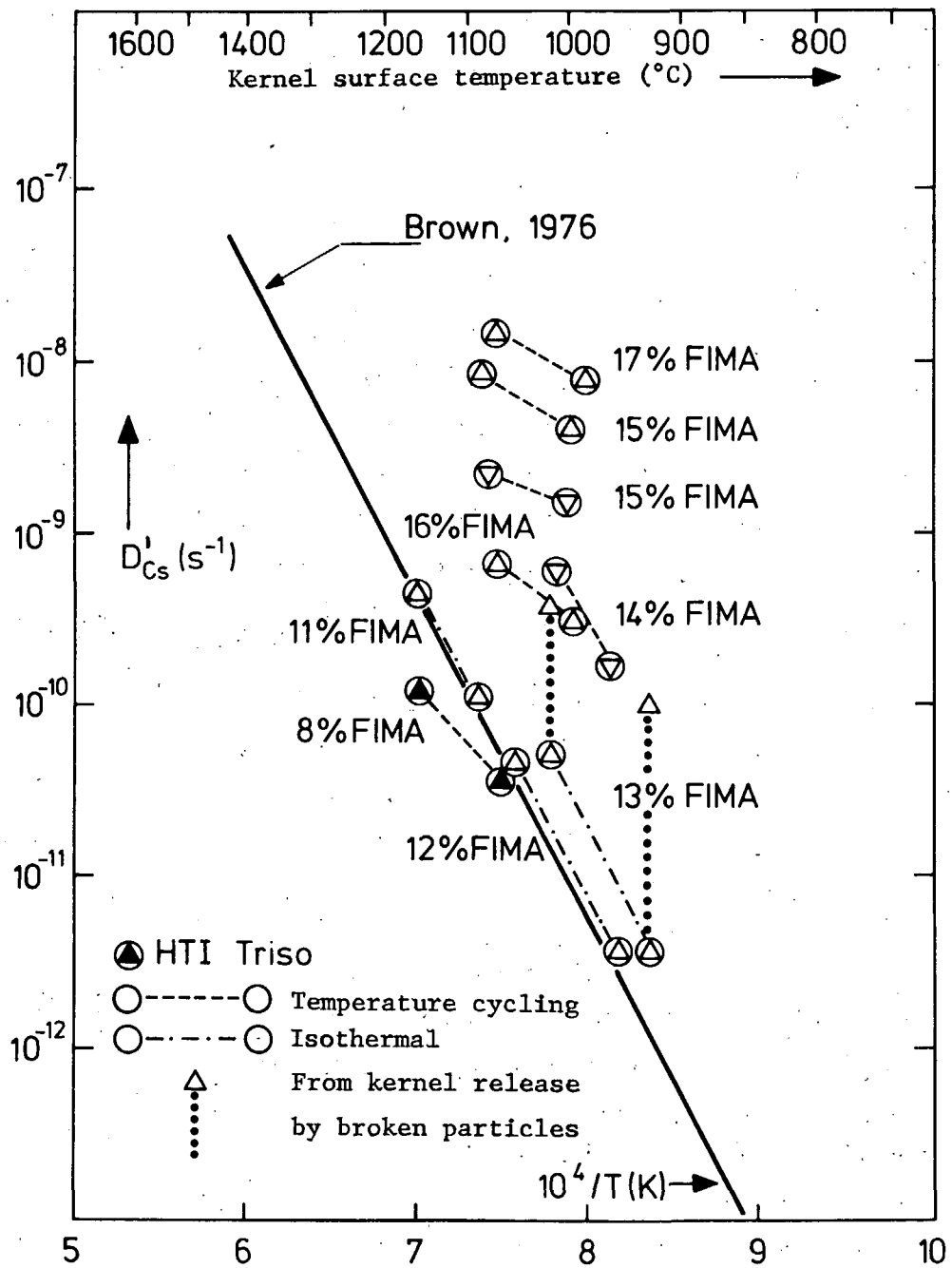

Fig. 2-13. Reduced diffusion coefficient of Cs in high-burnup $(Th,U)O_2$ obtained from measurement of Cs-137 kernel loss. Particles in sphere 11 of DR-K4 are denoted by "13 % FIMA"

2.7. FISSION PRODUCT RELEASE FROM CARBON DILUTED UO_2 FUEL

The influence of kernel porosity on fission product retention in the kernel has been demonstrated in the Dragon FPR 2 experiment (FPR = fission product retention). Fission product release was considerably higher from the porous (3 g/cm^3), carbon-diluted UO_2 than in undiluted UO_2. This result was expected (Nabielek et al., 1974). Fractional Cs-137 release from diluted and undiluted UO_2 is compared in Fig. 2-14. Release values approaching 100% were measured for the carbon-diluted fuels at temperatures >1300 K.

The fractional release was determined by gamma spectrometric measurements of the fission product inventory in TRISO coated particles and bare kernels irradiated to 5.9% FIMA (Lamb and Nabielek, 1976), shown on the top of Fig. 2-15.

At temperatures above 1330 K, there was a near-complete loss of Cs-137, Sb-125, and Sr-90. Ce-144 was partially lost, but Zr-95, Ru-103, and Ru-106 stayed with the fuel. From the drop in the Cs-134/Cs-137 ratio (bottom of Fig. 2-15), it can be assumed that xenon was released from the bare kernels in the early stages of irradiation. During the annealing for fission gases, there was only an initial burst, but no steady release rate could be obtained. Silver was below the detection limit in the bare kernels. It is expected that silver also was not retained in carbon-diluted kernels.

REFERENCES

Baker, H. T., et al., 1974, "Statistical Irradiation Studies on Dragon LE Series Coated Fuel Particles: Part II - Annealing and Radiochemical Results," Dragon Project Report 910.

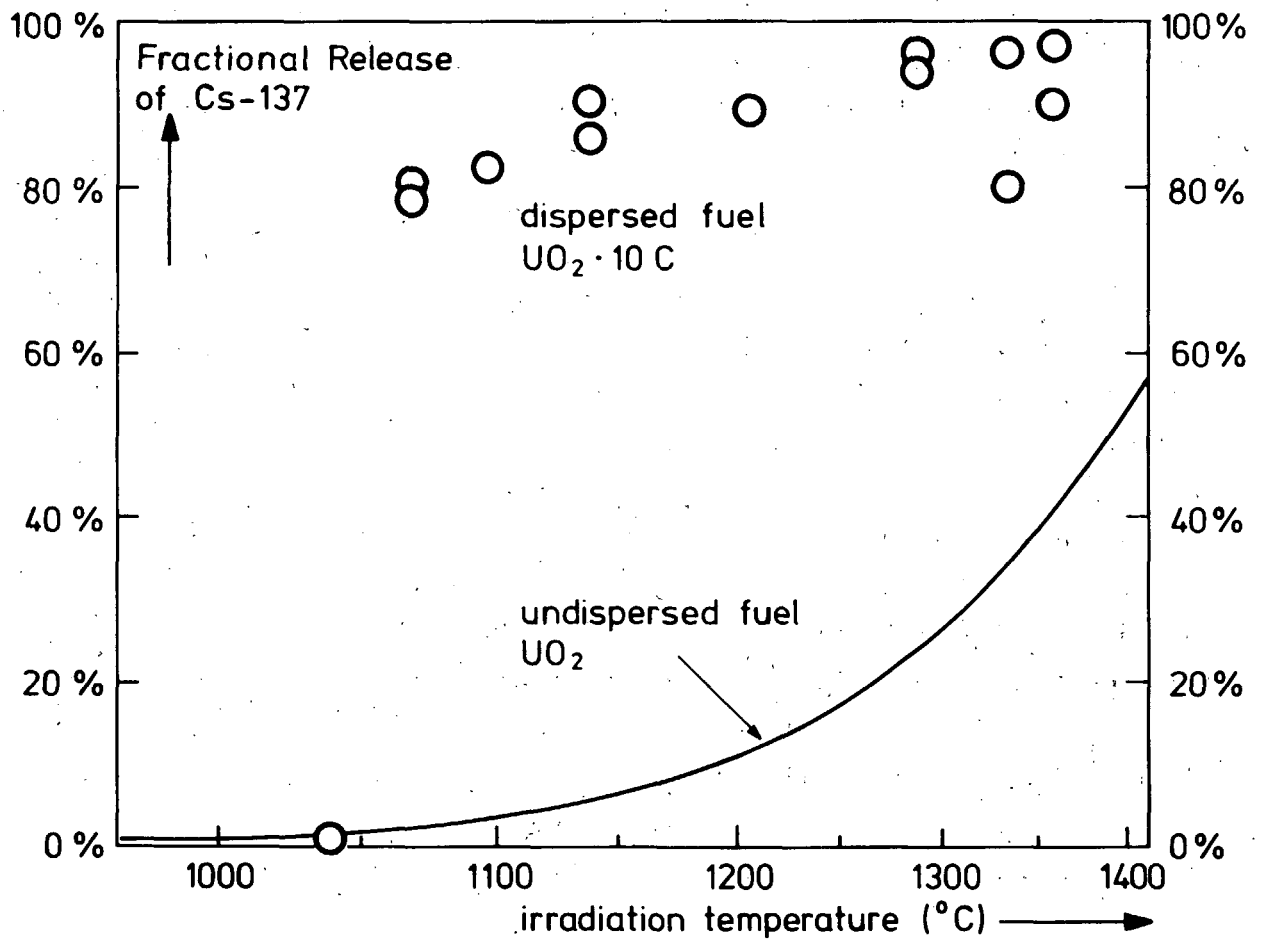

Fig. 2-14. Fractional release of Cs-137 as a function of irradiation temperature for carbon-diluted, high-enriched UO_2 fuel (kernel density 3 g/cm^3) compared to undispersed oxide fuel (kernel density 8 to 10 g/cm^3; Eq. 2-2)

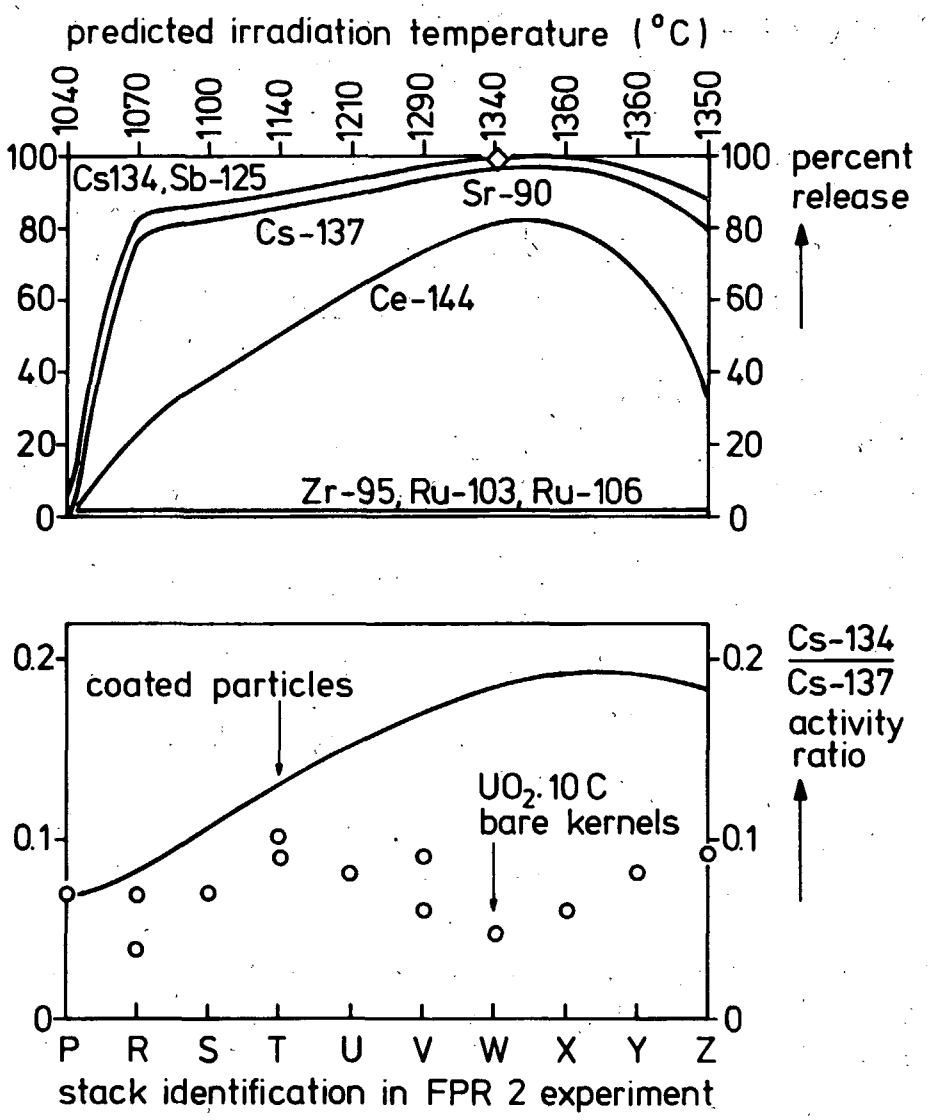

Fig. 2-15. Fission product release from bare, carbon-diluted UO_2 fuel (3 g x cm^{-3})

Bongartz, K., 1977; "Bestimmung der Versagensquote für ein TRISO-Brutteilchen mit mehreren Modifikationen in Abhängigkeit vom Abbrand mit Hilfe von Spannungsmodellrechnungen," KFA-IRW Technical Note 77/77.

Brown, P. E., et al., 1971; "The Emission of Fission Products from Bare UO_2 Fuel Kernels During Irradiation at High Temperature," unpublished data, presented in parts at the Int. Conf. on Physical Metallurgy of Reactor Fuel Elements, CEGB, Berkeley Nuclear Laboratories, September 2-7, 1973.

Brown, P. E., and R. L. Faircloth, 1976; "Metal Fission Product Behavior in HTR's - UO_2 Coated Particle Fuel," J. Nucl. Mat 59 29.

Brown, P. E., M. Brownsword, and E. W. Hooper, 1977a; "The Determination of Diffusion Coefficients for Cs and Ag in PyC and SiC by Post Irradiation Annealing of Coated Particle Fuels," UKAEA Harwell Report AERE-R-8603.

Brown, P. E., 1977b; UKAEA Harwell, private communication.

Burnette, R. D., W. E. Bell, and N. L. Baldwin, 1973; "Fission Product Retention Characteristics of HTGR Fuel," Proc. Int. Conf. Nuclear Fuel Performance, British Nuclear Energy Society, London.

Burnette, R. D., 1978; General Atomic Company, unpublished data.

Fessler, W., 1976; "Zusammenstellung und Auswertung von Gasmengenmessungen an beschichteten Brennstoffteilchen nach Bestrahlung," unpublished data.

Ford, L. H., N. S. Hibbert, and D. G. Martin, 1972; "Recent Developments of Coatings for GCFR and HTGCR Fuel Particles and their Performance," J. Nucl. Mat. 45, 139.

Förthmann, R., et al., 1974; "Chemical Behaviour in Irradiated HTGR Fuels," IAEA Symposium on Thermodynamics of Nuclear Materials, Paper 190/35, October 21-25, Vienna.

Förthmann, R., H. Grübmeier, and D. Stöver, 1977; "Metallic Fission Product Retention of Coated Particles with Ceramic Kernel Additives," Nucl. Techn. 35, 548.

Friskney, C. A., and K. A. Simpson, 1975a; "The Release of Cesium and Xenon from the UO_2 Kernels of Irradiated HTR Fuel Particles," J. Nucl. Mat. 57, 341.

Friskney, C. A., and K. A. Simpson, 1975b; "Fission Product Migration in the Coatings of Irradiated UO_2 HTR Fuel Particles," J. Nucl. Mat. 57, 333.

Friskney, C. A., 1975c; "Examination of Irradiated UO_2 HTR Fuel Particles," Dragon Project Technical Note 729.

Friskney, C. A., and K. A. Simpson, 1976; "Examination of Irradiated UO_2 HTR Fuel Particles - Behaviour of Fission Products Ba, Sr and Zr," Dragon Project Technical Note 762.

GA, 1975; "HTGR Fuels and Core Development Program Quarterly Progress Report for the Period Ending February 28, 1975," ERDA Report GA-A13353, General Atomic Company.

GA, 1976; "AIPA Fission Product Source Terms," HTGR Accident Initiation and Progression Analysis Status Report, Vol. 5, ERDA Report GA-A13617, General Atomic Company.

Good, P. D., and P. Giles, 1975; "The Post-Irradiation Measurement of Noble Fission Gas Release from the Charge III Low Enriched UO_2 Centre Rod Experiments," Dragon Project Report 922.

Groos, E., et al., 1977; "Fission Product Release from Coated Particles Embedded in Spherical Fuel Elements for HTR's," Nucl. Techn. 35, 509.

Harmon, D. P., and C. B. Scott, 1975; "Development and Irradiation Performance of LHTGR Fuel," ERDA Report GA-A13173, General Atomic Company.

Hick, M., H. Nabielek, and T. A. Harrison, 1973; "Mechanical Failure of Coated Particles Due to Internal Gas Pressure and Kernel Swelling," Dragon Project Report 828, Part II.

Hick, H., 1976; "Review of Unusual Particle Bursting Phenomena," Dragon Project Technical Note 760.

Lamb, D. N., and H. Nabielek, 1976; "Fission Product and Release from Carbon-Diluted Fuel," Dragon Project, unpublished data.

Lindemer, T. B., M. D. Allen, and J. M. Leitnaker, 1969; "Kinetics of the Graphite-Uranium Dioxide Reaction from 1400°C to 1756°C," J. Amer. Cer. Soc. 52, 233.

Montgomery, F. C., 1978; General Atomic Company, private communication.

Müller, A., 1976; "Freisetzung gasförmiger Spaltprodukte (Kr, Xe, J) aus Brennelementen fur gasgekühlte Hochtemperaturreaktoren," KFA Report Jül-1295, parts included in Groos, 1977.

Myers, B. F., and W. E. Bell, 1974; "Strontium Transport Data for HTGR Systems," USAEC Report GA-A13168, General Atomic Company.

Myers, B. F., and W. E. Bell, 1978a; "Cesium Transport Data for HTGR Systems," General Atomic Company, to be published.

Myers, B. F., 1977b; "Diffusion Coefficients of Fission Products Metals in Kernel Materials," General Atomic Company, unpublished data.

Myers, B. F., N. L. Baldwin, and W. E. Bell, 1977c; "Fission Gas Release from Fuel Particles and Fuel Rods," Nucl. Techn. 35, 501.

Myers, B. F., 1977d; "Comparison of Cesium and Strontium Diffusion in ThO_2 and UO_2 Fuel Kernels," General Atomic Company, unpublished data.

Myers, B. F., 1977e; "Release from Failed Oxide Particles During Temperature Transients," General Atomic Company, unpublished data.

Myers, B. F., 1977f; "Improved Estimate of the Dependence of R/B for Failed ThO_2 Fuel Particles on Burnup," General Atomic Company, unpublished data.

Nabielek, H., et al., 1974; "Fission Product Migration in HTR Fuel," Dragon Project Report 828, Part III.

Nabielek, H., and P. E. Brown, 1975; "The Release of Ag-110 m in HTR's," Dragon Project Technical Note 657, presented at the Reaktortagung 1975, Nürnberg.

Nabielek, H., 1976a; "The Mechanism of Silver Retention in Coated Particle Fuel," Dragon Project Technical Note 801.

Nabielek, H., 1976b; "Fission Product Retention in HTR Fuel," KFA/Dragon Final Status Report Meeting, April 28-29, Paper No. 8.

Nabielek, H., P. E. Brown, and P. Offermann, 1977; "Silver Release from Coated Particle Fuel," Nucl. Techn. 35, 483.

Offermann, P., 1977; "Silver Diffusion in Pyrocarbon," J. Nucl. Mat. 64, 249.

Pointud, M. L., and P. Chenebault, 1977; "Emission of Fission Gases by Failed Coated Oxide Fuel Particles," Nucl. Techn. 35, 494.

Reitsamer, G., G. Falta, and H. Nabielek, 1978; "Retention of Solid Fission Products in HTR Oxide Fuel," ANS Summer Meeting, San Diego, June 1978.

Schenk, W., 1978; "Untersuchungen zum Verhalten von beschichteten Brennstoffteilchen und Kugelbrennelementen bei Störfalltemperaturen," to be published as KFA Jül report.

Shepherd, J., G. G. Kinsella, and P. A. A. Scott, 1971; "The Prediction of Fission Gas Release in an Operating HTR," Dragon Project Report 789.

Stöver, D., and R. Hecker, 1977; "Cesium Release Data for BISO-Coated Particles," Nucl. Techn. 35, 465.

Voice, E. H., and V. C. Scott, 1972; "The Formation and Structure of SiC Pyrolytically Deposited in a Fluidized Bed of Microspheres," Special Ceramics 5, British Ceramics Society.

Voice, E. H., H. Walther, and J. York, 1973; "The Behaviour of Silicon Carbide Coatings in the HTR," Proc. Int. Conf. Nuclear Fuel Performance, British Nuclear Energy Society, London.

Zoller, P., 1976; "Das Transportverhalten der Spaltprodukte Cäsium und Strontium in beschichteten Brennstoffteilchen fur Hochtemperaturreaktoren unter Bestrahlungsbedingungen," KFA Report Jül-1324.

3. FUEL PARTICLE MECHANICAL PERFORMANCE

3.1. MECHANICAL PERFORMANCE MODELING

Successful modeling depends on the realistic input of material data and environmental conditions, and the correct and consistent specification of the relevant physical laws. In coated-particle fuel, the stresses in the coating layers due to internal gas pressure are calculated. Breakage of a coating layer is predicted when the maximum stress exceeds the given value of the material's strength. Particle failure in a number of irradiation experiments has been successfully described for TRISO particles (Hick, Nabielek, and Harrison, 1973; Martin and Hobbs, 1977; Bongartz, 1977) and dimensional changes of BISO particles can be predicted (Kaae et al., 1977). The work of Kaae, Martin, and Bongartz combines the spread in particle properties as obtained from production data with the strength (Weibull) statistics of PyC or SiC (measured or from the literature) to predict in-pile failure rates.

The application of stress model prediction is acceptable only for existing particle types where the required material data are available. Extrapolation to new coated particle concepts (e.g., the selection of a new low-enriched particle) is acceptable in the case of applying parametric variations to optimize the particle design because:

1. The actual broken particle fraction will be obtained from irradiation tests.

2. The change of material parameters is approximately known after many years of experience with an extremely wide variety of coated-particle designs and irradiation conditions in the U.K., FRG, and U.S.

A sensitive point is the structure and the strength of coating layers (especially pyrocarbon), which are known to depend on the radius of the coating layer according to the Weibull statistics and the fine details of coating conditions.

To improve neutron economy and to increase heavy metal loading, the LEU fissile kernel has to be larger than the HEU fissile kernel; therefore, the LEU fissile particle diameter and coating volume are also larger.

Peach Bottom irradiation results (Holzgraf et al., 1977) obtained on TRISO coated weak acid resin (WAR) particles of various diameters showed the OPyC survival fraction decreased with the increase of coating volume under stress (Fig. 3-1). Other TRISO coated particle irradiation data (Harmon and Scott, 1975) indicated that the critical anisotropy of OPyC for failure decreased as the particle diameter increased (Fig. 3-2). Since the stress levels during irradiation are higher for more anisotropic coatings, this implies that the coatings on larger particles fail at lower stress levels. The need of low anisotropic coating for the OPyC coating to survive on large particles has also been substantiated by Dragon and CEA data (Sayers, 1973; Janvier, 1973a; Graham, 1973). The sharp drop in survival fraction of OPyC volumes $\geq 5 \times 10^{-11}$ m^3 (9×10^7 μm^3 in Fig. 3-1) is surprising by comparison to 100% survival of propene-derived PyC at temperatures 800°C/1000°C/1200°C to doses 6.7×10^{25} m^{-2} EDN in Corail VI (Janvier, Moreau, and Voice, 1973a) with OPyC volume 18×10^{-11} m^3 (34 in the units of Fig. 3-1). Further investigations are needed to clarify this discrepancy. Low-enriched (9.5%) UO_2 600 μm LTI BISO particles have been irradiated to extremely high values of burnup and fluence in the KFA BR2-P12 experiment (see Table 3-1 for variation of PyC thickness). No complete assessment is available at this time. Preliminary visual, microradiographic, and ceramographic observations show no coating damage at all despite the increase of in-pile gas release. For interpretations of failure mechanisms, see Schenk (1978), Thiele and Bradley (1976), and Bradley and Thiele (1977).

TABLE 3-1
PARTICLE CHARACTERISTICS AND IRRADIATION BEHAVIOR OF
THE BR2-P12 EXPERIMENT

BR-P12 600 μm Kernel Dia. UO_2 9.5 % Enriched, LTI BISO	
Variant	PyC Volume (10^{-11} m^3)
Thin PyC	10
Medium PyC	23
Thick PyC	41

Irradiation Time (days)	Burnup FIMA (%)	Fluence (10^{25} cm^{-2}) (E>0.1 MeV)	R/B (Kr-85 m) All Variants
300	9-11	6.3 - 8.0	10^{-5}
500	14-17	11.5 - 13.5	10^{-2}
Irradiation temperatures 950° to 1120°C			

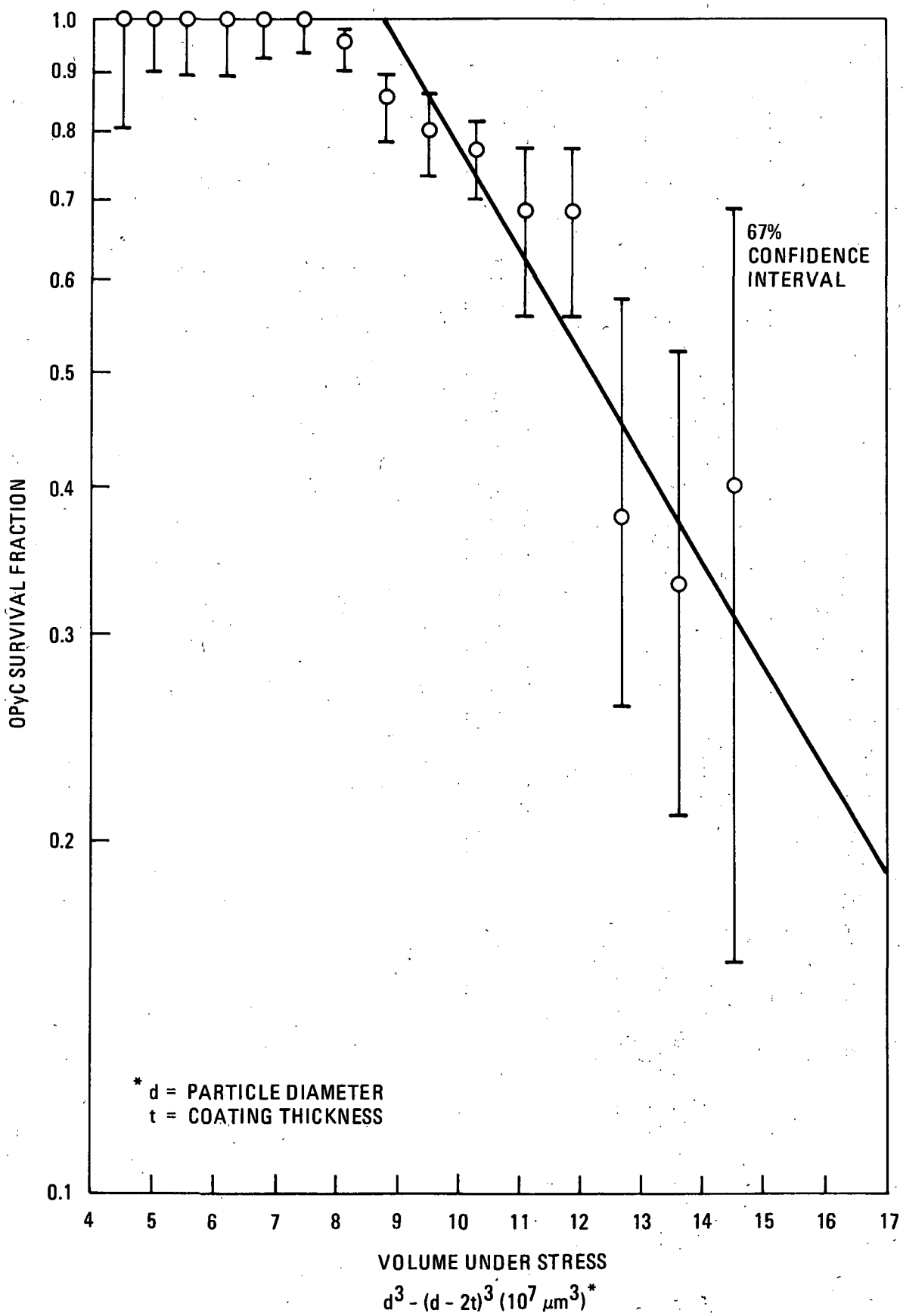

Fig. 3-1. Survival fraction of outer pyrocarbon layer versus parameter proportional to PyC volume (batch OR 1694, WAR)

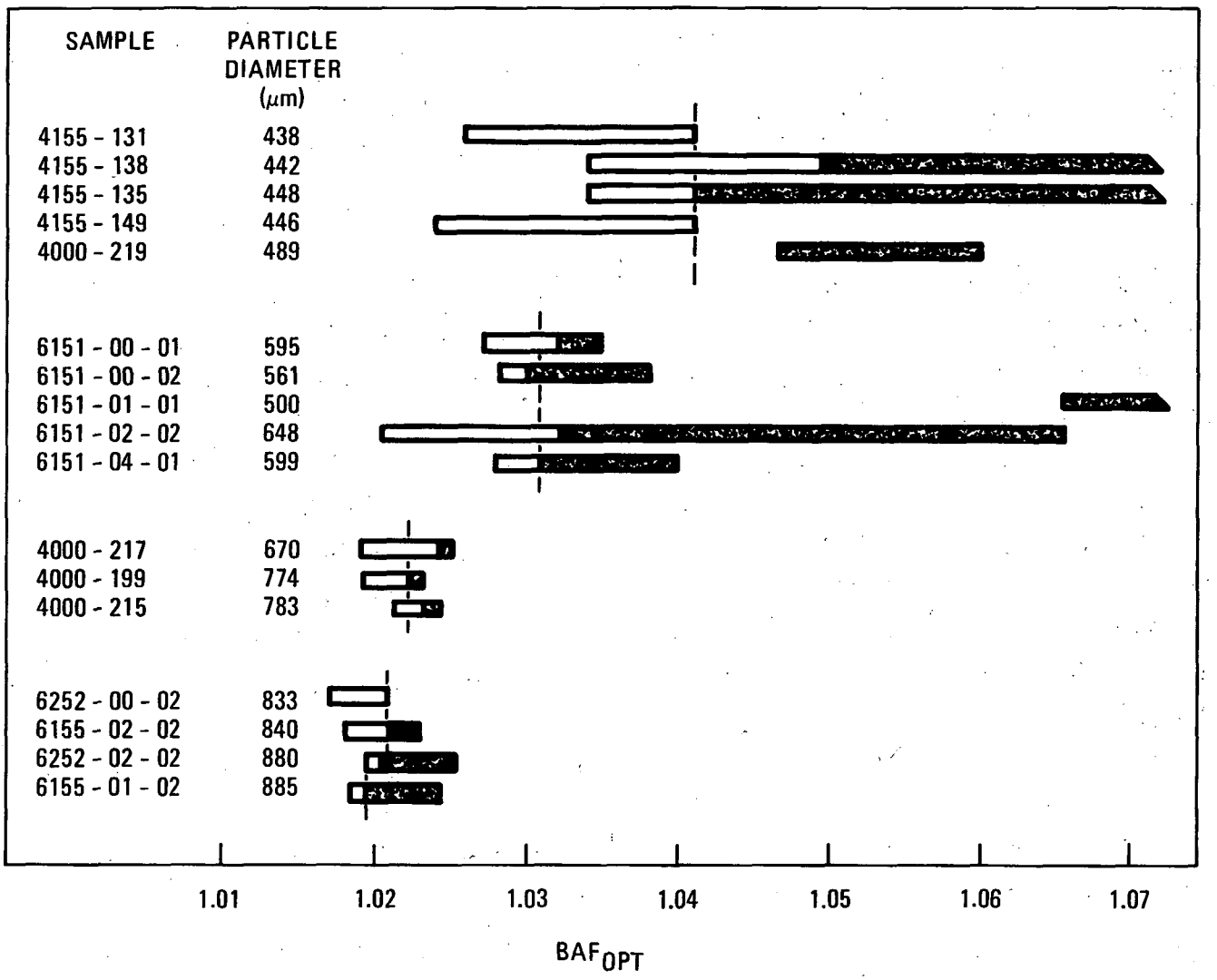

Note: Bars represent 95 percentile limits for anisotropy values within a batch of particles. Darkened region represents fraction of batch having failed OPyC coatings after irradiation to $\geq$ 6 x 10^{21} n/cm^2 at temperatures between 1050° and 1250°C. The approximation is made that the coatings having the highest anisotropies failed during irradiation. The larger diameter particles experience failure at lower BAF_{OPT} values.

Fig. 3-2. Outer pyrocarbon critical anisotropy values for different size TRISO fuel particles

It appears, from the point of view of particle design requirements, that the larger low-enriched uranium particles might require development work to produce coating structures and strengths (especially PyC) to survive the required service limits.

3.2. STABLE AND LONG-LIVED FISSION GAS RELEASE FROM THE FUEL KERNEL

The yield of stable and long-lived Kr and Xe isotopes is about 0.31 atom per fission. The release of Kr and Xe from the fuel kernel into the porous buffer represents a major cause of the pressure vessel failure of the fuel particle coating. Experimental measurements of the release of Kr and Xe isotopes in irradiated oxide particles showed that the internal release of Kr and Xe isotopes is burnup- and temperature-dependent. Conservative design practices require the assumption of 100% gas release from the kernel for purposes of stress calculations in the coating layers. Numerous studies of the gas release data have been conducted to correlate gas release with such parameters as burnup, temperature, kernel density, kernel diameter, particle heat rating, grain size, etc. To date no complete model has been developed.

The assessment of noble gas release from low-enriched UO_2 was attempted at different stages:

1. As a function of burnup (Janvier, Bruch, and Blanchard, 1973b) with irradiation temperature as a parameter (Formann, 1971).

2. As a function of irradiation temperature (Flowers, 1973; Wagner-Löffler et al., 1973a).

3. As a function of irradiation temperature and burnup and estimates on the influence of kernel density (Turnbull and Shipp, 1974).

In the final evaluation, Turnbull and Shipp (Horsley et al., 1976) proposed the following two-stage procedure:

1. A fraction F_B of gas atoms escapes from the grain interior to the grain boundaries by diffusion with

$$\log_{10} D' \text{ (Xe, Kr in } UO_2 \text{ and } (U,Pu)O_2,\ 1100 < T < 1820 \text{ K} = -2.30 - 8116/T \tag{3-1}$$

$$F_B = 1 - \frac{1}{15\ D't} + \frac{6}{D't} \sum_{n=1}^{\infty} \frac{e^{-n^2\pi^2 D't}}{n^4\pi^4} \tag{3-2}$$

where t = irradiation time, s,
T = irradiation temperature, K,
D' = reduced diffusion coefficient, s^{-1}.

2. There is retention at the grain boundaries. Only a fraction F_{gb} of F_B is released. F_{gb} varies with the total number of gas atoms reaching the grain boundaries given by F_B x Bu, where Bu is the burnup in % FIMA.

For low values of F_B x Bu, the retention at grain boundaries is complete; i.e.,

$$F_{gb} = 0 \qquad \text{for } F_B \text{ x Bu} < A_1 \ . \tag{3-3}$$

Above a critical saturation level A_2, no further retention is effective.

$$F_{gB} = 1 \qquad \text{for } F_B \text{ x Bu} > A_2 \ . \tag{3-4}$$

For simplicity, a linear function is assumed in the intermediate region:

$$F_{gb} = \frac{F_B \times Bu - A_1}{A_2 - A_1} \qquad \text{for } A_1 \leqq F_B \times Bu \leqq A_2 \quad . \tag{3-5}$$

The overall release is given by $F = F_{gb} \times F_B$.

Using $A_1 = 0.5$ and $A_2 = 5.0$, a large number of measured Xe and Kr release results on 600 to 800 μm kernel diameter, low-enriched UO_2 (20% porosity) HTI TRISO particles can be described by this mechanism, the irradiation conditions being:

Irradiation time	60 to 300 days
Burnup	1.3% to 13% FIMA
Irradiation temperature	880° to 1500°C

Higher density (5% porosity) kernels were shown to have better retention. If this model is applied to dense UO_2 kernels of diameters ≦600 μm, the term $F_B \times Bu$ has to be corrected for kernel volume and density.

For dense ThO_2 and $(Th,U)O_2$ fuels, Myers et al. (1977) derived an expression on the basis of Lindemer's data, which predict the release of long-lived and stable fission gases with the equivalent sphere formula and a single burnup and temperature dependent diffusion coefficient (see Figs. 2-12 and 3-3).

$$\log_{10}\overline{D'} \{Xe,Kr,I,Te,Se,Br \text{ in } (Th,U)O_2,\ 1170 < T < 1650\ K\}$$

$$= -5.94 - \frac{5463}{T} + \frac{3.24}{1 + 11/Bu} \quad . \tag{3-6}$$

This type of representation has been chosen to compare a number of experimental results. The effective diffusion coefficient $\overline{D'}$ computed via the equivalent sphere model from measured release values (and irradiation time) is plotted versus irradiation temperature with burnup (% FIMA) as a

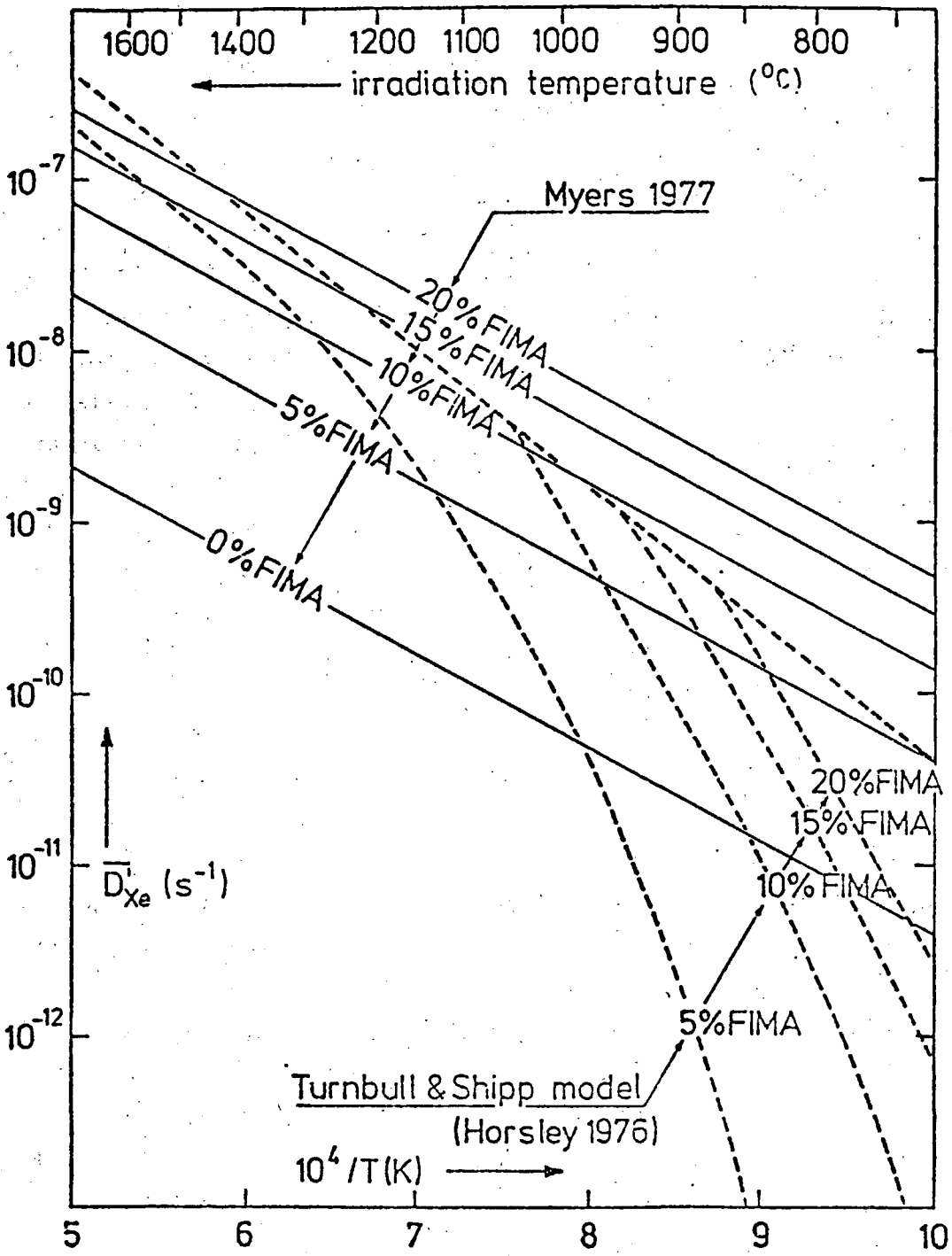

Note: This effective reduced diffusion coefficient, when applied within the equivalent sphere model, gives the internal fractional release of xenon (and krypton) which is measured after crushing of coated particles.

Fig. 3-3. Reduced diffusion coefficient of xenon versus irradiation temperature in the Myers formalism and in the Turnbull & Shipp model

parameter (Figs. 3-4 and 3-5). The prediction of the Turnbull-Shipp model can be shown on the $\overline{D'}$ versus 1/T plot by assuming a relationship between burnup Bu and irradiation time t. For the purpose of Fig. 3-3, the relation t (days) = 20 x Bu (% FIMA), which is typical for the evaluated tests, is used. Myers' predictions were meant to represent upper limits and are therefore higher in the HTR operating range of 1000° to 1250°C and 10% FIMA. More recent Dragon and UKAEA particles show better retention of xenon than predicted by the Turnbull-Shipp model. (See Fig. 3-4; for HTR3 Xe release, see also Fig. 3-8). Results on dense, sol-gel, UO_2 fuels are shown in Fig. 3-5. The DR-P4 (Met 4 stress model experiment) kernels produced by KEMA were coated by HOBEG; DR-P5 was produced by KFA; and fuel for experiments BR2-P11, BR2-P12, and FRJ2-P15 was produced by HOBEG. Only the latter produces a consistent set of results. Further measurements and evaluation of results on already irradiated, low-enriched, dense, UO_2 fuel should be completed when postirradiation measurements on the new design of the low-enriched fissile particles are planned.

While the above treatment describes the stable fission gas release characteristics on the basis of the reduced diffusion coefficient D', empirical formulas have also been given by various authors to correlate the fractional release F with the burnup. Janvier et al. (1973b) measured the release of stable and long-lived fission gases from UO_2 kernels (10% to 20% porosity) irradiated at 1000° to 1400°C to 2% to 4% FIMA. The fractional release F can be related to the burnup (% FIMA) by the equation F = 0.16 (% FIMA) - 0.2 for burnup between 1.5% and 7% FIMA. Above 7% FIMA, the release is almost 100% of the stable fission gas formed during the irradiation. No significant influence of temperature (1000° to 1400°C) and porosity (10% to 20%) was observed. Kania et al. (1976) measured the release of stable Kr + Xe from sol-gel ThO_2 and $Th_{0.81}U_{0.19}O_2$ kernels, which were irradiated in the temperature range 1150° to 1600°C in ORNL HT-12 through HT-15 and HRB-6 capsules and test GAC P13LC4T6. The upper bound of the data points can be described by the relationships

$$F = 0.10 \text{ (\% FIMA) for } 0 \leq \text{FIMA} \lesssim 6\% \quad ,$$

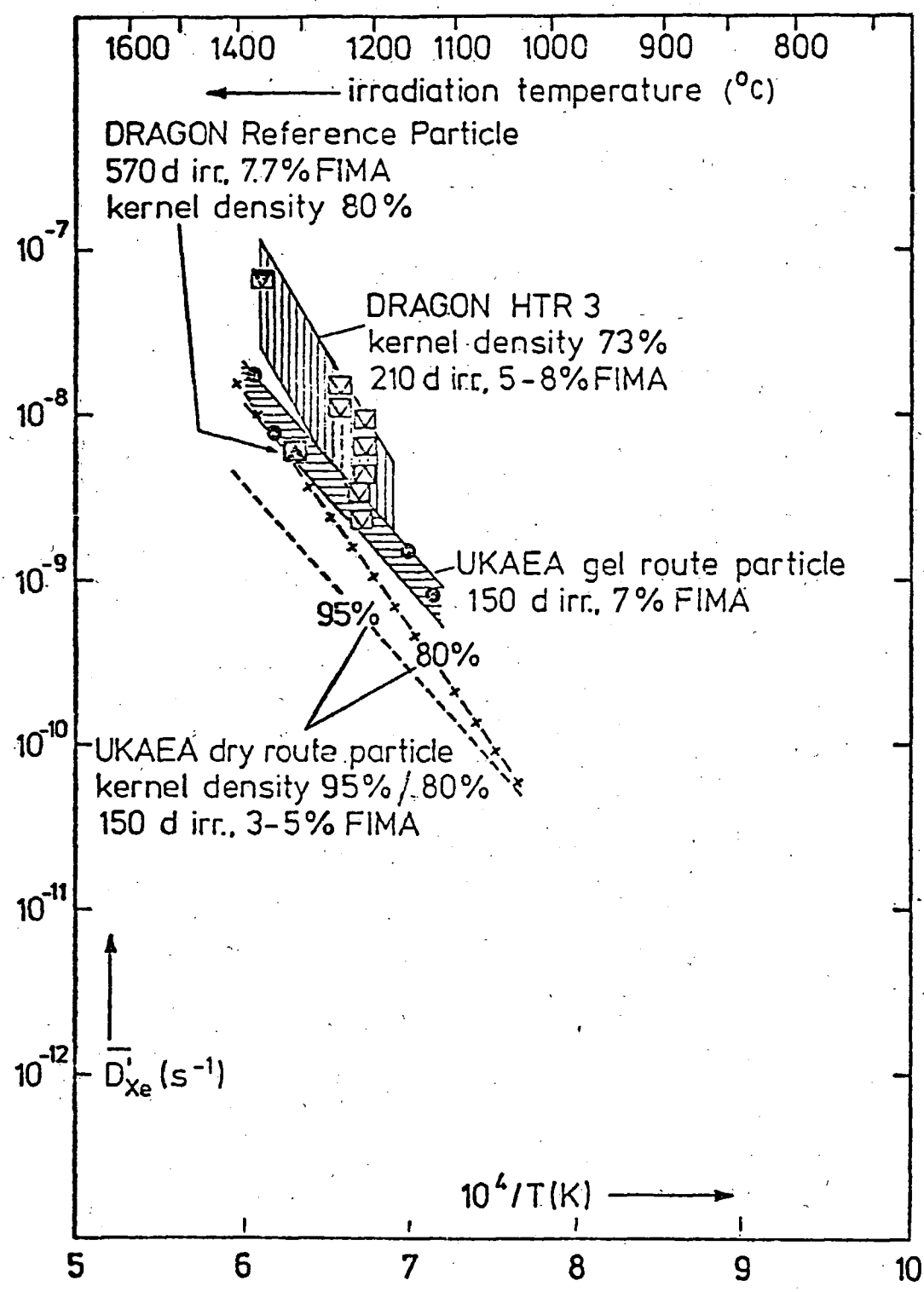

Fig. 3-4. Reduced diffusion coefficient of xenon versus irradiation temperature from gas measurements of Dragon and UKAEA LEU particles that have not been included in Turnbull & Shipp fit

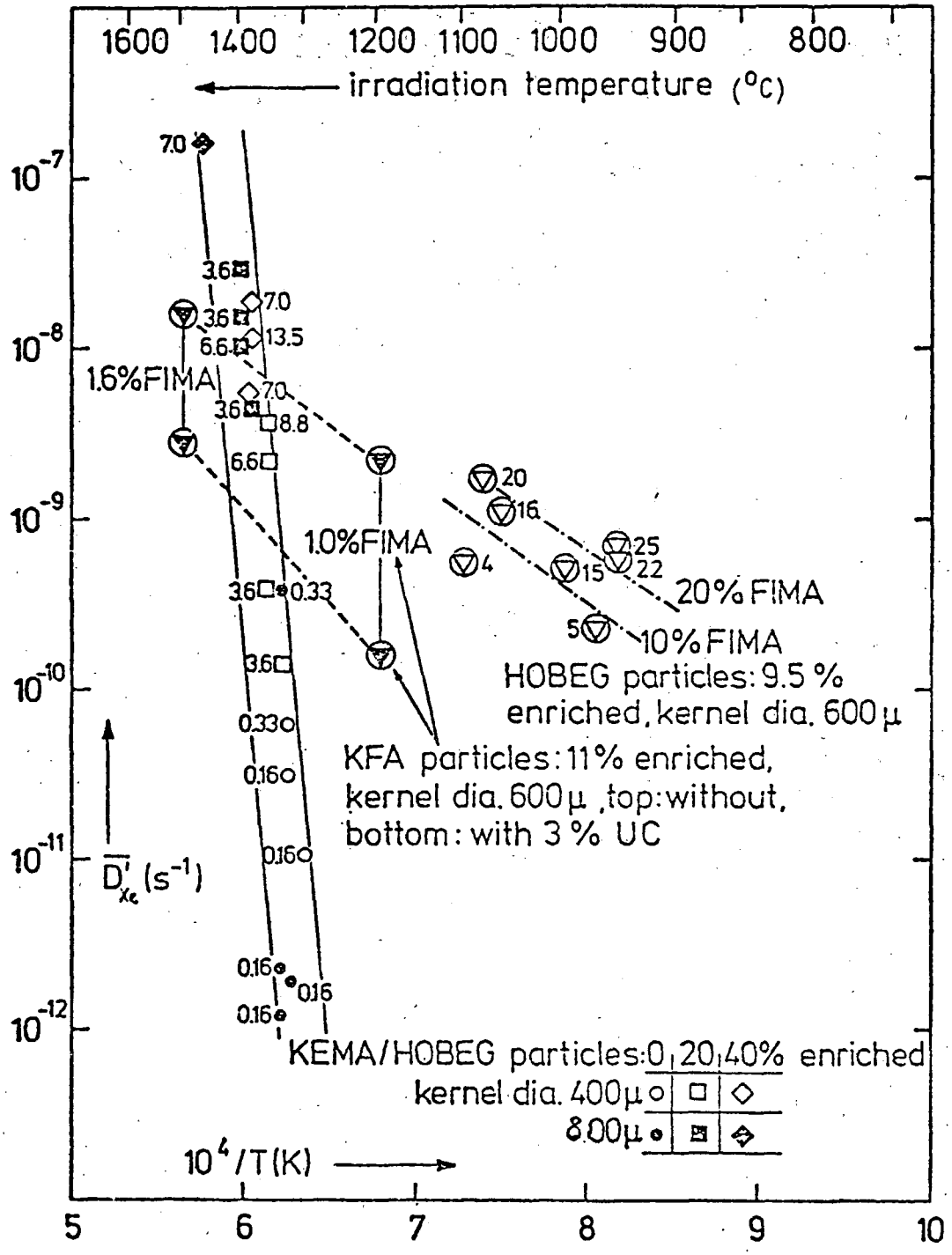

Note: KEMA/HOBEG particles: DR-P4 (Met 4) experiment
KFA particles: DR-P5 (Met 5) experiment
HOBEG particles: BR2-P11, BR2-P12, FRJ2-P15
Numbers adjacent to symbols indicate burnup (% FIMA)

Fig. 3-5. Reduced diffusion coefficient of xenon versus irradiation temperature for dense, low-enriched UO_2 particles

$$F = 0.45 + 0.025 \text{ (\% FIMA)} \text{ for } 6\% \leq \text{FIMA} \leq 22\% \quad .$$

These empirical formulas seem to indicate that for the burnups (10% to 20% FIMA) required for the LEU fuel under consideration, the fractional release of the stable fission gases can be expected to be very high.

3.3. INTERNAL CO RELEASE

3.3.1. CO Release Measurements

The release of CO from irradiated oxide kernels represents a major contributor to the gas pressure inside an irradiated fuel particle. When fissile atoms undergo fissioning in an oxide kernel, there are not enough fission product atoms produced, which can tie up the released oxygen atoms by forming stable oxides. The excess oxygen atoms then react with the carbon buffer to form CO (also a small amount of CO_2*) inside the fuel particle.

Because of the difference in fission product yields, the heavy fissile atoms such as the plutonium isotopes produce more excess oxygen atoms than the uranium isotopes. The design of LEU fuel particles, which contain more plutonium atoms bred from U-238 than the HEU fuel particles, has to take the contribution of CO pressure into account. In addition to the mechanical effect of CO pressure buildup, the presence of CO may be required for the oxygen transport from the hot to the cold side during the amoeba migration of the kernel.

The theoretical number of excess oxygen atoms formed per fission event in an oxide kernel can be calculated from the fission yields, the isotopic composition of the kernel, and the valence states of the fission products.

It can be assumed with some certainty that in oxide fuel the following oxides exist at HTGR operating conditions: ZrO_2, SrO, BaO, and (Y, La, RE†)O_2 (in solid solution with UO_2). The ZrO_2, SrO, and BaO do not interact

*The CO_2 contribution is less than 1% except at low temperatures and high burnup.

†Rare earths Ce, Pr, Nd, Pm, Sm, Eu, Gd, and Tb.

with other fission products to tie up additional oxygen as solid oxides (Lindemer, 1977). $(Cs,Rb)_2UO_4$ should be stable at temperatures below 1000°C (Lindemer, 1977), which helps reduce the oxygen and cesium pressures considerably.

The yields of oxygen-binding fission products from various fissile isotopes (Meek and Rider, 1977) and the calculated number of "free" oxygen atoms per fission are shown in Table 3-2. From the data in Table 3-2, the (theoretically minimum) number of free oxygen atoms per fission is given by

O/F = 0.09 x (fraction U-233 fissions) + 0.13 x (fraction U-235 fissions)

+ 0.62 x (fraction Pu-239 fissions) + 0.60 x (fraction Pu-241 fissions)

and the number of CO moles released can be calculated by multiplication with burnup and kernel volume divided by heavy metal molar volume (24.6 cm^3 for UO_2).

The determination of CO content in irradiated particles is not a simple matter. When it was suspected that the 10-minute heat treatment before crushing the particle and making the gas measurement might not achieve the in-pile CO equilibrium value, the annealing temperature was raised to 1800°C. Eventually, it was realized that this procedure led to values for the CO release that were too high. A series of comparative measurements were therefore made in different laboratories to establish the techniques and procedures (Hick, Nabielek, and Wagner-Löffler, 1975; Horsley et al., 1976; Lindemer, 1977; Strigl and Proksch, 1977), which are believed to yield the true CO release in the particle at the end of the irradiation.

The reversibility of the attainment of thermodynamic equilibrium has been demonstrated (Proksch and Strigl, 1975, 1600° to 1200°C; Lindemer, 1977, 2000° to 1400°C and 1700° to 1100°C). However, irreversible changes can occur (Proksch and Strigl, 1975) when the inner pyrocarbon layer is damaged and CO is gettered by SiC, or when the release of Sr (and perhaps Cs) reduces the oxygen getters in the particle.

TABLE 3-2
YIELD OF OXYGEN BINDING FISSION PRODUCTS FROM THE VARIOUS FISSILE ISOTOPES (MEEK AND RIDER, 1977) AND CALCULATED NUMBER OF FREE OXYGEN ATOMS PER FISSION

	Number of Atoms Formed per Fission			
	U-233	U-235	Pu-239	Pu-241
Zr	0.326	0.310	0.189	0.157
Sr	0.124	0.096	0.035	0.026
Ba	0.060	0.068	0.061	0.069
Y, La, RE[(a)]	0.536	0.542	0.452	0.496
	Free Oxygen Atoms per Fission			
For trivalent RE	0.360	0.403	0.849	0.847 theoretical maximum
For tetravalent RE	0.092	0.132	0.623	0.599 theoretical minimum
Cs, Rb	0.185	0.165	0.151	0.157

[(a)] RE = rare earths

Kania et al. (1976) measured the oxygen from irradiated ThO_2 and HEU $Th_{0.81}U_{0.19}O_2$ particles (Fig. 3-6). Lindemer (1977) proposed the following equation to correlate the oxygen release as CO in these particles:

$$\log_{10}(O/F) = -0.13 - \frac{3214}{T} + \log_{10}(Bu) \qquad (3\text{-}7)$$

for the burnup (% FIMA) range $3 < Bu < 23\%$, and equilibration temperature $1325 < T < 2270$ K with $O/F \leq 0.36 + 0.05$ (U-235 fission fraction). The oxygen release represented by Eq. 3-7 was shown (Lindemer, 1977) to be reasonably consistent with that predicted from thermodynamic data for the oxides of the fuel and the fission products. Figure 3-7 shows the plots of Eq. 3-7 for Bu = 5%, 10%, and 20% FIMA. The same figure shows the CO measurement results from HEU Dragon driver fuel (Strigl, 1977). The oxygen release from the carbon-dilute driver fuel is lower than that for the ThO_2 and $(Th,UO)O_2$ particles. In the Dragon project, it has always been assumed that CO production and amoeba migration are to a large degree suppressed in carbon-diluted fuel (Wagner-Loffler, 1976).

In Fig. 3-8, the measured releases of oxygen per plutonium fission in low-enriched fuels are plotted against annealing temperatures. Following Horsley et al. (1976), the contribution of U-235 fissions is neglected. No systematic dependence on irradiation temperature and burnup can be recognized. The measured values in most cases are significantly lower than the theoretical minimum value of O/F = 0.6. For each single experiment, the release is higher at higher irradiation (or annealing) temperature.

A number of interesting effects can be noticed with the Dragon advanced coating experiment Colibri HTR3 (Strigl, Proksch, and Peschta, 1975; see Fig. 3-9). These are:

1. The irradiation temperature dependence of internal CO and Xe release.

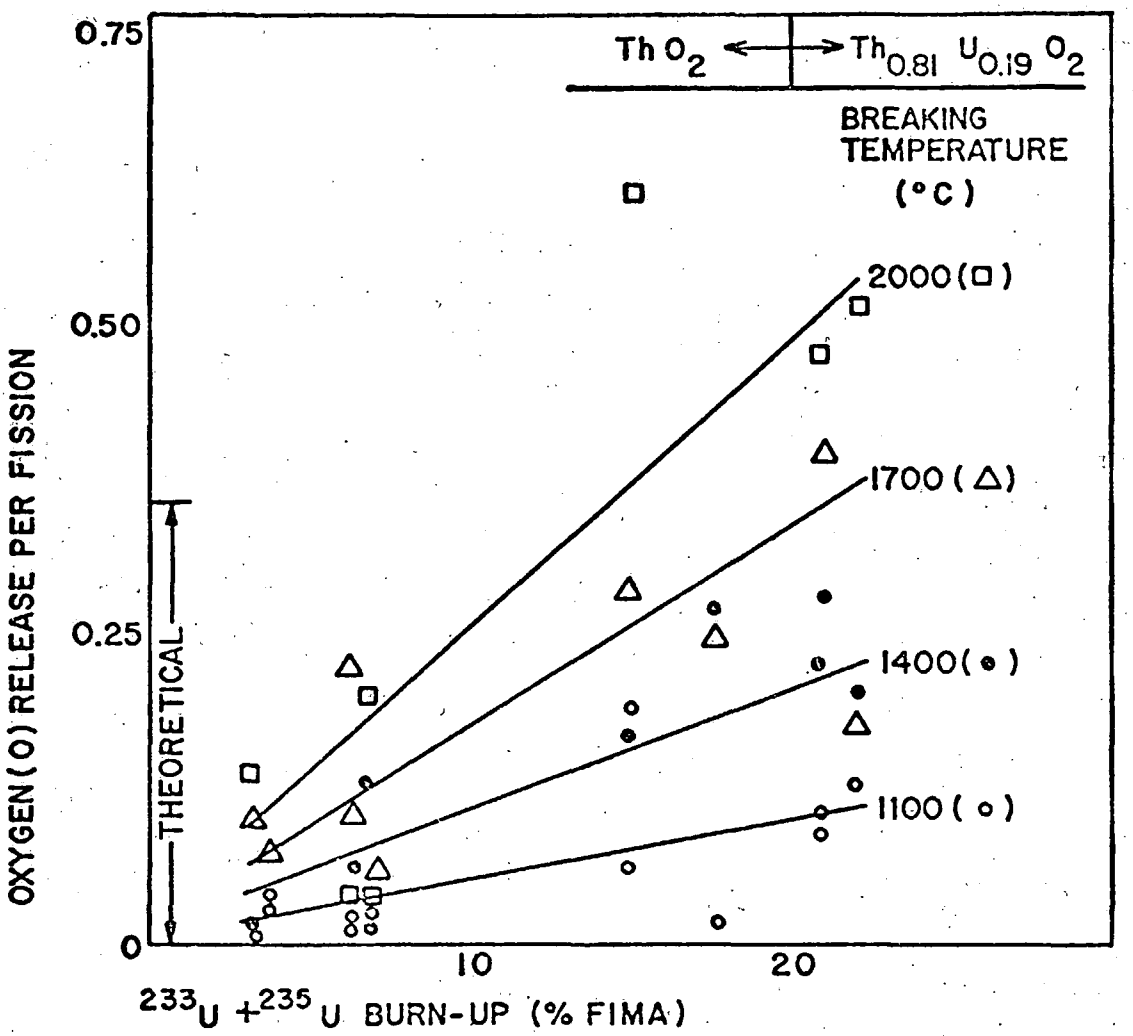

Fig. 3-6. Experimental atomic oxygen release per fission in ThO_2 and $Th_{0.81}U_{0.19}O_2$ particles as a function of U-233 plus U-235 burn-up and equilibration temperature

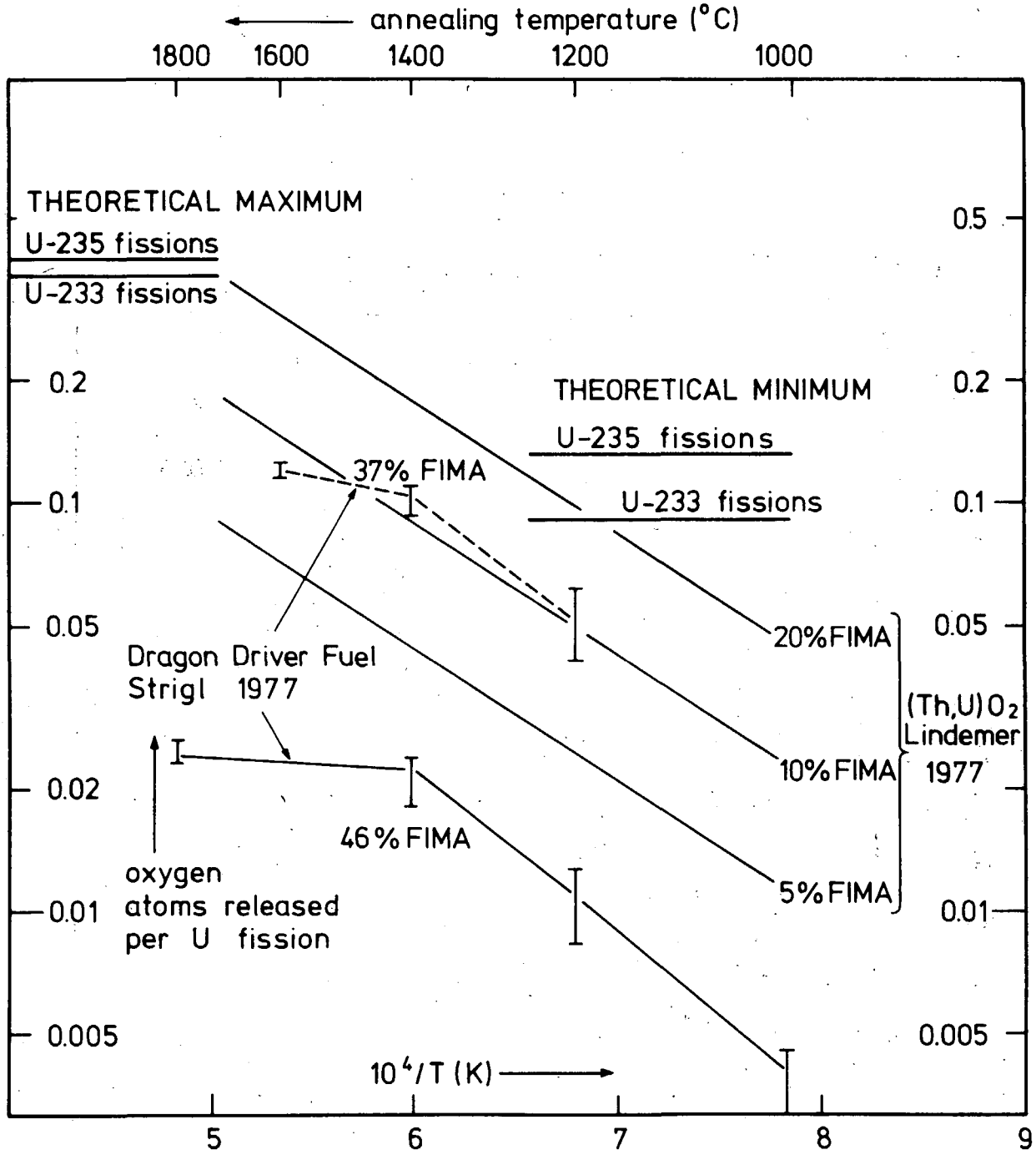

Note: Horizontal lines ("theoretical") from Table 3-2, sloping parallel lines from Eq. 3-7, single measured values from CO measurements on Dragon Driver fuel (FE X055: 37 % FIMA, 1350 - 1400°C irradiation temperature, 200 days irradiation; FE X157: 46 % FIMA, 1130 - 750°C irradiation temperature, 550 days irradiation)

Fig. 3-7. Free oxygen atoms per uranium fission versus equilibration temperature before crushing particles for CO measurement

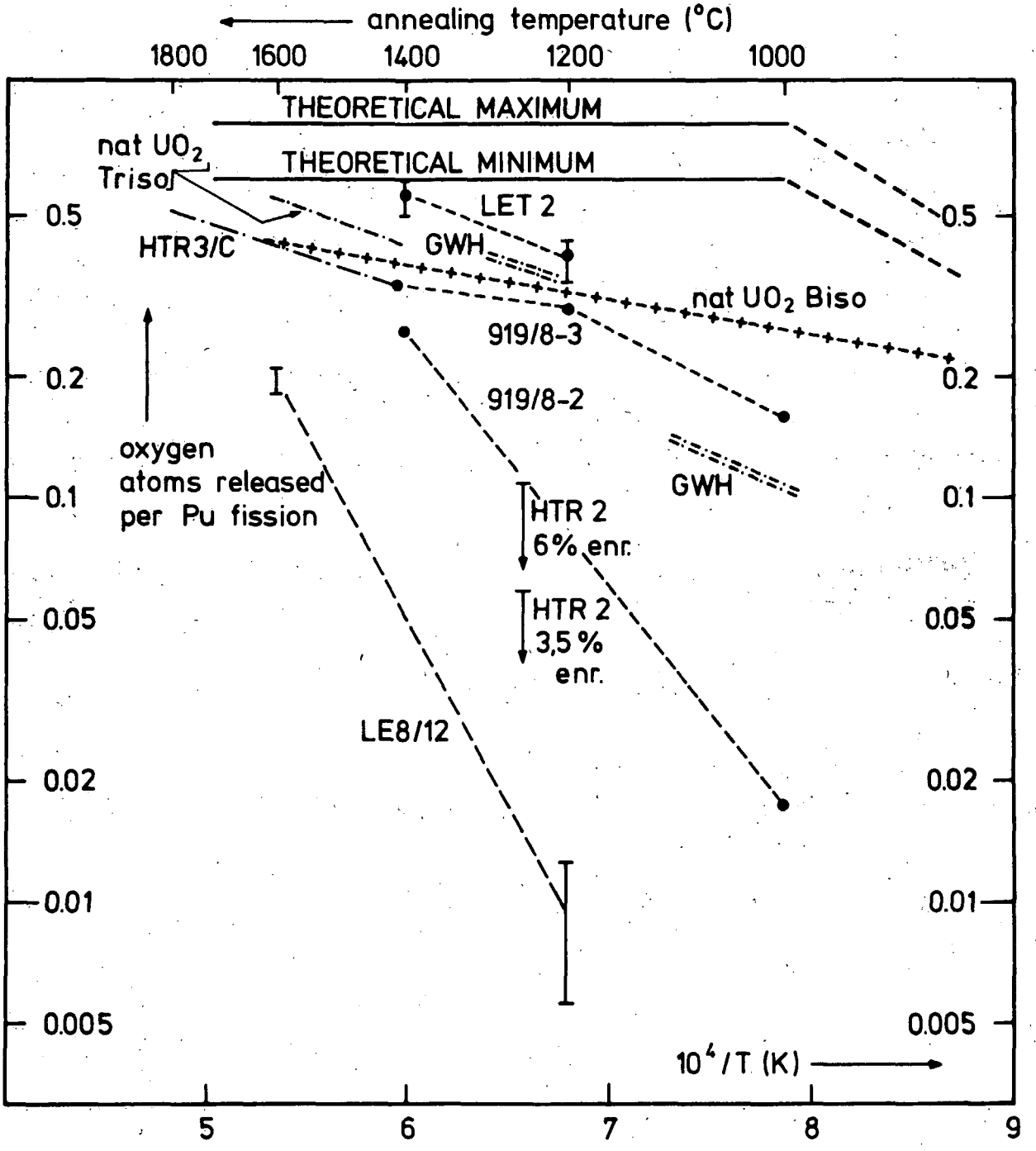

Fig. 3-8. Free oxygen atoms per plutonium fission versus equilibration temperature measurements from G. W. Horsley (GWH), T. B. Lindemer (nat. UO_2 BISO/TRISO), and A. Strigl (others)

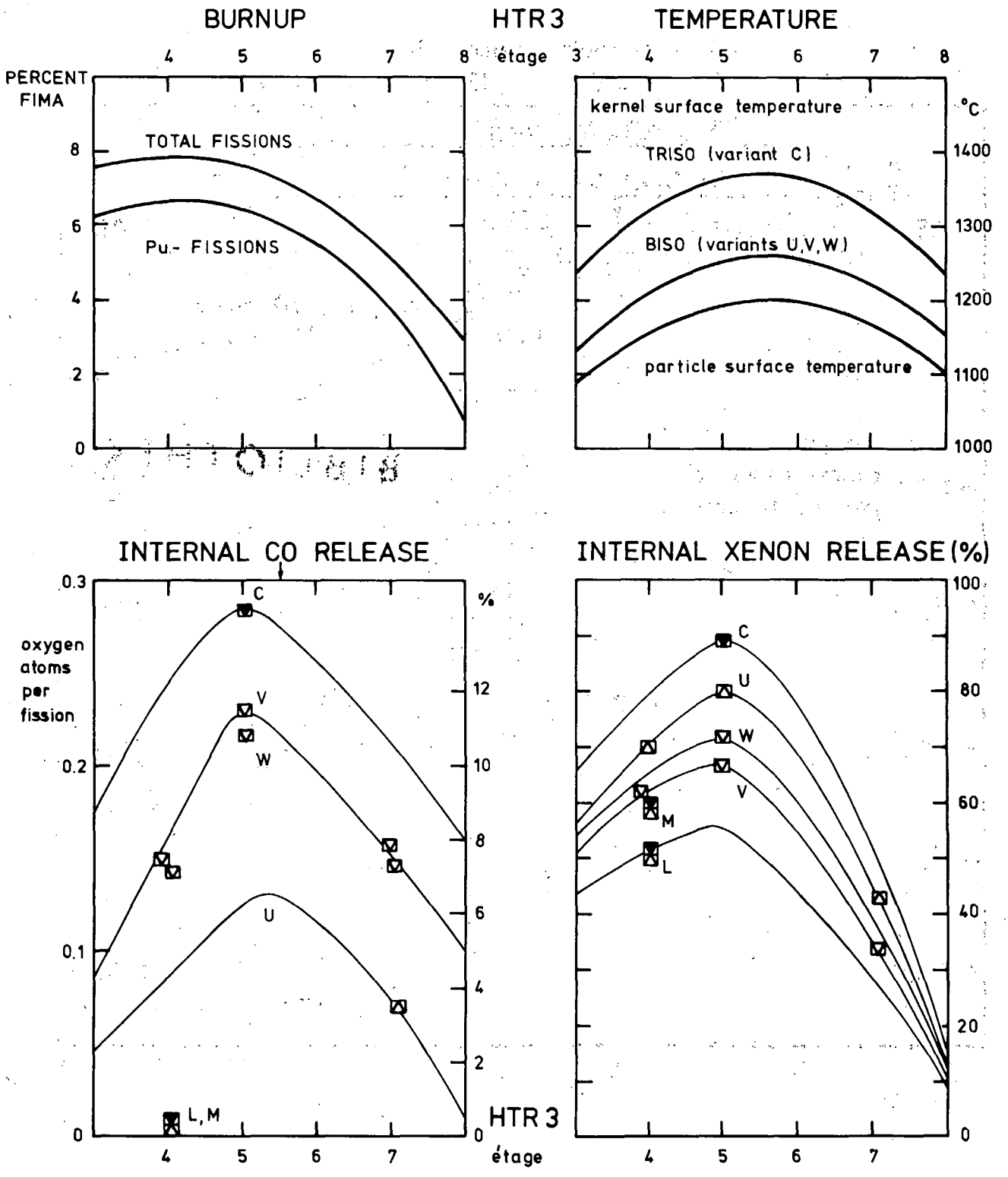

Fig. 3-9. Dragon advanced coating experiment Colibri HTR 3, irradiated in the Osiris reactor for 207 days

2. Increased CO with higher (x2) internal release of cesium in variants V, W (LTI BISO) versus U (HTI BISO).

3. Complete suppression of CO when IPyC is broken (variants L, M; no corrosion of SiC).

Neglecting enhanced and suppressed CO release, the irradiation temperature dependence of CO release responsible for the pressure contribution is shown in Fig. 3-10. An estimated mean value through the shaded area is given by

$$\log_{10}(O/F_{Pu}) = 1.36 - \frac{3100}{T} \qquad (3\text{-}8)$$

for $1270 < T \leq 1670$ K and Bu $\leq$ 8% FIMA.

By comparison, only a small number of CO measurements are available for dense, sol-gel, low-enriched UO_2 kernels. The results from DR-P4 (Met 4) and DR-P5 (KFA contribution to the MET 5 experiment) are below the line given above. The CO measurements on BR2-P12 and FRJ2-P15 9.5% enriched UO_2 fuel have not yet been reported.

Further work on CO release is required because the prediction of CO pressure is one of the most important aspects of LEU fuel particle development.

3.3.2. Oxygen Getters and Buffers

The CO pressure in irradiated fuel particles can be reduced by using oxygen getters or buffers, which combine with the oxygen released from the kernel during irradiation. The getters and buffers that have been demonstrated and the consequences of using them are:

1. SiC addition to the kernel or the buffer layer (Horsley et al., 1975; improved silver retention, Brown and Faircloth, 1976).

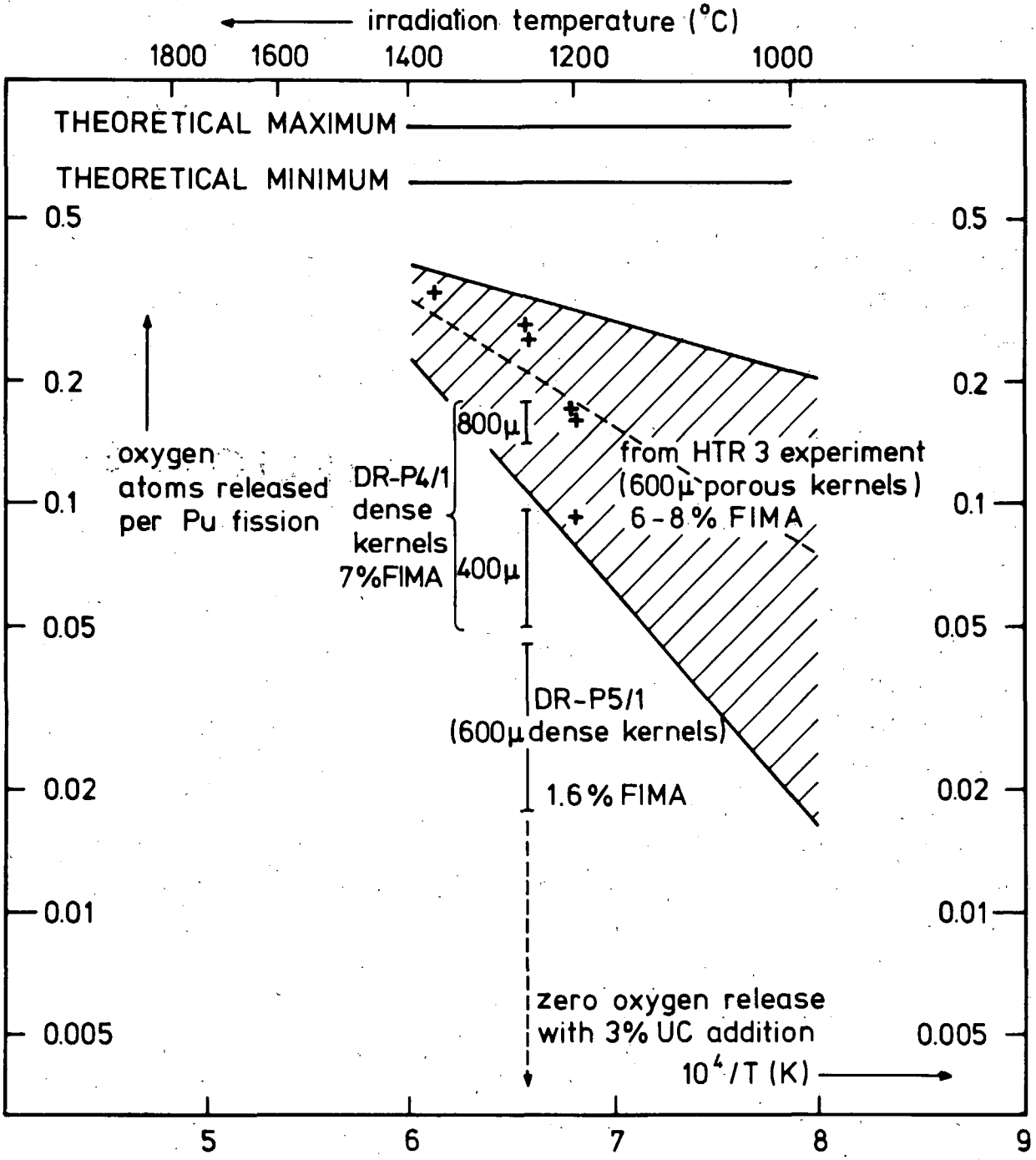

Fig. 3-10. Free oxygen per plutonium fission versus irradiation temperature with burnup as a parameter

2. Carbon addition to the kernel (Dragon driver fuel, see Fig. 3-7; Strigl and Proksch, 1977; increased Sr, Cs, Ru, Ce release, Nabielek, 1976).

3. Carbide addition in dense kernels (Naoumidis, 1972; Naoumidis and Thiele, 1974; increased strontium release, Thiele, 1975).

4. Carbide addition in WAR kernels (Homan et al., 1977, increased fission gas release due to porosity in kernel).

5. Trivalent rare earths (Steemers, 1975).

Estimates for the minimum amounts of additives for gettering the free oxygen atoms released during irradiation are given in Table 3-3. In-pile evaluation of various oxygen getters and buffers has been carried out in various laboratories. The results obtained appear to be very promising.

TRISO coated, low-enriched (4%) UO_2 kernels containing Ce_2O_3 (5 mole %) as an oxygen getter, and SiC (5 mole %) and ZrC (2.5 to 5 mole %) as oxygen buffers, have been irradiated by Harwell and Dragon workers in their Dido 918/8 experiment (Steemers, 1975; Horsley et al., 1975) at temperatures up to 1250°C and burnup of 6% FIMA. Postirradiation gas analysis in the temperature range of 1000° to 1600°C showed that SiC, ZrC, and Ce_2O_3 were equally effective in reducing CO pressure in irradiated particles to negligible values. The ZrC additive did not stop the amoeba migration of the UO_2 kernels, but the SiC and the Ce_2O_3 additives eliminated or reduced it. Moreover, the SiC additive also lowered substantially the release of Ag-110m from the UO_2 kernels. Thus, the use of oxygen buffers and getters offers an effective means for lowering the CO pressure in irradiated oxide particles, and at the same time provides other benefits to the irradiation performance of oxide fuel particles.

Carbide containing (3% UC) low-enriched, dense oxide kernels has been irradiated in the DR-P5 and FRJ2-P12 experiments (maximum 8% FIMA) and

TABLE 3-3

MINIMUM FRACTION OF KERNEL GETTER OR BUFFER REQUIRED FOR COMPLETE SUPPRESSION OF CO (AND AMOEBA) IN OXIDE KERNELS (CALCULATED BY USE OF INFORMATION FROM TABLE 3-2)

Assumptions: 20% enriched UO_2 fissile particle
27% FIMA final burnup
33% relative contribution of plutonium fissions

1. Silicon Carbide in UO_2 Kernel ($SiC \rightarrow SiO_2$)

$$\text{Minimum fraction SiC} = \frac{[(1/3) \times 0.62 + (2/3) \times 0.13] \times 0.27}{2 \text{ oxygen atoms per silicon atom}} = 0.040$$

2. Oxycarbide Kernel

With carbide additions, the trivalent state of rare earths is assumed (i.e., 0.85 oxygen atoms per Pu fission).

$$\text{Minimum fraction } UC_2 = \frac{[(1/3) \times 0.85 + (2/3) \times 0.40] \times 0.27}{2 \text{ oxygen atoms per uranium atom}} = 0.074$$

3. Trivalent Rare Earths

According to Lindemer (1977), the maximum oxidation state should be $\leq Ce\ O_{1.65}$ to control μ_{O_2} enough to prevent amoeba. Therefore, the minimum fraction initial $Ce\ O_{1.5}$ is

$$\frac{[(1/3) \times 0.62 + (2/3) \times 0.13] \times 0.27}{0.15 \text{ oxygen atoms per cerium atom}} = 0.53$$

similar kernels of medium enrichment have been irradiated in BR2-P14/16/18/19 and R2-P5 (maximum of 70% FIMA) experiments. Preliminary investigations (Grübmeier et al., 1978) show qualitatively that the UC addition suppresses CO formation and amoeba migrations, but causes a small release of barium and rare earths. In the absence of a UC additive, the release of barium and rare earths in UO_2 is suppressed. The slight increase in barium and rare earth release is probably caused by the lowering of the oxygen potential in UO_2 by the UC additive.

REFERENCES

Bongartz, K., 1977; "Bestimmung der Versagensquote für ein TRISO-Bruttenilchen mit mehreren Modifikationen in Abhängigkeit vom Abbrand mit Hilfe von Spannungs-modellrechnungen," KFA-IRW Technical Note 77/77.

Bradley, R. A., and B. A. Thiele, 1977; "Neutron-Induced Permeability of PyC-Coated HTGR Fuel Particles," Nucl. Techn. 35, 353.

Brown, P. W., and R. L. Faircloth, 1976; "Metal Fission Product Behavior in HTR's - UO_2 Coated Particle Fuel," J. Nucl. Mat. 59, 29.

Flowers, R. H., 1973; "A Comparison Between Fractional Releases of Active and Stable Rare Gas Isotopes from Oxide Kernels," AERE Harwell, unpublished data.

Formann, E., 1971; "A Summary of Gas-Pressure Build-up Within a Coated Particle," Dragon Project Technical Note 146.

Graham, L. W., and H. Hick, 1973; "Performance Limits of Coated Particle Fuel," Proc. Int. Conf. Nuclear Fuel Performance, British Nuclear Energy Society, London.

Grübmeier, H., et al., 1978; "Charakterisierung und Spaltproduktverhalten in karbidhaltigen oxidischen Brennstoffteilschen," Reaktortagung 1978, Hannover.

Harmon, D. P., and C. B. Scott, 1975; "Development and Irradiation Performance of LHTGR Fuel," ERDA Report GA-A13173, General Atomic Company.

Hick, H., H. Nabielek, and T. A. Harrison, 1973; "Mechanical Failure of Coated Particles Due to Internal Gas Pressure and Kernel Swelling," Dragon Project Report 828.

Hick, H., H. Nabielek, and M. Wagner-Löffler, 1975; "Summary of a Round Table Discussion on Amoeba Mechanisms in Oxide Fuel Particles," Dragon Project Report 919.

Holzgraf, J. F., et al., 1977; "Postirradiation Examination Evaluation of Peach Bottom Fuel Test Element FTE-14 and 15," General Atomic Company, to be published.

Homan, F. J., et al., 1977; "Stoichiometric Effects on Performance of High-Temperature Gas-Cooled Reactor Fuels From the U-C-O System," Nuclear Technology 35, 428.

Horsley, G. W., et al., 1975; "An Irradiation Experiment (919/8) to Examine the Influence of Getters on the Irradiation Behavior of UO_2 Kernel Coated Particle Fuel," AERE Report R8018.

Horsley, G. W., et al., 1976; "Influence of Irradiation Temperature, Burnup, and Fuel Composition on Gas Pressure in Coated Particle Fuels," J. Am. Cer. Soc. 59, 1.

Janvier, J. C., C. Moreau, and E. H. Voice, 1973a; "The Behaviour of PyC Fuel Coatings at High Fast Neutron Dose," Proc. Int. Conf. Nuclear Fuel Performance, British Nuclear Energy Society, London.

Janvier, J. C., M. Bruch, and R. Blanchard, 1973b; "Fission Gas Pressure Evolution in Irradiated Coated Particles," Proc. Int. Conf. Nuclear Fuel Performance, British Nuclear Energy Society, London.

Kaae, J. L., et al., 1977; "Prediction of BISO Particle Behaviour During Irradiation with a Stress-Analysis Model," Nucl. Techn. 35, 368.

Kania, M. J., et al., 1976; "Irradiation Performance of HTGR Fertile Fuel in HFIR Target Capsules HT-12 through HT-15," ORNL Report TM-5305.

Lindemer, T. B., 1977; "Measurement and Interpretation of CO and Kr + Xe in Irradiated ThO_2-Containing HTGR Fuel Particles," J. Am. Cer. Soc. 60, 409.

Martin, D. G., and J. E. Hobbs, 1976; "Some Calculations of the Failure Statistics of Coated Fuel Particles," AERE Harwell Report R-8724.

Meek, M. E., and B. F. Rider, 1977; "Compilation of Fission Product Yields," General Electric Report NEDO-12154-2.

Myers, B. F., et al., 1977; "The Behavior of Fission Gases in HTGR Fuel Materials," DOE Report GA-A13723, General Atomic Company.

Nabielek, H., 1976; "Fission Product Retention in HTR Fuel," KFA/Dragon Final Status Report Meeting, April 28-29, Paper No. 8.

Naoumidis, A., 1972; "Brenn- und/oder Brutelement für Kernreaktoren sowie Verfahren zum Herstellen von Brenn- und/oder Brutelementen," Patentschrift 22 15, 907 (April 1).

Naoumidis, A., and B. Thiele, 1974; "Studies on the Amoeba Effect: Carbon Transport in Coated Fuel Particles under the Influence of a Temperature Gradient," IAEA Symposium on Thermodynamics of Nuclear Materials, SM-190/36.

Proksch, E., and A. Strigl, 1975; "Some Aspects of the Kinetics of the Attainment of CO Equilibrium in Oxide HTR Fuel Particles," Dragon Project Report 957.

Schenk, W., 1978; "Untersuchungen zum Verhalten von beschichteten Brennstoffteilchen und Kugelbrennelementen bei Störfalltemperaturen," KFA-Jül report, to be published.

Sayers, J. B., et al., 1973; "Coated Particle Fuels for the Low Enriched Fuel Cycle HTR," Proc. Int. Conf. Nuclear Fuel Performance, British Nuclear Energy Society, London.

Steemers, T. C., 1975; "DIDO 919/8: An HTGR Fuel Particle Experiment in Which Kernel Oxygen Getters are Evaluated," Dragon Project Report 962.

Strigl, A., E. Proksch, and G. Peschta, 1975; "Determination of Internal Gas Release of Fuel Particles from the Colibri HTR3 Experiment," Dragon Project Technical Note 72.

Strigl, A., and E. Proksch, 1977; "Restoration of Carbon Monoxide Equilibrium in Porous Oxide HTR Fuel Particles," Nucl. Technol. 35, 386.

Thiele, B. A., 1975; "Results on the Post Irradiation Examination of Met V/2 (DR-P5/2)," KFA-IRW Technical Note 7/75.

Thiele, B., and R. A. Bradley, 1976; "Neutron-Induced Permeability of BISO Coated HTR Fuel Particles," Int. Conf. World Nuclear Power, ANS/ENS, Washington, D.C.

Turnbull, J. A., and R. Shipp, 1974; "The Release of Stable Rare Gases from the Kernels of Coated Particles During Irradiation," Central Electricity Generating Board, unpublished data.

Wagner-Löffler, M., et al., 1973; "The Signficiance of Gas-Pressure Building in Coated Particles," Proc. Int. Conf. Nuclear Fuel Performance, British Nuclear Energy Society, London.

Wagner-Löffler, M., 1976; "Agglomeration in Carbon-Diluted UO_2 Fuel," Dragon Project, unpublished data.

4. CHEMICAL PERFORMANCE

This section discusses two physico chemical phenomena that can affect the irradiation performance of LEU oxide particles: (1) the migration of oxide kernels in a temperature gradient and (2) the interaction of fission products with SiC coatings.

4.1. THERMAL MIGRATION (AMOEBA) IN OXIDE SYSTEMS

4.1.1. Migration Mechanism

When coated oxide particles are irradiated at high temperatures in a thermal gradient (e.g., in a fuel rod), the kernels tend to migrate towards the hot side, leaving a carbon deposit on the cold side. If the migration continues through the buffer layer and the kernel comes into contact with the inner pyrocarbon coating, the interaction with fuel components and fission products weakens the coating and leads to coating failure.

The mechanism controlling oxide kernel migration is not as well defined as that for the carbide kernel migration (Gulden, 1972). The merits and the drawbacks for the various mechanisms proposed were presented at a meeting organized by the Dragon project in 1975 (Hick, Nabielek, and Wagner-Löffler, 1975), but no general agreements were reached. Lindemer and his co-workers at ORNL (Lindemer and Olstad, 1974a; and de Nordwall, 1974b; and de Nordwall and Olstad, 1975; and Pearson, 1976, 1977) derived the carbon transport rates from the first principles for $CO-CO_2$ diffusion control, CO disproportionation control, and solid state diffusion control, and compared the experimentally determined transport rates as a function of radial positions in a fuel rod with the predicted rates. They concluded that the solid-state diffusion process controls the kernel migration rates in UO_2, ThO_2, PuO_{2-x}, and $Th_{0.8}U_{0.2}O_2$ particles and that the kernel migration

coefficient (cm^2 K/s), which is used for describing carbide kernel migration data, can adequately correlate the oxide kernel migration data. Smith (1976) of GA made several interesting observations on the thermal migration of ThO_2 kernels. He found that ThO_2 kernels could exhibit two types of migration modes. These modes were characterized by kernel shape during migration and the kernel-coating interface at the hot side, although the migration kinetics were not affected. The kernel became elongated in the direction of the temperature gradient in some cases, and carbon precipitates were found in the grain boundaries of the kernel. There was an incubation period for the migration process, and it decreased with the increase of burnup and temperature. It was concluded that solid-state diffusion of carbon down the temperature gradient and Th and O up the temperature gradient controlled the migration rate.

Regardless of what the controlling mechanism for the migration is, the presence of high oxygen potential in the oxide appears to be essential to the migration process for UO_2 since the lowering of the oxygen potential by adding oxygen getters or buffers (Steemers, 1975; Horsley et al., 1975a; Noaumidis, 1973) to the kernel does suppress kernel migration. However, the UO_2 kernel migration behavior does not seem to be affected by burnup and fuel enrichment. This seems to imply that the migration process is insensitive to oxygen potential once the oxygen potential is above a certain threshold.

4.1.2. Thermal Migration Data of Oxide Fuel

A wealth of thermal migration data for a variety of fuel types is included in the references cited earlier. Figure 4-1, a summary of the data for oxide fissile fuels, is similar to the plot drawn by Wagner-Löffler (1977). The Y-axis of Fig. 4-1 consists of the kernel migration coefficient (KMC), which was first used by Gulden (1972) to describe the solid-state diffusion-controlled thermal migration in carbide fuel. Use of the KMC to describe the thermal migration in fuel systems without an established controlling mechanism is discussed in detail by Lindemer and Pearson (1977).

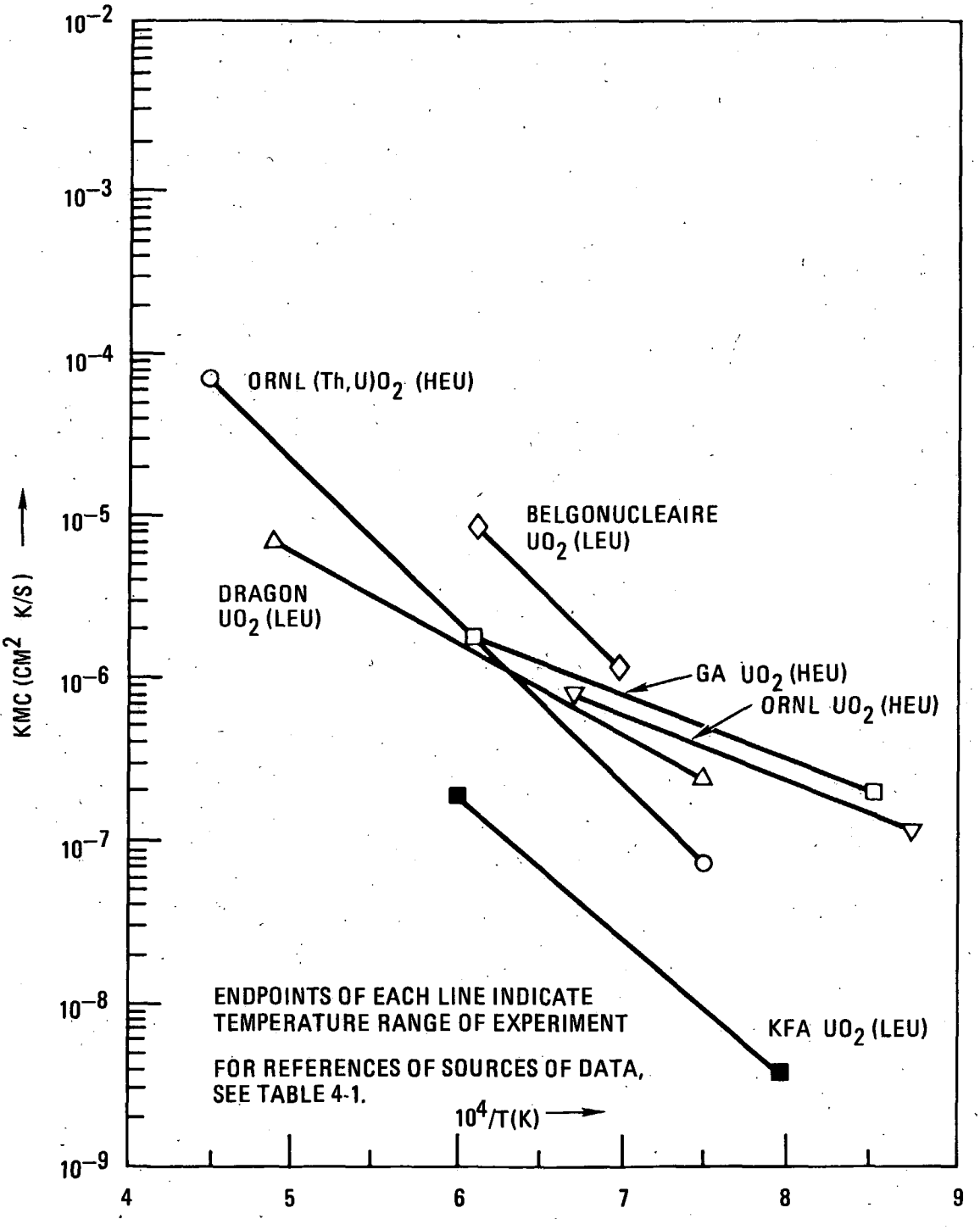

Fig. 4-1. Kernel migration coefficient of oxide fuel particles

The GA, ORNL, and Dragon project UO_2 data all fall close to one another, although the fuel enrichment of the Dragon UO_2 is much lower than that of the GA and ORNL UO_2. On this basis it is probably safe to assume that all the kernel migration coefficients of HEU oxide fuel particles can be used for establishing LEU/MEU oxide fuel particle design. This assumption should be confirmed with further experiments using dense LEU/MEU UO_2, $(Th,U)O_2$, and uranium oxycarbide kernels. The Belgonucleaire UO_2 data are higher and the KFA UO_2 data are considerably lower than the ORNL, GA, and Dragon project UO_2 data in the plot. Further experiments should be planned to resolve these discrepancies.

The variation of kernel migration coefficient with temperature, according to Lindemer and Pearson (1977), can be written as

$$\log_{10}(KMC) = a - \frac{b}{T} \quad .$$

Table 4-1 lists the "a" and "b" values for the plots shown in Fig. 4-1. It should be emphasized that Fig. 4-1 represents a large volume of data, and that the amount of scattering around each plot is substantial. Interested readers can refer back to the references cited for details. From Fig. 4-1, it can be seen that at temperatures below 1350°C UO_2 exhibits a larger tendency to migrate under a thermal gradient than $(Th,U)O_2$.

4.1.3. Means for Reducing Oxide Kernel Thermal Migration

The migration of oxide kernels in a thermal gradient can be reduced by lowering the oxygen potential of the kernel. Various means for achieving this goal are described in Section 3.

4.2. SiC CORROSION

When the inner high density pyrocarbon layer of an oxide fuel particle is broken or permeable, the silicon carbide layer is exposed to the

TABLE 4-1
KMC PARAMETERS FOR THE PLOTS SHOWN IN FIG. 4-1

Fuel Type	Source of Data	Temp. Range of Experiment (°C)	a	b	Reference
HEU $(Th,U)O_2$	ORNL	1100 - 1900	-0.82	7830	Lindemer and Pearson, 1977
HEU UO_2	GA	900 - 1350	-3.58	3540	Scott, Harmon, and Holzgraf, 1976
HEU UO_2	ORNL	900 - 1200	-2.77	4800	Lindemer and Pearson, 1977
LEU UO_2	Dragon	1100 - 1700	-2.05	6300	Wagner-Loffler, 1977
LEU UO_2	Belgonucleaire	1200 - 1350	0.36	9000	Thomson, 1975
LEU UO_2	KFA	900 - 1400	-2.09	7650	Mehner, 1977

gaseous rare gas/CO/CO_2 environment within the particle as well as the fission products and the oxide kernel.

Corrosion of an SiC coating layer causes two effects:

1. A certain thickness of material is converted to a reaction product of probably lower strength.

2. The reaction front proceeds along grain boundaries and introduces the equivalent of large microcracks.

In terms of mechanical performance, the first effect can be described by assigning a reduced thickness to the SiC coating layer, and the second effect can probably be described by assigning a modified Weibull modulus to the statistical description of the strength distribution. Both of these descriptions will have to be based on an evaluation of SiC quality control data (grain size, free silicon, etc., Weibull distribution of unirradiated material) together with metallographic observations (corrosion depth, microcrack size) and bursting strength measurements (Weibull distribution of irradiated and annealed material).

Two modes of SiC corrosion have been observed in irradiated coated particles (Hick, 1976):

1. In oxide fuels, SiC corrosion involving the formation and transport of SiO gas due to a thermal gradient when the internal CO has access to the SiC because of failed inner PyC coating layer.

2. In carbide fuels, SiC corrosion due to a chemical reaction with fission products (Ce, Nd, La, and Pr).

Other fission products (e.g., Sr and Pd) may react with SiC in either an oxide or a carbide fuel environment.

4.2.1. Reaction With CO

Two mechanisms of SiC corrosion involving CO and SiO have been established at typical HTGR operating conditions. In both mechanisms, it is assumed that the initial breach in the PyC and the subsequent corrosion of the SiC occur at the hot end.

The first mechanism (Flowers and Horsley, 1968) involves the oxidation of SiC by high pressure CO to form a protective layer of silica:

$$2\ CO + SiC \rightleftarrows SiO_2 + 3\ C \quad . \tag{4-1}$$

This silica is then reduced to silicon monoxide by SiC:

$$SiO_2 + SiC \rightleftarrows 2\ SiO + C \quad , \tag{4-2}$$

which diffuses through the void volume of the particle to the cool end of the temperature gradient, where it reacts with CO to reform silica:

$$CO + SiO \rightleftarrows SiO_2 + C \quad . \tag{4-3}$$

Reaction 4-3, therefore, acts as a sink for SiO formed in reaction 4-2. Reaction 4-1 eventually stops because it reduces the CO pressure to its equilibrium value. However, when all the SiO_2 has been removed from the site of corrosion by reaction 4-2, more SiO is formed either by the low pressure corrosion reaction between CO and SiC by reaction 4-4 or by the SiC extracting oxygen from the UO_2 kernel.

$$CO + SiC \rightleftarrows SiO + 2\ C \quad . \tag{4-4}$$

The second mechanism involves a different route for the formation of SiO, and relies on intimate contact between the kernel and the SiC layer. In low CO pressures, UO_2 and SiC react to form SiO according to reaction 4-5:

$$UO_2 + 2\ SiC \rightleftarrows UC_2 + 2\ SiO \quad , \tag{4-5}$$

$$UC_2 + 2\ CO \rightleftarrows UO_2 + 4\ C \quad , \tag{4-6}$$

provided that (1) the CO pressure is above that in Eq. 4-6 and (2) reaction 4-6 is kinetically feasible. UO_2 will be reformed and carbon deposited. In fact, the UO_2 behaves as a catalyst. The SiO formed reacts with CO in the cooler regions of the particle by either reaction 4-3 or reaction 4-7, depositing SiO_2 + C or SiO_2 + SiC, respectively.

$$3\ SiO + CO \rightleftarrows SiC + 2\ SiO_2 \quad . \tag{4-7}$$

At temperatures below 1600 K (P_{CO} < 1 MPa), both gas and solid phase corrosion mechanisms are thermodynamically possible and the SiC layers should, therefore, be protected from contact with either the kernel or the gaseous atmosphere within the particle (Crofts and Swan, 1973).

SiC is proposed as a getter for the excess oxygen formed as a result of uranium and plutonium thermal fissioning (Horsley, 1973). If the gas phase corrosion mechanism operates, it will be sufficient to include SiC anywhere within the free gas space of the particle. The effectiveness of SiC gettering CO has been demonstrated by a series of irradiation experiments at Harwell, both with SiC in the kernel and in the buffer layer (Horsley, Davies, and Weldrich, 1975b).

Surprisingly, no signs of SiC corrosion were observed in the Dragon Colibri HTR 3 experiment with low-enriched uranium TRISO fuel particles (207 days, 9% FIMA, maximum particle surface temperature 1250°C), even in the case with direct UO_2 kernel/SiC contact. This particle variety had only a 20-μm inner PyC layer designed to break within the first days of irradiation (Voice, 1975).

On the whole, extremely little SiC corrosion has been observed in the Dragon project's high-temperature irradiation experiments with porous,

low-enriched and carbon-diluted, high-enriched (driver) UO_2 fuel (temperatures up to 2000 K) (Wagner-Löffler, 1975). Furthermore, chlorine (see Section 4.2.3) could not be detected in Dragon and UKAEA HTI/TRISO particles, but traces of SiC were shown to be present in the kernel and buffer (Rose, 1973). The corrosion of SiC in the DR-P5 experiment (KFA particles in the Dragon MET 5 experiment) cannot be explained other than by the poor quality of the silicon carbide.

4.2.2. Strontium Corrosion

Strontium has been shown to be the most influential in attacking SiC in high-temperature irradiations (>1750 K) even when the pyrocarbon layer is intact. Eighteen percent enriched UO_2 TRISO particles (800 μm kernel diameter) irradiated for one year to 4% FIMA at a mean temperature of 1820 K were found to have retained the rare gases (Kr and Xe), but had released strontium and barium.

The results implied that the pyrocarbon coatings had remained intact, but the silicon carbide coating had lost its integrity. To substantiate this apparent failure of the silicon carbide coating, particles were examined for the distribution of fission products in the coating layers. Microprobe scans indicated that although cesium was present predominantly in the inner pyrocarbon layer, it was not detectable in the silicon carbide and outer pyrocarbon layers. Radiochemical analysis showed that strontium release from the particles as Sr-90 was variable, being as much as 20% in some cases. Metallographic examination of the coating layers showed attack of the silicon carbide layer, also to a variable extent. Most particles showed some indication of attack occurring on the inner side of the silicon carbide layer, nearest to the kernel, but for others the complete layer had been affected. The microprobe scans showed that the attack could be associated with the presence of strontium since this element could not be detected beyond the point at which attack was no longer visible. No significant amounts of strontium were found in the pyrocarbon layers. It is tentatively proposed that strontium reacted with the silicon carbide, forming strontium silicate or silicide. At the inner pyrocarbon-silicon

carbide interface, ruthenium, rhodium, and palladium were found. It is generally assumed that these metals, because of their refractory nature, stay preferentially with the UO_2 kernel. As they were not detected in the inner pyrocarbon layer, the actual transport mechanism to the interface is open to speculation, but it could be associated with carbon monoxide pressure and carbonyl formation. It is possible that the mechanism needs only to account for ruthenium movement because, once at the interface, rhodium and palladium will be produced as a result of beta decay of ruthenium. These elements, especially palladium, are well known for their catalytic activity, and they could have some bearing on the strontium-silicon carbide reaction. However, since both the strontium reactions with silicon carbide and the possible migration of ruthenium require the presence of carbon monoxide, the suppression of CO formation by the addition of oxygen getters in the kernel could eliminate the silicon carbide attack (Brown and Faircloth, 1976).

Suzuki and Iseki (1973) studied the reaction between SiC and SrO. They found the reaction between SiC and SrO began at about 1000°C, and the products varied with the oxygen content in the atmosphere. In air, strontium silicate was formed, while in an oxygen-free atmosphere strontium carbide and strontium silicate were observed. The reactions between SiC and these fission products in an irradiated fuel particle are, therefore, strongly dependent upon the oxygen potential in the particle.

4.2.3. Rare Earth Attack

The interaction of the rare earth fission products with SiC, and the subsequent corrosion, have been studied in great detail in carbide fuel particles. These effects are practically absent in oxide fuels because of the greatly improved kernel retention of Sr and rare earths as oxides. Two reactions have been observed:

1. Reaction of the inner SiC surface on the cooler side (Pearson and Lindemer, 1977).

2. Reaction with the inner SiC surface on the hotter side when chlorine is present (Grübmeier, Naoumidis, and Thiele, 1977).

Reactions between SiC and CeO_2 have been studied by Suzuki and Iseki (1973). When heated in air, no reaction between SiC and CeO_2 was observed up to 1500°C. In vacuum, the reaction between SiC and CeO_2 began at about 1100°C, and with increasing temperature, $Ce_4(SiO_4)_3$, $CeSi_2$, and CeC_2 phases were successively observed.

4.2.4. Palladium Attack

Due to the difference in fission product spectrum between uranium and plutonium isotopes, the irradiated LEU fuel particles are expected to contain more noble metal fission products such as Ag and Pd. Ag is known to diffuse rapidly through pyrocarbon coating (see Section 2). It is believed that Pd may do the same. Pd has been shown to attack SiC. When Pd is brought into contact with SiC at high temperatures (1000° to 1300°C), the Si moves into the Pd to form the Pd-Pd_2Si liquid eutectic phase (melting point 800°C), leaving a carbon residue (Yang, 1976). The reaction between Pd and SiC has also been studied by Suzuki, Iseki, and Imanaka (1977). The reaction was found to begin at 1000°C, and the products were Pd_2Si and Pd_3Si. Silver also forms a low melting eutectic (melting point 830°C) with silicon and has a high diffusion rate in SiC (Nabielek, 1977). However, no chemical compatibility study between Ag and SiC has been reported.

Pd phase was found at the SiC inner pyrocarbon interface in plutonium-containing fuel particles irradiated in FTE-13 in the Peach Bottom reactor, and localized attack of SiC was observed. Pd attack of SiC coating was found in low-enriched (6%) UC_2 WAR particles irradiated in fuel rods in the HRB-4 capsule to burnups of 85% U-235, 20% U-238, and 14% Th-232 (Homan et al., 1976). Details on Pd-SiC interaction observed at ORNL are given in Appendix C.

It is interesting to note that no Pd-SiC reaction was observed in the Dragon project's irradiation tests on TRISO low-enriched UO_2, and in the

Studsvik irradiation of TRISO particles containing plutonium oxide (20% Pu_2O_3, 80% PuO_2, dispersed in carbon at Pu/O ratios of 1:30.5 and 1:21) to 37% FIFA at 1200° to 1450°C and 20% FIFA at 1850°C (Barr et al., 1967).

It appears that more controlled irradiation tests of LEU fuel particles are needed in order to define the conditions for the Pd-SiC interaction to occur, in addition to the study of Ag transport through SiC.

REFERENCES

Barr, P., et al., 1967; "High Temperature Irradiation Experiments on Plutonium-Bearing Coated Particle Fuel," Plutonium as a Reactor Fuel, IAEA, Vienna.

Brown, P. E., and R. L. Faircloth, 1976; "Metal Fission Product Behaviour in High Temperature Reactors - UO_2 Coated Particle Fuel," J. of Nucl. Mat 59, 29-41.

Crofts, J. A., and T. Swan, 1973; "Reactions Between UO_2, SiC and CO in an HTGR Fuel Particle," Central Electricity Generating Board, unpublished data.

Flowers, R. H., and G. W. Horsley, 1968; "The Influence of Oxide Kernels on the Manufacture and Performance of Coated Particle Fuel," Atomic Energy Research Establishment (U.K.) Report R5949.

Grübmeier, H., A. Naoumidis, and B. A. Thiele, 1977; "Silicon Carbide Corrosion in HTGR Fuel Particles," KFA Report Jül-1382.

Gulden, T. D., 1972; "Carbon Thermal Diffusion in the UC_2-C System," J. Amer. Ceramic Soc. 55, 14-18.

Hick, H., H. Nabielek, and M. Wagner-Löffler, 1975; "Summary of a Round Table Discussion on Amoeba Mechanisms in Oxide Fuel Particles," Dragon Project Report 919.

Hick, H., 1976; "Outline of Proposed Total Core Integration for a Non-Steady Irradiation History," (Generalization of Fuel Failure Criteria), Dragon Project Technical Note 763.

Homan, F. J., et al., 1976; "Irradiation Performance of HTGR Fuel Rods in HFIR Experiments HRB-4 and -5," ORNL Report 5115.

Horsley, G. W., 1973; UKAEA Harwell, private communication.

Horsley, G. W., et al., 1975a; "An Irradiation Experiment (919/8) to Examine the Influence of Getters on the Irradiation Behavior of UO_2 Kernel Coated Particle Fuel," AERE Report R8018.

Horsley, G. W., J. M. Davies, and G. J. Weldrich, 1975b; "The Behaviour of UKAEA Fuels in the Dragon Met. V(3) Experiment," UKAEA Harwell, unpublished data.

Lindemer, T. B., and R. A. Olstad, 1974a; "HTGR Fuel Kernel Migration Data for the Th-U-C-O System as of April 1, 1974," ORNL Report TM-4493.

Lindemer, T. B., and H. J. De Nordwall, 1974b; "An Analysis of Chemical Failure of Coated UO_2 and Other Oxide Fuel in the High Temperature Gas-Cooled Reactor," ORNL Report TM-4926.

Lindemer, T. B., H. J. de Nordwall, and R. A. Olstad, 1975; Thermodynamics of Nuclear Materials 1974, Vol. I, pp. 163-71, International Atomic Energy Agency.

Lindemer, T. B., and R. L. Pearson, 1976; "Kernel Migration in HTGR Fuels for the Th-U-C-O-N System," ORNL Report TM-5207.

Lindemer, T. B., and R. L. Pearson, 1977; "Kernel Migration for HTGR Fuels From the System Th-U-Pu-C-O-N," J. Amer. Cer. Soc. 60, 5-14.

Mehner, A. W., 1977; KFA, private communication.

Nabielek, H., 1977; "Silver Release from Coated Particle Fuel," KFA Report Jül-1407.

Naoumidis, A., 1973; "Suppressing the Amoeba Effect in Coated Particles with Carbide Kernels for the High Temperature Reactor," J. Nuclear Materials 48 (2), 118-24.

Pearson, R. L., and T. B. Lindemer, 1977; "The Interaction of LaC_2 and NdC_2 with SiC in HTGR Particles," to be published in the Proceedings of the American Nuclear Society Thermal Reactor Safety Meeting, August 1-5, Sun Valley, Idaho.

Rose, K. S. B., 1973; UKAEA Harwell, private communication.

Scott, C. B., D. P. Harmon, and J. F. Holzgraf, 1976; "Postirradiation Examination of Capsules P13R and P13S," ERDA Report GA-A13827, General Atomic Company.

Smith, C. L., 1976; "Migration of ThO_2 Kernels Under the Influence of a Temperature Gradient," General Atomic Report GA-A14058.

Steemers, T. C., 1975; "DIDO 919/8: A HTR Fuel Particle Experiment in Which Kernel Oxygen Getters are Evaluated," Dragon Project Report 962.

Suzuki, H., and T. Iseki, 1973; "Reactions Between SiC and SrO at High Temperatures," Nucl. Sci. Technol. 10 (6), 360-366.

Suzuki, H., R. Iseki, and T. Imanaka, 1977; "Reactions Between SiC and Pd on CeO_2 at High Temperatures," Nucl. Sci. Technol. 14 (6), 438-442.

Thomson, J. M., 1975; "Study of the Chemical Failure of UO_2 Low Enriched Particles," Dragon Project Technical Note 702.

Voice, E. H., 1975; Dragon project (now UKAEA Dounreay), private communication.

Wagner-Löffler, M., 1975; Dragon project (now OSGAE Seibersdorf), private communication.

Wagner-Löffler, M., 1977; "Amoeba Behavior of UO_2 Coated-Particle Fuel," Nucl. Technol. 35 (2), 392-402.

Yang, L., 1976; General Atomic Company, unpublished data.

5. CONCLUSIONS AND DISCUSSION

This review has revealed that a large amount of available information can be used for the prediction of the irradiation performance of LEU/MEU fuel particles. Some of the information, however, needs further confirmation and refinement. Furthermore, some of the problem areas covered are not unique to LEU/MEU fuel particles. Solutions to these problem areas are therefore beneficial to both LEU/MEU and HEU systems. The essential findings are discussed below.

5.1. PLUTONIUM TRANSPORT

Pu-238, which is derived from U-235, represents a potential radiological hazard if it is released in significant quantities to the primary circuit. Since the U-235 inventory in a LEU/MEU core is approximately the same as that in a HEU core, plutonium release is important to both LEU/MEU and HEU systems.

Plutonium release from intact TRISO particles is probably negligible at typical HTGR operating temperatures. For failed particles, the release should vary with the composition of the phases in the kernel, with carbides having a higher release rate than oxides. Oxycarbides may have a much higher release rate than either carbides or oxides. However, this has to be confirmed experimentally since the measured vapor pressure of plutonium oxycarbide appears to be in error. The compositions of the phases present in irradiated uranium oxycarbide kernels, and the vapor pressure of plutonium over these phases, have been calculated from thermodynamic data (see Appendix A). Besmann concluded that plutonium is present in solid solution in the corresponding uranium phases, and plutonium release should be much less than that for plutonium carbide (see Appendix A). In view of the uncertainties in the thermodynamic data, and the neglect of the fission product effect, experimental measurements of plutonium release from

irradiated and laser-failed uranium oxide, carbide, and oxycarbide (of various O/U ratios) particles in helium are needed to check these calculations. Moreover, the release rate should be affected by the conversion of the oxide or oxycarbide phase to carbide and the hydrolysis of the carbide in moist helium. The measurements should, therefore, be carried out as a function of the CO and moisture contents of the helium environment. These results will provide important inputs during the selection of our primary LEU/MEU fuel candidate.

Preliminary observation indicates that graphite surrounding the fuel body may be an effective trap for plutonium. However, no detailed measurements of the sorption characteristics of plutonium over graphite have been made. For cases where plutonium release from heavy metal contamination in a fuel body is higher than the allowed release, it is important to be able to show that graphite can trap the plutonium released.

5.2. FISSION PRODUCT TRANSPORT

The diffusion of cesium, barium, strontium, and fission gases in oxide kernels is of interest to both LEU/MEU and HEU fuel systems. Data (reduced diffusion coefficient D') available from fuel kernels of different enrichment (LEU or HEU), density (porous kernel prepared by powder agglomeration, dense kernel prepared by gel-precipitation method), and composition [UO_2, $(Th,U)O_2$, and ThO_2] have been compared. Agreement is observed in some cases, but not in others. Since the grain size and diffusion distance vary with kernel fabrication method, composition, and burnup, caution has to be exercised in using D' values for one type of kernel structure to calculate the release from other types of kernel structures. To gain a better understanding of how D' varies with kernel structures, controlled experiments should be carried out at low burnups with kernels of well-characterized porosity, surface area, composition, and grain size. The studies should then be extended to high burnups, and the kernels should again be carefully examined for their structure and composition after the irradiation. The results will provide the basis for extrapolating available D' values to kernels of different structures. Uranium oxycarbide, which represents one of the LEU/MEU

fuel candidates, may have two or three uranium-containing phases, depending upon the composition and stoichiometry of the fuel. It would be extremely interesting to study the fission product release from such a multiphase fuel material.

The release of fission gases from failed particles is expected to be dependent upon the susceptibility of the kernel to hydrolysis. Oxide fuels that do not react with moisture may be converted to carbide after coating failure, and the carbide fuel can then react with the moisture. Information on the effects of kernel conversion and hydrolysis on fission product release is extremely useful in controlling helium coolant activity and fission product plateout. Experiments designed for providing such information are of great importance to both LEU/MEU and HEU fuel development. Of the major LEU/MEU fuel candidates, UO_2 is not subjected to hydrolysis in moist helium, but the behavior of uranium oxycarbide may vary with composition and stoichiometry. All promising LEU/MEU fuel materials should be included in these studies.

Because of the high inventory of silver in irradiated LEU/MEU fuel particles and its hard gamma irradiation, silver release is much more important in LEU/MEU fuel than in HEU fuel. Like plutonium, silver release from BISO particles is much higher from BISO than TRISO particles, and graphite is also an effective trap. Silver, however, is released from TRISO particles to various degrees at irradiation temperatures above 1450 K. To prevent silver release from setting the performance limit, a developmental program must be initiated to improve silver retention in fuel bodies. This includes studies of silver transport in SiC, improvement of SiC coating (e.g., nitrogen doping) for silver retention, use of additives to the oxide kernel to reduce silver release, and determination of sorption characteristics of silver in graphite as a function of temperature.

5.3. FUEL PARTICLE MECHANICAL PERFORMANCE

The development of stress-strain models for predicting fuel particle performance is of interest to both LEU/MEU and HEU fuel systems. The

LEU/MEU fuel particles, however, are in general larger than the HEU fuel particles because of neutronic and fuel cycle cost requirements. There are indications that, in agreement with Weibull's statistics on the strength of brittle materials, coatings of larger diameter have lower strength and higher failure probability. However, this is not substantiated by some of the experimental results available. More work is needed to relate pyrocarbon and SiC strengths with coating volume (or area) and coating conditions. Controlled irradiation experiments using particles of various sizes and coating strengths should be carried out to provide information for checking the validity of the stress-strain models and to establish the relationship between coating diameter and failure probability.

Stable fission gas release, which is one of the major contributions to pressure vessel failure of the fuel particle, is also a problem of interest to both LEU/MEU and HEU fuel systems. Models, diffusion equations, and empirical formulas describe the observed results. For the burnup planned for the LEU/MEU fuel system, the release appears to be high. More carefully planned experiments, however, are needed to relate the structures of the kernel, temperature, and burnup with the release.

Because of the high free oxygen yield for plutonium fissioning, the CO pressure in irradiated LEU/MEU fuel particles is expected to be much higher than that in irradiated HEU fuel particles of the same design. Higher CO pressure leads to pressure vessel failure and amoeba failure. The theoretical maximum and minimum values of excess oxygen per fission can be calculated from the fission yields of different fissile nuclides. Most of the experimentally observed values for porous UO_2, dense $(Th,U)O_2$, and dense ThO_2, however, fall below the theoretical minimum values. More CO measurements on irradiated dense UO_2 and uranium oxycarbide particles should be made for comparison. It is expected that better understanding by careful evaluation of existing and additional experimental data may overcome the present pessimistic assumptions on CO release.

The use of oxygen getters or buffers (SiC, UC, ZrC, and Ce_2O_3) for lowering the CO pressure have shown promise in a number of irradiation

experiments. The lowering of oxygen potential in the kernel, however, does cause a small increase (compared with that for UO_2) in the release of barium and rare earth fission products. Further irradiation experiments and postirradiation studies are needed to select the getter (or buffer) material, to define the optimum concentration, and to assess the overall consequences of using oxygen getters or buffers.

5.4. FUEL PARTICLE CHEMICAL PERFORMANCE

The kernel migration coefficients of HEU oxide fuel particles can probably be used for establishing the LEU/MEU oxide fuel particle design. This assumption, however, should be confirmed with further experiments using dense LEU/MEU UO_2, $(Th,U)O_2$, and uranium oxycarbide kernels. The discrepancy between the Belgonucleaire, KFA, and ORNL-Dragon-GA UO_2 KMC data should be resolved. Complete understanding of the UO_2 migration mechanism is still lacking. No data exist for the KMC values of uranium oxycarbide particles of various compositions and stoichiometries. Efforts should be made to obtain this information for a better understanding of the UO_2 thermal migration process. Oxygen getters and buffers should be developed to reduce the oxygen potential in LEU/MEU fuel particles, which will diminish the amoeba effect and lower CO pressure.

The localized attack of the SiC coating by the noble metal fission product Pd may put a limit on fuel performance. More work is needed to determine whether the release of Pd varies with kernel composition (carbide, oxide, or oxycarbide) or if, like Ag, it can be reduced by use of kernel additives. The development of a better coating (e.g., ZrC) that might resist Pd attack could improve the performance of the LEU/MEU fuel particles. In-pile irradiation experiments should be planned to define the temperature and burnup for the Pd-SiC reaction concurrently with the study of silver transport through SiC.

The LEU fuel particle performance information available in the literature has provided a broad data base for the development of LEU/MEU fuel systems. With confirmation and refinement of these data, and a carefully

planned program for resolving the critical problems uncovered by our past experiences, it should not be difficult to develop a licensable fuel system to meet the demand of LEU/MEU HTGR systems.

6. RECOMMENDED LEU/MEU FUEL DEVELOPMENT PROGRAM

The critical problems that may limit the performance of the LEU/MEU fuel particles have been established as:

1. Plutonium release from failed fuel particles.
2. Silver release from fuel particles.
3. Failure of pyrocarbon coatings on large LEU/MEU fuel particles.
4. Excessive CO pressure in LEU/MEU fuel particles.
5. Amoeba migration of LEU/MEU oxide kernels.
6. Pd attack of the SiC coating.

The LEU/MEU fuel development program should be formulated with these critical problems in mind. The recommended program is summarized below.

6.1. PLUTONIUM RELEASE

1. Determine the plutonium release from irradiated and laser-failed UC_2 particles, UO_2 particles, and uranium oxycarbide particles of different compositions and stoichiometries as a function of temperature and impurity contents (CO, H_2O) in the helium environment.

2. Compare the phases present and the plutonium release data with that calculated from thermodynamic information.

3. Study the sorption and diffusion of plutonium in graphite.

6.2. SILVER RELEASE

1. Study the diffusion of silver in SiC, improved SiC (nitrogen-doped), and ZrC coatings.

2. Develop silver getter in the kernel (e.g., SiC) or in the carbon buffer coating.

3. Study the sorption and diffusion behavior of silver in graphite as a function of temperature.

6.3. COATING FAILURE ON LARGE PARTICLES

1. Determine the Weibull parameters for pyrocarbon and SiC coatings deposited under various conditions.

2. Irradiate LEU fuel particles of various diameters and compare the failure fractions with those deduced from the stress-strain model, using coating strength data generated under item 1.

3. Develop stronger coatings (e.g., a Si-alloyed pyrocarbon coating) to replace the outer pyrocarbon coating of TRISO particles.

4. Improve the strength of the SiC coating by optimizing production techniques.

6.4. CO PRESSURE IN LEU/MEU FUEL PARTICLES

1. Determine the amount of CO released from irradiated dense LEU/MEU sol-gel kernels.

2. Develop carbide-buffered LEU/MEU fuel particles with lower oxygen potential and CO pressure. Examples are (1) uranium oxycarbide of various compositions and stoichiometries and (2) SiC and ZrC buffered UO_2.

3. Study metallic fission product release (e.g., Cs, Sr, and rare earths) from carbide-buffered LEU/MEU fuel particles.

6.5. AMOEBA MIGRATION OF LEU/MEU OXIDE KERNELS

1. Study the amoeba migration of LEU/MEU UO_2 kernels to gain a better understanding of the migration mechanism and to explain the discrepancies that exist in some of the literature data on UO_2.

2. Develop carbide-buffered LEU/MEU fuel particles of lower oxygen potential and reduced amoeba migration. Study the amoeba migration of uranium oxycarbide of various compositions and stoichiometries, and SiC and ZrC buffered UO_2.

6.6. Pd ATTACK OF SiC COATING

1. Establish the degree and morphology of Pd attack on SiC coatings as a function of fuel kernel composition (carbide, oxide, and oxycarbide), temperature, and burnup.

2. Develop Pd getters (e.g., SiC and ZrC) for trapping Pd in the kernel or the buffer coating.

3. Develop coatings that are resistant to Pd attack (e.g., ZrC).

6.7. ADDITIONAL EFFORTS

In addition to the program outlined above for resolving the problem areas that limit LEU/MEU fuel particle performance, additional efforts are needed to establish the fission product (metallic and gaseous) release as a function of kernel fabrication methods and kernel structures (porosity, surface area, density, grain size, etc.). This work is of generic interest to both LEU/MEU and HEU fuel systems.

To implement the above-described program, four major tasks are required.

1. Kernel Development

This task is mainly process-oriented. The main objective is to develop the process for the preparation of the large LEU/MEU kernels needed and the characterization of these kernels. Uranium oxycarbide kernels and carbide-buffered kernels for CO pressure and amoeba migration control are of particular interest.

2. Coating Development

This task is also mainly process-oriented. The main objective is to develop the processes for the deposition of Si-alloyed pyrocarbon for higher strength, ZrC coating for resisting Pd attack, and carbon buffer coatings containing oxygen getters for reducing CO pressure and the amoeba effect, and the characterization of these coatings.

3. Fuel Irradiation

The main objective of this task is to evaluate the in-pile irradiation performance of various LEU/MEU fuel particle designs, either in loose particle form or in fuel rods. Particle breakage, fission product-coating interaction, and amoeba migration as a function of kernel composition, particle diameter, and temperature burnup are of particular interest. The results, when combined with the postirradiation annealing results, serve as the basis for the selection of the reference LEU/MEU fuel.

4. Postirradiation Annealing Studies

This task includes the study of:

a. Plutonium release from irradiated and laser-failed LEU/MEU fuel particles as a function of kernel composition and the

impurity contents (CO, H_2O) of a helium environment. The sorption characteristics of plutonium in graphite will also be determined.

b. Amoeba migration and CO pressure measurements to determine the effectiveness of oxygen getters and buffers.

c. Silver and other metallic and gaseous fission products released as a function of kernel composition, structures, and coating structures.

d. Short-lived fission gas release from irradiated and laser-failed LEU/MEU fuel particles as a function of kernel compositions, structures, and impurity contents (CO, H_2O) of a helium environment.

e. SiC-fission product interaction. The information defines the temperature and burnup for which the Pd-SiC interaction becomes appreciable. The effectiveness of ZrC to resist Pd attack, and the possibility of trapping Pd and Ag in the kernel or the buffer coating, will be evaluated. The effect of oxygen getters and buffers on the release of rare earths from oxide kernels, and the reaction with the SiC coating, will be studied. The reported temperature threshold for the attack of SiC by Sr will be checked.

ACKNOWLEDGMENTS

The authors wish to acknowledge the support received from the staffs at KFA Jülich, General Atomic Company, and Oak Ridge National Laboratory. We are also grateful for the help given by European laboratories, in particular the Oesterreichische Studiengesellschaft für Atomenergie in Seibersdorf, the UKAEA establishments in Harwell and Winfrith, the Research Laboratory of the Central Electricity Generating Board in Berkeley, Great Britain, the Commissariat à L'Energie Atomique in Grenoble, and Belgonucleaire, Brussels.

APPENDIX A
THERMOCHEMICAL EQUILIBRIA IN MEU HTGR FUEL

T. M. Besmann
Oak Ridge National Laboratory

A chemical thermodynamic assessment of the U-Pu-C-O system was made in the range of compositions of interest to MEU HTGR fuel. The computer program SOLGASMIX-PV (Besmann, 1977), which calculates complex chemical equilibria, was used to determine the stable phases in the system and calculate partial pressures.

SOLGASMIX-PV was run at 1400, 1600, 1800, and 2000 K using the species and thermodynamic data listed in Table A-1. The outputs for the four cases given below are given in Table A-2.

Overall Composition	% Conversion	Pu/(U + Pu)	Phases Determined to be Present
$U_{0.93}Pu_{0.07}C_{0.19}O_{1.8}$	10	0.07	$U_{1-x}Pu_xC_{1.5} + U_{1-y}Pu_yO_{2-0.5y} + C$
$U_{0.93}Pu_{0.07}C_{0.475}O_{1.5}$	25	0.07	$U_{1-x}Pu_xC_{1.5} + U_{1-y}Pu_yO_{2-0.5y} + C$
$U_{0.99}Pu_{0.01}C_{0.19}O_{1.8}$	10	0.01	$U_{1-x}Pu_xC_{1.5} + U_{1-y}Pu_yO_{2-0.5y} + C$
$U_{0.93}Pu_{0.07}C_{0.1}O_{1.8}$	-	0.07	$U_{1-x}Pu_xC_{1.5} + U_{1-y}Pu_yO_{2-0.5y} + U_{1-z}Pu_zC_{1-\ell}O_\ell$

Initially, the fuel was assumed to be 10% or 25% converted to $UC_{1.9}$ with no excess carbon. Plutonium ratios [Pu/(U + Pu)] of 0.01 and 0.07 were considered to represent bred-in plutonium. The calculations were performed assuming that the following ideal solid or liquid solutions represent the respective condensed phases: $UC_{1.5} + PuC_{1.5}$ represents $U_{1-x}Pu_xC_{1.5}$; $UC_{1.9} + PuC_{1.5}$ represents $U_{1-k}Pu_kC_{1.9-0.4k}$; $UO_2 + PuO_{1.5}$ represents $U_{1-y}Pu_yO_{2-0.5y}$; $UO + PuO + UC + PuC$ represents $U_{1-z}Pu_zC_{1-\ell}O_\ell$; and $U + Pu$ represents $U_{1-m}Pu_m$. These are considered reasonably good assumptions in the light of available data (Potter and Roberts, 1968; Potter, 1970; Besmann, 1977).

TABLE A-1

THERMODYNAMIC DATA

Species	Temperature (K)	ΔH_f° (kJ/mol)	ΔS_f° (J/mol·K)	Reference
$CO_{(g)}$	1800	-117290	84.39	JANAF (1971)
$CO_{2(g)}$	1800	-396220	0.13	JANAF (1971)
$U_{(g)}$	1800	493230	113.1	Oetting et al. (1976)
$Pu_{(g)}$	1800	326800	88.83	Oetting et al. (1976)
$PuO_{(g)}$	1600-2150	-119000	41.0	Ackerman and Chandrasekharaiah (1974)
$PuO_{2(g)}$	1600-2150	-471100	-28.0	Ackerman and Chandrasekharaiah (1974)
$PuC_{2(g)}$	1800	569000	210.0	(a)
$UO_{(g)}$	1800-2200	-37000	43.1	Ackerman and Chandrasekharaiah (1974)
$UO_{2(g)}$	1600-2200	-508400	-22.8	Ackerman and Chandrasekharaiah (1974)
$UO_{3(s)}$	1200-1500	-840000	-81.2	Ackerman and Chandrasekharaiah (1974)
$UC_{2(g)}$	-	642300	162.0	Tetenbaum et al. (1975)
$UC_{(s)}$	1800	-110000	-0.86	Tetenbaum et al. (1975)
$UO_{(s)}$	1800	-544100	-96.43	(b)
$PuC_{(s)}$	1800	-32550	123.0	Tetenbaum et al. (1975)
$PuO_{(s)}$	1800	-557300	-92.33	(b)
$UC_{1.5}$	1800	-100900	10.6	Tetenbaum et al. (1975)
$PuC_{1.5(s)}$	1800	-82130	-3.92	Tetenbaum et al. (1975)
$UC_{1.9(s)}$	1800	-89100	11.2	Potter and Rand (1977)
$UO_{2(s)}$	1800	-1088230	-175.41	Rand et al. (1977)
$PuO_{1.5(s)}$	1600-2150	-83600	-133.5	Ackerman and Chandrasekharaiah (1974)

(a) Calculated from the free energy functions of Faircloth et al. (1968) and the ΔH_f° and S_{298}° of Schumm et al. (1973) for the analogous species $CeC_{2(g)}$.

(b) Calculated following the method of Potter (1972).

TABLE A-2

U-Pu-C-O SYSTEM OUTPUTS FROM PROGRAM SOLGASMIX-PV
(T = 1400.00 K; P = 1.000D 00 ATM)

	X*/MOLE[a]	Y/MOLE[b]	P/ATM[c]	ACTIVITY[d]
AR	0.10000D-01	0.10000D-01	0.99998D 00	0.99998D 00
CO	0.0	0.16305D-06	0.16305D-04	0.16305D-04
CO2	0.0	0.44273D-14	0.44273D-12	0.44273D-12
U	0.0	0.15260D-18	0.15260D-16	0.15260D-16
PU	0.0	0.29197D-14	0.29197D-12	0.29197D-12
O2	0.90000D 00	0.71822D-29	0.71820D-27	0.71820D-27
PUO	0.0	0.10667D-13	0.10667D-11	0.10667D-11
PUO2	0.0	0.97486D-18	0.97485D-17	0.97485D-16
PUC2	0.0	0.57283D-17	0.57282D-15	0.57282D-15
UO	0.0	0.54743D-16	0.54742D-14	0.54742D-14
UO2	0.0	0.20525D-15	0.20525D-13	0.20525D-13
UO3	0.0	0.11535D-19	0.11535D-17	0.11535D-17
UC2	0.0	0.14996D-21	0.14996D-19	0.14996D-19
			MOLE FRACTION[e]	
UC	0.0	0.0	0.0	0.0
UO	0.0	0.0	0.0	0.0
PUC	0.0	0.0	0.0	0.0
PUO	0.0	0.0	0.0	0.0
			MOLE FRACTION	
UC1.5	0.0	0.82032D-01	0.99245D 00	0.99245D 00
PUC1.5	0.0	0.62398D-03	0.75491D-02	0.75491D-02
			MOLE FRACTION	
UC1.9	0.0	0.0	0.0	0.0
PUC1.5	0.0	0.0	0.0	0.0
			MOLE FRACTION	
UO2	0.0	0.84797D 00	0.92437D 00	0.92437D 00
PUO1.5	0.0	0.69376D-01	0.75627D-001	0.75627D-01
			MOLE FRACTION	
U	0.93000D 00	0.0	0.0	0.0
PU	0.70000D-01	0.0	0.0	0.0
C	0.19000D 00	0.66016D-01		

[a] Quantities of each element in its reference state.

[b] Moles of each species present at equilibrium.

[c] Partial pressure of the gases.

[d] Chemical activity of each species.

[e] Mole fraction of each species in each solution.

TABLE A-2 (continued)

(T = 1600.00 K; P = 1.000D 00 ATM)

	X*/MOLE	Y/MOLE	P/ATM	ACTIVITY
AR	0.10000D-01	0.10000D-01	0.99907D 00	0.99907D 00
CO	0.0	0.92853D-05	0.92767D-03	0.72767D-03
CO2	0.0	0.25283D-11	0.25260D-09	0.25260D-09
U	0.0	0.90022D-16	0.89939D-14	0.89939D-14
PU	0.0	0.27231D-12	0.27206D-10	0.27206D-10
O2	0.90000D 00	0.28896D-24	0.28869D-22	0.28869D-22
PUO	0.0	0.16624D-11	0.16608D-09	0.16608D-09
PUO2	0.0	0.69441D-15	0.69376D-13	0.69376D-13
PUC2	0.0	0.71998D-14	0.71931D-12	0.71931D-12
UO	0.0	0.21793D-13	0.21773D-11	0.21773D-11
UO2	0.0	0.10372D-12	0.10363D-10	0.10363D-10
UO3	0.0	0.33203D-16	0.33173D-14	0.33173D-14
UC2	0.0	0.43853D-18	0.43812D-16	0.43812D-16
			MOLE FRACTION	
UC	0.0	0.0	0.0	0.0
UO	0.0	0.0	0.0	0.0
PUC	0.0	0.0	0.0	0.0
PUO	0.0	0.0	0.0	0.0
			MOLE FRACTION	
UC1.5	0.0	0.81946D-01	0.99129D 00	0.99129D 00
PUC1.5	0.0	0.72026D-03	0.87109D-02	0.87109D-02
			MOLE FRACTION	
UC1.9	0.0	0.0	0.0	0.0
PUC1.5	0.0	0.0	0.0	0.0
			MOLE FRACTION	
UO2	0.0	0.84804D 00	0.92448D 00	0.92448D 00
PUO1.5	0.0	0.69280D-01	0.75524D-01	0.75524D-01
			MOLE FRACTION	
U	0.93000D 00	0.0	0.0	0.0
PU	0.70000D-01	0.0	0.0	0.0
C	0.19000D 00	0.65964D-01		

TABLE A-2 (continued)

(T = 1800.00 K; P = 1.000D 00 ATM)

	X*/MOLE	Y/MOLE	P/ATM	ACTIVITY
AR	0.10000D-01	0.10000D-01	0.97850D 00	0.97850D 00
CO	0.0	0.21975D-03	0.21502D-01	0.21502D-01
CO2	0.0	0.35951D-09	0.35178D-07	0.35178D-07
U	0.0	0.13124D-13	0.12842D-11	0.12842D-11
PU	0.0	0.94567D-11	0.92533D-09	0.92533D-09
O2	0.90000D 00	0.11245D-20	0.11003D-18	0.11003D-18
PUO	0.0	0.86071D-10	0.84220D-08	0.84220D-08
PUO2	0.0	0.11724D-12	0.11472D-10	0.11472D-10
PUC2	0.0	0.18904D-11	0.18497D-09	0.18497D-09
UO	0.0	0.23402D-11	0.22899D-09	0.22899D-09
UO2	0.0	0.13409D-10	0.13120D-08	0.13120D-08
UO3	0.0	0.16611D-13	0.16254D-11	0.16254D-11
UC2	0.0	0.22206D-15	0.21728D-13	0.21728D-13
			MOLE FRACTION	
UC	0.0	0.0	0.0	0.0
UO	0.0	0.0	0.0	0.0
PUC	0.0	0.0	0.0	0.0
PUO	0.0	0.0	0.0	0.0
			MOLE FRACTION	
UC1.5	0.0	0.82005D-C1	0.99026D 00	0.99026D 00
PUC1.5	0.0	0.80619D-03	0.97353D-02	0.97353D-02
			MOLE FRACTION	
UC1.9	0.0	0.0	0.0	0.0
PUC1.5	0.0	0.0	0.0	0.0
			MOLE FRACTION	
UO2	0.0	0.84799D 00	0.92456D 00	0.92456D 00
PUO1.5	0.0	0.69194D-01	0.75441D-01	0.75441D-01
			MOLE FRACTION	
U	0.93000D 00	0.0	0.0	0.0
PU	0.70000D-C1	0.0	0.0	0.0
C	0.19000D 00	0.65563D-01		

TABLE A-2 (continued)

(T = 2000.00 K; P = 1.000D 00 ATM)

	X*/MOLE	Y/MOLE	P/ATM	ACTIVITY
AR	0.10000D-01	0.10000D-01	0.73420D 00	0.73420D 00
CO	0.0	0.36202D-02	0.26580D 00	0.26580D 00
CO2	0.0	0.24862D-07	0.18253D-05	0.18253D-05
U	0.0	0.92584D-12	0.67975D-10	0.67975D-10
PU	0.0	0.21203D-09	0.15567D-07	0.15567D-07
O2	0.90000D 00	0.10979D-17	0.80609D-16	0.80609D-16
PUO	0.0	0.26563D-08	0.19503D-06	0.19503D-06
PUO2	0.0	0.93147D-11	0.68389D-09	0.68389D-09
PUC2	0.0	0.21382D-09	0.15699D-07	0.15699D-07
UO	0.0	0.12926D-09	0.94901D-08	0.94901D-08
UO2	0.0	0.85912D-09	0.63077D-07	0.63077D-07
UO3	0.0	0.31422D-11	0.23070D-09	0.23070D-09
UC2	0.0	0.42414D-13	0.31140D-11	0.31140D-11
			MOLE FRACTION	
UC	0.0	0.0	0.0	0.0
UO	0.0	0.0	0.0	0.0
PUC	0.0	0.0	0.0	0.0
PUO	0.0	0.0	0.0	0.0
			MOLE FRACTION	
UC1.5	0.0	0.83635D-01	0.98934D 00	0.98934D 00
PUC1.5	0.0	0.90080D-03	0.10656D-01	0.10656D-01
			MOLE FRACTION	
UC1.9	0.0	0.0	0.0	0.0
PUC1.5	0.0	0.0	0.0	0.0
			MOLE FRACTION	
UO2	0.0	0.84637D 00	0.92452D 00	0.92452D 00
PUO1.5	0.0	0.69099D-01	0.75480D-01	0.75480D-01
			MOLE FRACTION	
U	0.93000D 00	0.0	0.0	0.0
PU	0.70000D-01	0.0	0.0	0.0
C	0.19000D 00	0.59577D-01		
IHC002I STOP	00000			

TABLE A-2 (continued)

(T = 1400.00 K; P = 1.000D 00 ATM)

	X*/MOLE	Y/MOLE	P/ATM	ACTIVITY
AR	0.10000D-01	0.10000D-01	0.99998D 00	0.99998D 00
CO	0.0	0.16202D-06	0.16202D-04	0.16202D-04
CO2	0.0	0.43715D-14	0.43714D-12	0.43714D-12
U	0.0	0.15239D-18	0.15239D-16	0.15239D-16
PU	0.0	0.34516D-14	0.34515D-12	0.34515D-12
O2	0.75000D 00	0.70915D-29	0.70914D-27	0.70914D-27
PUO	0.0	0.12530D-13	0.12530D-11	0.12530D-11
PUO2	0.0	0.11379D-17	0.11379D-15	0.11379D-15
PUC2	0.0	0.67718D-17	0.67717D-15	0.67717D-15
UO	0.0	0.54321D-16	0.54320D-14	0.54320D-14
UO2	0.0	0.20238D-15	0.20238D-13	0.20238D-13
UO3	0.0	0.11302D-19	0.11302D-17	0.11302D-17
UC2	0.0	0.14975D-21	0.14975D-19	0.14975D-19
			MOLE FRACTION	
UC	0.0	0.0	0.0	0.0
UO	0.0	0.0	0.0	0.0
PUC	0.0	0.0	0.0	0.0
PUO	0.0	0.0	0.0	0.0
			MOLE FRACTION	
UC1.5	0.0	0.23094D 00	0.99108D 00	0.99108D 00
PUC1.5	0.0	0.20795D-02	0.89243D-02	0.89243D-02
			MOLE FRACTION	
UC1.9	0.0	0.0	0.0	0.0
PUC1.5	0.0	0.0	0.0	0.0
			MOLE FRACTION	
UO2	0.0	0.69906D 00	0.91144D 00	0.91144D 00
PUO1.5	0.0	0.67920D-01	0.88556D-01	0.88556D-01
			MOLE FRACTION	
U	0.93000D 00	0.0	0.0	0.0
PU	0.70000D-01	0.0	0.0	0.0
C	0.47500D 00	0.12547D 00		

TABLE A-2 (continued)

(T = 1600.00 K; P = 1.000D 00 ATM)

	X*/MOLE	Y/MOLE	P/ATM	ACTIVITY
AR	0.10000D-01	0.1000D-01	0.99908D 00	0.99908D 00
CO	0.0	0.92288D-05	0.92203D-03	0.92203D-03
CO2	0.0	0.24977D-11	0.24954D-09	0.24954D-09
U	0.0	0.89881D-16	0.89798D-14	0.89798D-14
PU	0.0	0.32078D-12	0.32048D-10	0.32048D-10
O2	0.75000D 00	0.28545D-24	0.28519D-22	0.28519D-22
PUO	0.0	0.19464D-11	0.19446D-09	0.19446D-09
PUO2	0.0	0.80809D-15	0.80735D-13	0.80735D-13
PUC2	0.0	0.84813D-14	0.84735D-12	0.84735D-12
UO	0.0	0.21627D-13	0.21607D-11	0.21607D-11
UO2	0.0	0.10230D-12	0.10221D-10	0.10221D-10
UO3	0.0	0.32550D-16	0.32520D-14	0.32520D-14
UC2	0.0	0.43784D-18	0.43743D-16	0.43743D-16
			MOLE FRACTION	
UC	0.0	0.0	0.0	0.0
UO	0.0	0.0	0.0	0.0
PUC	0.0	0.0	0.0	0.0
PUO	0.0	0.0	0.0	0.0
			MOLE FRACTION	
UC1.5	0.0	0.23071D 00	0.98974D 00	0.98974D 00
PUC1.5	0.0	0.23920D-02	0.10261D-01	0.10261D-01
			MOLE FRACTION	
UC1.9	0.0	0.0	0.0	0.0
PUC1.5	0.0	0.0	0.0	0.0
UO2	0.0	0.69929D 00	0.91184D 00	0.91184D 00
PUO1.5	0.0	0.67608D-01	0.88158D-01	0.88158D-01
			MOLE FRACTION	
U	0.93000D 00	0.0	0.0	0.0
PU	0.70000D-01	0.0	0.0	0.0
C	0.47500D 00	0.12534D 00		

TABLE A-2 (continued)

(T = 1800.00 K; P = 1.000D 00 ATM

	X*/MOLE	Y/MOLE	P/ATM	ACTIVITY
AR	0.10000D-01	0.10000D-01	0.97862D 00	0.97862D 00
CO	0.0	0.21843D-03	0.21376D-01	0.21376D-01
CO2	0.0	0.35526D-09	0.34767D-07	0.34767D-07
U	0.0	0.13100D-13	0.12820D-11	0.12820D-11
PU	0.0	0.11104D-10	0.10867D-08	0.10867D-08
O2	0.75000D 00	0.11112D-20	0.10875D-18	0.10875D-18
PUO	0.0	0.10048D-09	0.98327D-08	0.98327D-08
PUO2	0.0	0.13606D-12	0.13315D-10	0.13315D-10
PUC2	0.0	0.22198D-11	0.21723D-09	0.21723D-09
UO	0.0	0.23222D-11	0.22725D-09	0.22725D-09
UO2	0.0	0.13227D-10	0.12945D-08	0.12945D-08
UO3	0.0	0.16290D-13	0.15942D-11	0.15942D-11
UC2	0.0	0.22165D-15	0.21691D-13	0.21691D-13
			MOLE FRACTION	
UC	0.0	0.0	0.0	0.0
UO	0.0	0.0	0.0	0.0
PUC	0.0	0.0	0.0	0.0
PUO	0.0	0.0	0.0	0.0
			MOLE FRACTION	
UC1.5	0.0	0.23061D 00	0.98857D 00	0.98857D 00
PUC1.5	0.0	0.26670D-02	0.11433D-01	0.11433D-01
			MOLE FRACTION	
UC1.9	0.0	0.0	0.0	0.0
PUC1.5	0.0	0.0	0.0	0.0
			MOLE FRACTION	
UO2	0.0	0.69939D 00	0.91218D 00	0.91218D 00
PUO1.5	0.0	0.67333D-01	0.87819D-01	0.87819D-01
			MOLE FRACTION	
U	0.93000D 00	0.0	0.0	0.0
PU	0.70000D-01	0.0	0.0	0.0
C	0.47500D 00	0.12487D 00		

TABLE A-2 (continued)

(T = 2000.00 K; P = 1.000D 00 ATM)

	X*/MOLE	Y/MOLE	P/ATM	ACTIVITY
AR	0.10000D-01	0.1000D-01	0.73572D 00	0.73572D 00
CO	0.0	0.35922D-02	0.26428D 00	0.26428D 00
CO2	0.0	0.24528D-07	0.18046D-05	0.18046D-05
U	0.0	0.92223D-12	0.67850D-10	0.67850D-10
PU	0.0	0.24789D-09	0.18237D-07	0.18237D-07
O2	0.75000D 00	0.10832D-17	0.79694D-16	0.79694D-16
PUO	0.0	0.30878D-08	0.22718D-06	0.22718D-06
PUO2	0.0	0.10766D-10	0.79209D-09	0.79209D-09
PUC2	0.0	0.24998D-09	0.18392D-07	0.18392D-07
UO	0.0	0.12802D-09	0.94186D-08	0.94186D-08
UO2	0.0	0.84605D-09	0.62245D-07	0.62245D-07
UO3	0.0	0.30767D-11	0.22636D-09	0.22636D-09
UC2	0.0	0.42248D-13	0.31083D-11	0.31083D-11
			MOLE FRACTION	
UC	0.0	0.0	0.0	0.0
UO	0.0	0.0	0.0	0.0
PUC	0.0	0.0	0.0	0.0
PUO	0.0	0.0	0.0	0.0
UC1.5	0.0	0.23210D 00	0.98752D 00	0.98752D 00
PUC1.5	0.0	0.29340D-02	0.12484D-01	0.12484D-01
			MOLE FRACTION	
UC1.9	0.0	0.0	0.0	0.0
PUC1.5	0.0	0.0	0.0	0.0
			MOLE FRACTION	
UO2	0.0	0.69790D 00	0.91233D 00	0.91233D 00
PUO1.5	0.0	0.67066D-01	0.87671D-01	0.87671D-01
			MOLE FRACTION	
U	0.93000D 00	0.0	0.0	0.0
PU	0.70000D-01	0.0	0.0	0.0
C	0.47500D 00	0.11886D 00		
IH0002I STOP	00000			

TABLE A-2 (continued)

(T = 1400.00 K; P = 1.000D 00 ATM)

	X*/MOLE	Y/MOLE	P/ATM	ACTIVITY
AR	0.10000D-01	0.10000D-01	0.99998D 00	0.99998D 00
CO	0.0	0.16811D-06	0.16811D-04	0.16811D-04
CO2	0.0	0.47062D-14	0.47061D-12	0.47061D-12
U	0.0	0.15360D-18	0.15360D-16	0.15360D-16
PU	0.0	0.40446D-15	0.40446D-13	0.40446D-13
O2	0.90000D 00	0.76345D-29	0.76344D-27	0.76344D-27
PUO	0.0	0.15235D-14	0.15235D-12	0.15235D-12
PUO2	0.0	0.14355D-18	0.14355D-16	0.14355D-16
PUC2	0.0	0.79354D-18	0.79353D-16	0.79353D-16
UO	0.0	0.56811D-16	0.56810D-14	0.56810D-14
UO2	0.0	0.21961D-15	0.21961D-13	0.21961D-13
UO3	0.0	0.12725D-19	0.12725D-17	0.12725D-17
UC2	0.0	0.15094D-21	0.15094D-19	0.15094D-19
			MOLE FRACTION	
UC	0.0	0.0	0.0	0.0
UO	0.0	0.0	0.0	0.0
PUC	0.0	0.0	0.0	0.0
PUO	0.0	0.0	0.0	0.0
			MOLE FRACTION	
UC1.5	0.0	0.97424D-01	0.99895D 00	0.99895D 00
PUC1.5	0.0	0.10199D-03	0.10458D-02	0.10458D-02
			MOLE FRACTION	
UC1.9	0.0	0.0	0.0	0.0
PUC1.5	0.0	0.0	0.0	0.0
			MOLE FRACTION	
UO2	0.0	0.90258D 00	0.98903D 00	0.98903D 00
PUO1.5	0.0	0.98980D-02	0.10968D-01	0.10968D-01
			MOLE FRACTION	
U	0.99000D 00	0.0	0.0	0.0
PU	0.10000D-01	0.0	0.0	0.0
C	0.19000D 00	0.43711D-01		

TABLE A-2 (continued)

(T = 1600.00 K; P = 1.000D 00 ATM

	X*/MOLE	Y/MOLE	P/ATM	ACTIVITY
AR	0.10000D-01	0.10000D-01	0.99904D 00	0.99904D 00
CO	0.0	0.95683D-05	0.95591D-03	0.95591D-03
CO2	0.0	0.26847D-11	0.26821D-09	0.26821D-09
U	0.0	0.90706D-16	0.90620D-14	0.90620D-14
PU	0.0	0.37746D-13	0.37710D-11	0.37710D-11
O2	0.90000D 00	0.30683D-24	0.30654D-22	0.30654D-22
PUO	0.0	0.23745D-12	0.23722D-10	0.23722D-10
PUO2	0.0	0.10221D-15	0.10211D-13	0.10211D-13
PUC2	0.0	0.99801D-15	0.99706D-13	0.99706D-13
UO	0.0	0.22628D-13	0.22606D-11	0.22606D-11
UO2	0.0	0.11097D-12	0.11086D-10	0.11086D-10
UO3	0.0	0.36605D-16	0.36570D-14	0.36570D-14
UC2	0.0	0.44186D-18	0.44144D-16	0.44144D-16
			MOLE FRACTION	
UC	0.0	0.0	0.0	0.0
UO	0.0	0.0	0.0	0.0
PUC	0.0	0.0	0.0	0.0
PUO	0.0	0.0	0.0	0.0
			MOLE FRACTION	
UC1.5	0.0	0.97416D-01	0.99879D 00	0.99879D 00
PUC1.5	0.0	0.11777D-03	0.12074D-02	0.12074D-02
			MOLE FRACTION	
UC1.9	0.0	0.0	0.0	0.0
PUC1.5	0.0	0.0	0.0	0.0
			MOLE FRACTION	
UO2	0.0	0.89258D 00	0.98905D 00	0.98905D 00
PUO1.5	0.0	0.98822D-02	0.10950D-01	0.10950D-01
			MOLE FRACTION	
U	0.99000D 00	0.0	0.0	0.0
PU	0.10000D-01	0.0	0.0	0.0
C	0.19000D 00	0.43689D-01		

TABLE A-2 (continued)

(T = 1800.00 K; P = 1.000D 00 ATM)

	X*/MOLE	Y/MOLE	P/ATM	ACTIVITY
AR	0.10000D-01	0.10000D-01	0.97785D 00	0.97785D 00
CO	0.0	0.22648D-03	0.22146D-01	0.22146D-01
CO2	0.0	0.38162D-09	0.37317D-07	0.37317D-07
U	0.0	0.13244D-13	0.12951D-11	0.12951D-11
PU	0.0	0.13124D-11	0.12833D-09	0.12833D-09
O2	0.90000D 00	0.11936D-20	0.11672D-18	0.11672D-18
PUO	0.0	0.12302D-10	0.12030D-08	0.12030D-08
PUO2	0.0	0.17259D-13	0.16877D-11	0.16877D-11
PUC2	0.0	0.26234D-12	0.25653D-10	0.25653D-10
UO	0.0	0.24323D-11	0.23784D-09	0.23784D-09
UO2	0.0	0.14353D-10	0.14036D-08	0.14036D-08
UO3	0.0	0.18314D-13	0.17909D-11	0.17909D-11
UC2	0.0	0.22408D-15	0.21912D-13	0.21912D-13
			MOLE FRACTION	
UC	0.0	0.0	0.0	0.0
UO	0.0	0.0	0.0	0.0
PUC	0.0	0.0	0.0	0.0
PUO	0.0	0.0	0.0	0.0
			MOLE FRACTION	
UC1.5	0.0	0.97514D-01	0.99865D 00	0.99865D 00
PUC1.5	0.0	0.13184D-03	0.13501D-02	0.13501D-02
			MOLE FRACTION	
UC1.9	0.0	0.0	0.0	0.0
PUC1.5	0.0	0.0	0.0	0.0
			MOLE FRACTION	
UO2	0.0	0.89249D 00	0.98906D 00	0.98906D 00
PUO1.5	0.0	0.98682D-02	0.10936D-01	0.10936D-01
			MOLE FRACTION	
U	0.99000D 00	0.0	0.0	0.0
PU	0.10000D-01	0.0	0.0	0.0
C	0.19000D 00	0.43304D-01		

TABLE A-2 (continued)

(T = 2000.00 K; P = 1.000D 00 ATM)

	X*/MOLE	Y/MOLE	P/ATM	ACTIVITY
AR	0.10000D-01	0.10000D-01	0.72635D 00	0.72635D 00
CO	0.0	0.37675D-02	0.27365D 00	0.27365D 00
CO2	0.0	0.26638D-07	0.19348D-05	0.19348D-05
U	0.0	0.94453D-12	0.68606D-10	0.68606D-10
PU	0.0	0.29738D-10	0.21600D-08	0.21600D-08
O2	0.90000D 00	0.11763D-17	0.85444D-16	0.85444D-16
PUO	0.0	0.38357D-09	0.27860D-07	0.27860D-07
PUO2	0.0	0.13848D-11	0.10058D-09	0.10058D-09
PUC2	0.0	0.29990D-10	0.21783D-08	0.21783D-08
UO	0.0	0.13576D-09	0.98611D-08	0.98611D-08
UO2	0.0	0.92904D-09	0.67480D-07	0.67480D-07
UO3	0.0	0.349830-11	0.25410D-09	0.25410D-09
UC2	0.0	0.43270D-13	0.31429D-11	0.31429D-11
			MOLE FRACTION	
UC	0.0	0.0	0.0	0.0
UO	0.0	0.0	0.0	0.0
PUC	0.0	0.0	0.0	0.0
PUO	0.0	0.0	0.0	0.0
			MOLE FRACTION	
UC1.5	0.0	0.99274D-01	0.99852D 00	0.99852D 00
PUC1.5	0.0	0.14700D-03	0.14785D-02	0.14785D-02
			MOLE FRACTION	
UC1.9	0.0	0.0	0.0	0.0
PUC1.5	0.0	0.0	0.0	0.0
			MOLE FRACTION	
UO2	0.0	0.89073D 00	0.98906D 00	0.98906D 00
PUO1.5	0.0	0.98530D-02	0.109410-01	0.10941D-01
			MOLE FRACTION	
U	0.99000D 00	0.0	0.0	0.0
PU	0.10000D-01	0.0	0.0	0.0
C	0.19000D 00	0.37102D-01		
IHC002I STOP	00000			

TABLE A-2 (continued)

(T = 1400.00K; P = 1.0000 00 ATM)

	X*/MOLE	Y/MOLE	P/ATM	ACTIVITY
AR	0.10000D-01	0.10000D-01	0.10000D 01	0.10000D 01
CO	0.0	0.20570D-07	0.20570D-05	0.20570D-05
CO2	0.0	0.22981D-15	0.22981D-13	0.22981D-13
U	0.0	0.90118D-18	0.90118D-16	0.90118D-16
PU	0.0	0.11099D-13	0.11099D-11	0.11099D-11
O2	0.90000D 00	0.12158D-29	0.12158D-27	0.12158D-27
PUO	0.0	0.16684D-13	0.16684D-11	0.16684D-11
PUO2	0.0	0.62738D-18	0.62737D-16	0.62737D-16
PUC2	0.0	0.20474D-17	0.20474D-15	0.20474D-15
UO	0.0	0.13301D-15	0.13301D-13	0.13301D-13
UO2	0.0	0.20520D-15	0.20519D-13	0.20519D-13
UO3	0.0	0.47448D-20	0.47448D-18	0.47448D-18
UC2	0.0	0.83262D-22	0.83262D-20	0.83262D-20
			MOLE FRACTION	
UC	0.0	0.47089D-01	0.98967D 00	0.98967D 00
UO	0.0	0.25558D-03	0.53714D-02	0.53714D-02
PUC	0.0	0.41620D-04	0.87472D-03	0.87472D-03
PUO	0.0	0.19428D-03	0.40832D-02	0.40832D-02
			MOLE FRACTION	
UC1.5	0.0	0.35074D-01	0.99513D 00	0.99513D 00
PUC1.5	0.0	0.17175D-03	0.48728D-02	0.48728D-02
			MOLE FRACTION	
UC1.9	0.0	0.0	0.0	0.0
PUC1.5	0.0	0.0	0.0	0.0
			MOLE FRACTION	
UO2	0.0	0.84758D 00	0.92412D 00	0.92412D 00
PUO1.5	0.0	0.69592D-01	0.75877D-01	0.75877D-01
			MOLE FRACTION	
U	0.93000D 00	0.0	0.0	0.0
PU	0.70000D-01	0.0	0.0	0.0
C	0.10000D 00	0.0		

TABLE A-2 (continued)

(T = 1600.00 K; P = 1.000D 00 ATM)

	X*/MOLE	Y/MOLE	P/ATM	ACTIVITY
AR	0.10000D-01	0.10000D-01	0.99991D 00	0.99991D 00
CO	0.0	0.85427D-06	0.85420D-04	0.85420D-04
CO2	0.0	0.83608D-13	0.83601D-11	0.83601D-11
U	0.0	0.69609D-15	0.69603D-13	0.69603D-13
PU	0.0	0.12660D-11	0.12659D-09	0.12659D-09
O2	0.90000D 00	0.37299D-25	0.37296D-23	0.37296D-23
PUO	0.0	0.27779D-11	0.27777D-09	0.27777D-09
PUO2	0.0	0.41707D-15	0.41704D-13	0.41704D-13
PUC2	0.0	0.21969D-14	0.21967D-12	0.21967D-12
UO	0.0	0.60569D-13	0.60564D-11	0.60564D-11
UO2	0.0	0.10361D-12	0.10360D-10	0.10360D-10
UO3	0.0	0.11922D-16	0.11921D-14	0.11921D-14
UC2	0.0	0.22255D-18	0.22253D-16	0.22253D-16
			MOLE FRACTION	
UC	0.0	0.46651D-01	0.98155D 00	0.98155D 00
UO	0.0	0.50159D-03	0.10554D-01	0.10554D-01
PUC	0.0	0.83547D-04	0.17579D-02	0.17579D-02
PUO	0.0	0.29187D-03	0.61409D-02	0.61409D-02
			MOLE FRACTION	
UC1.5	0.0	0.35323D-01	0.99474D 00	0.99474D 00
PUC1.5	0.0	0.18663D-03	0.52557D-02	0.52557D-02
			MOLE FRACTION	
UC1.9	0.0	0.0	0.0	0.0
PUC1.5	0.0	0.0	0.0	0.0
			MOLE FRACTION	
UO2	0.0	0.84752D 00	0.92427D 00	0.92427D 00
PUD1.5	0.0	0.69438D-01	0.75726D-01	0.75726D-01
			MOLE FRACTION	
U	0.93000D 00	0.0	0.0	0.0
PU	0.70000D-01	0.0	0.0	0.0
C	0.10000D 00	0.0		

TABLE A-2 (continued)

(T = 1800.00 K; P = 1.000D 00 ATM)

	X*/MOLE	Y/MOLE	P/ATM	ACTIVITY
AR	0.10000D-01	0.10000D-01	0.99843D 00	0.99843D 00
CO	0.0	0.15769D-04	0.15744D-02	0.15744D-02
CO2	0.0	0.84040D-11	0.88908D-09	0.83908D-09
U	0.0	0.12120D-12	0.12101D-10	0.12101D-10
PU	0.0	0.49922D-10	0.49843D-08	0.49843D-08
O2	0.90000D 00	0.11694D-21	0.11676D-19	0.11676D-19
PUO	0.0	0.14801D-09	0.14778D-07	0.14778D-07
PUO2	0.0	0.65676D-13	0.65572D-11	0.65572D-11
PUC2	0.0	0.50422D-12	0.50343D-10	0.50343D-10
UO	0.0	0.70397D-11	0.70286D-09	0.70286D-09
UO2	0.0	0.13139D-10	0.13119D-08	0.13119D-08
UO3	0.0	0.53024D-14	0.52941D-12	0.52941D-12
UC2	0.0	0.10361D-15	0.10345D-13	0.10345D-13
			MOLE FRACTION	
UC	0.0	0.46108D-01	0.97085D 00	0.97085D 00
UO	0.0	0.84183D-03	0.17726D-01	0.17726D-01
PUC	0.0	0.14339D-03	0.30192D-02	0.30192D-02
PUO	0.0	0.39893D-03	0.84000D-02	0.84000D-02
			MOLE FRACTION	
UC1.5	0.0	0.35622D-01	0.99441D 00	0.99441D 00
PUC1.5	0.0	0.20019D-03	0.55885D-02	0.55885D-02
			MOLE FRACTION	
UC1.9	0.0	0.0	0.0	0.0
PUC1.5	0.0	0.0	0.0	0.0
			MOLE FRACTION	
UO2	0.0	0.84743D 00	0.92445D 00	0.92445D 00
PUO1.5	0.0	0.69257D-01	0.75552D-01	0.75552D-01
			MOLE FRACTION	
U	0.93000D 00	0.0	0.0	0.0
PU	0.70000D-01	0.0	0.0	0.0
C	0.10000D 00	0.0		

TABLE A-2 (continued)

(T = 2000.00 K; P = 1.000D 00 ATM)

	X*/MOLE	Y/MOLE	P/ATM	ACTIVITY
AR	0.10000D-01	0.10000D-01	0.98353D 00	0.98353D 00
CO	0.0	0.16741D-03	0.16465D-01	0.16465D-01
CO2	0.0	0.34857D-09	0.34283D-07	0.34283D-07
U	0.0	0.75196D-11	0.73957D-09	0.73957D-09
PU	0.0	0.94661D-09	0.93103D-07	0.93103D-07
O2	0.90000D 00	0.75339D-19	0.74099D-17	0.74099D-17
PUO	0.0	0.35955D-08	0.35363D-06	0.35363D-06
PUO2	0.0	0.38227D-11	0.37597D-09	0.37597D-09
PUC2	0.0	0.39851D-10	0.39195D-08	0.39195D-08
UO	0.0	0.31829D-09	0.31305D-07	0.31305D-07
UO2	0.0	0.64141D-09	0.63085D-07	0.63085D-07
UO3	0.0	0.71125D-12	0.69954D-10	0.69954D-10
UC2	0.0	0.14380D-13	0.14144D-11	0.14144D-11
			MOLE FRACTION	
UC	0.0	0.45887D-01	0.95795D 00	0.95795D 00
UO	0.0	0.12768D-02	0.26656D-01	0.26656D-01
PUC	0.0	0.22250D-03	0.46451D-02	0.46451D-02
PUO	0.0	0.51483D-03	0.10748D-01	0.10748D-01
			MOLE FRACTION	
UC1.5	0.0	0.35605D-01	0.99411D 00	0.99411D 00
PUC1.5	0.0	0.21080D-03	0.58856D-02	0.58856D-02
			MOLE FRACTION	
UC1.9	0.0	0.0	0.0	0.0
PUC1.5	0.0	0.0	0.0	0.0
			MOLE FRACTION	
UO2	0.0	0.84723D 00	0.92464D 00	0.92464D 00
PUO1.5	0.0	0.69052D-01	0.75361D-01	0.75361D-01
			MOLE FRACTION	
U	0.93000D 00	0.0	0.0	0.0
PU	0.70000D-01	0.0	0.0	0.0
C	0.10000D 00	0.0		
IHO002I STOP	00000			

A.1. U-Pu-C-O PHASE EQUILIBRIA

Potter (1970) has drawn a pseudo-ternary phase diagram for the U-Pu-C-O system in which he suggests that the sesquicarbide ($MC_{1.5}$, where M is the actinide) is stabilized with respect to the dicarbide by the presence of plutonium. This appears likely because of the similar free energies of formation of $UC_{1.9}$ and $UC_{1.5}$, and the fact that plutonium does not form a dicarbide. The presence of plutonium would thus increase the stability of the sesquicarbide, and since the difference in the free energies of formation of the phases is small, the $MC_{1.5}$ phase probably forms. This is supported by the results of the SOLGASMIX-PV calculations where free carbon plus $U_{1-x}Pu_xC_{1.5}$ forms in preference to $U_{1-k}Pu_kC_{1.9-0.4k}$.

In his phase diagram, Potter (1970) does not indicate the plutonium concentration at which the dicarbide decomposes yielding carbon and the sesquicarbide. The calculations indicate that the limit is at a value of $Pu/U + Pu < 0.01$, which seems reasonable.

The most important conclusion, therefore, is that at equilibrium a dicarbidedioxide fuel, which initially contained no free carbon, reacts to form sesquicarbide and free carbon due to bred-in plutonium.

A.2. FISSION PRODUCT EFFECTS ON PHASE EQUILIBRIA

Using the thermal fission product yields of Meek and Rider (1974) and the analysis of Homan et al. (1977), it is possible to determine the influence of the fission products on the phase equilibria of the fuels. The fission yields of the metals and the compounds they form are listed below.

Species	Percent/U-235 Fission
$(RE^*,La,Y)O_{1.5}$	61
ZrC	37
BaC_2	6.8
SrC_2	9.6

*Rare earths

Thus 0.915 oxygen atoms and 0.698 carbon atoms are required per fission to form the fission product phases. Table A-3 illustrates an oxygen and carbon balance for fuel at 20% FIMA.

The balance of the released oxygen shown in Table A-3 must react with the actinide carbide to form free carbon and oxide. If this occurs, the fraction of carbon atoms released equals 0.160 and 0.109 for the 15% and 25% converted fuel, respectively. The fuel, therefore, still contains free carbon since that released by the formation of the oxide exceeds the deficit in the carbon balance for the converted fuel. Note that the results of the SOLGASMIX-PV calculations indicate some partitioning of plutonium among the phases, but this has been ignored as it does not significantly influence the results.

A.3. PARTIAL PRESSURES OF PLUTONIUM-CONTAINING SPECIES

The equilibrium partial pressures of the various vapor species are indicated in the output from the SOLGASMIX-PV calculations. The sums of the pressures of the plutonium-containing species (essentially PuO and Pu) are plotted versus reciprocal temperatures in Fig. A-1. It can be seen from these results that the pressures are somewhat sensitive to both plutonium concentration in the condensed phases and to the phases present, but only slightly sensitive to the amount of each phase. Dropping the plutonium concentration from a Pu/U + Pu = 0.07 to the value Pu/U + Pu = 0.01 decreases the pressure by a factor of 7. Moving from the phase field containing monoxycarbide to that containing carbon instead reduces the pressure by a factor of 2.

A.4. AREAS OF UNCERTAINTY AND SUGGESTIONS FOR FUTURE WORK

The greatest uncertainty is in the concentration of plutonium necessary to make the sesquicarbide plus carbon more stable that the dicarbide. In the unlikely event that it is appreciably greater than Pu/(U + Pu) = 0.01, the sesquicarbide would only form if there were insufficient available carbon to form the dicarbide (i.e., after some burning). In the even more

TABLE A-3

OXYGEN AND CARBON BALANCE AT 20% FIMA AND Pu/U + Pu = 0.07

	10% Converted		25% Converted	
	Oxygen	Carbon	Oxygen	Carbon
Released				
Due to fission	1.8 x 0.2 = 0.36	0.19 x 0.2 = 0.038	1.5 x 0.2 = 0.30	0.475 x 0.2 = 0.095
Due to $MC_{1.9} \rightarrow MC_{1.5} + 0.4C$	-	0.04	-	0.1
Due to $UO_2 \rightarrow (PuO_{1.5})^{(a)}_{UO_2}$	0.315	-	0.0263	-
Reacted				
Form fission product compounds	0.915 x 0.2 = 0.183	0.698 x 0.2 = 0.14	0.915 x 0.2 = 0.183	0.698 x 0.2 = 0.14
Balance	0.209	-0.062	0.143	0.055

(a) Denotes $PuO_{1.5}$ dissolved in UO_2 due to transmutation of U-238.

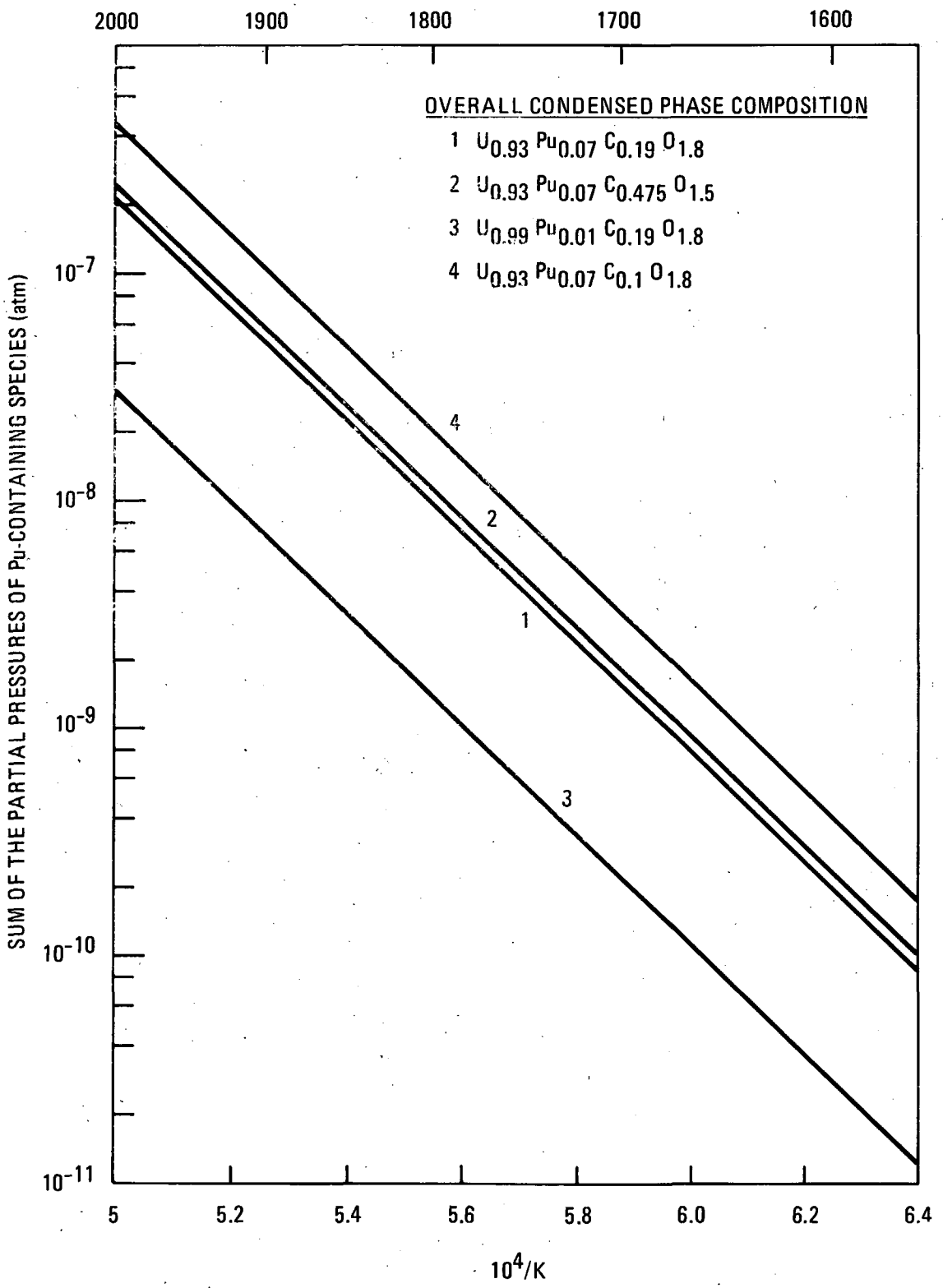

Fig. A-1. Sum of Pu-containing species over U-Pu-C-O of various compositions as a function of reciprocal temperatures

unlikely situation that the sesquicarbide is unstable with respect to the dicarbide and monoxycarbide, as appears to be the case in the U-C-O system (Potter, 1972), then the system would enter a dicarbide plus monoxycarbide plus dioxide phase region. The plutonium-containing species' pressures over this region would be less than those over that containing the sesquicarbide.

The questions about phase equilibria noted above could be answered with a series of experiments in which samples are prepared with compositions in the ranges of interest and annealed at the appropriate temperatures. Examination, by X-ray diffractometry, of the phases present should indicate the proper phase equilibria.

The next most important question is whether the various solutions, treated as ideal, do exhibit ideal solution behavior. There is still a question as to the ideality of the $UC_{1-x}O_x$ solid solution (Potter, 1972) as well as to the $U_{1-z}Pu_zC_{1-\ell}O_\ell$ solid solution. This is presently under investigation by Lindemer and Besmann of ORNL using equilibrium CO pressure measurement over systems of various compositions.

A.5. CONCLUSIONS

1. Although an MEU fuel may initially contain only $UC_{1.9}$ and UO_2, the breeding in of significant amounts of plutonium (>1%) will, at thermodynamic equilibrium, likely cause the dicarbide to decompose to the sesquicarbide plus carbon.

2. Fission products generated in the fuel will react to form oxides and carbides. Even at low initial concentrations of $UC_{1.9}$ (10% conversion) and considerable burnups (20% FIMA), however, enough carbon is free to form fission product carbides without decomposing the actinide sesquicarbide to monoxycarbide.

3. Should the monoxycarbide form, its effect on the plutonium-bearing species partial pressures is not great, increasing their sum by only a factor of 2. The pressures are considerably more sensitive to the concentration of plutonium in the system.

REFERENCES

Ackerman, R. J., and M. S. Chandrasekharaiah, Proc. Symposium on the Thermodynamics of Nuclear Materials, 1974; Vienna, Vol. 2 (October), p. 3.

Besmann, T. M., 1975; "SOLGASMIX-PV, A Computer Program to Calculate Equilibrium Relationships in Complex Chemical Systems," ORNL Report ORNL/TM-5775 (April).

Besmann, T. M., 1975; J. Nuc. Mater. 67, p. 77.

Faircloth, R. L., R. H. Flowers, and F. C. W. Pummery, 1968; J. Inorg. Nucl. Chem. 30, p. 499.

Homan, F. J., et al., 1977; Nuc. Tech. 35(2), p. 428.

JANAF, 1971; Thermochemical Tables, D. R. Stull and A. Prophet, ets., Second Ed., U. S. Government Printing Office, Washington.

Meak, M. E., and B. F. Rider, 1974;"Compilation of Fission Product Yields," General Electric Report NEDO-12154-1 (January).

Oetting, F. L., M. H. Rand, and R. J. Ackerman, 1976; The Chemical Thermodynamics of Actinide Elements and Compounds, Part I, "The Actinide Elements," IAEA, Vienna.

Potter, P. E., and W. G. Roberts, 1968; "Inhomogeneity in Sintered Uranium-Plutonium Carbides and Oxycarbides," AERE Report AERE-R 5661 (January).

Potter, P. E., 1970; Plutonium 1970 and Other Actinides, W. N. Miner, ed., The Metallurgical Society, p. 859.

Potter, P. E., 1972; J. Nuc. Mater. 42, p. 1.

Potter, P. E., and M. H. Rand, 1977; unpublished assessment.

Rand, M. H., et al., 1977; unpublished assessment.

Schumm, R. H., et al., 1973; U. S. NBS Technical Note 270-7.

Tetenbaum, M., A. Sheth, and W. Olson, 1975; "A Review of the Thermodynamics of the U-C, Pu-C, and U-Pu-C Systems," ANL Report ANL-AFP-8.

APPENDIX B
IRRADIATION TEST OF LOW-ENRICHED FUEL IN THE FRG

R. Gontard
Kernforschungsanlage Jülich

Irradiation tests carried out in the past years have led to the accumulation of extensive experience with LEU oxide fuel. Spherical fuel elements were used in different material test reactors to test the coated particles, which were in the form of compacts or coupons as well as loose. The reactors used were:

1. BR2, Mol, Belgium
2. HFR, Petten, Netherlands
3. R2, Studsvik, Sweden
4. DR Dragon reactor, Winfrith, Great Britian
5. FRJ2 (Dido), KFA Jülich, Federal Republic of Germany
6. AVR, KFA Jülich, Federal Republic of Germany

Particle design and irradiation experiment data are given in Tables B-1 (HOBEG fuel) and B-2 (fuel produced at KFA) along with remarks on post-irradiation examination results.

The designation used to identify experiments consists of three parts: (1) the reactor used, (2) the kind of experiment (P = particle, K = sphere, M = matrix), and (3) the number of the experiment. For instance, BR2-P10 means particle experiment number 10 in the BR2 reactor.

TABLE B-1

LEU FUEL PRODUCED AT HOBEG

Particle Batch	Experiment	Kernel				Coating										Irradiation						Postirradiation Examination		
							Buffer		Inner PyC		SiC		Outer PyC												
		Composition	Enrichment (%)	Density (g/cm^3)	Diameter (µm)	BISO/TRISO	Thickness (µm) Dep. from: C_2H_2	Density (g/cm^3)	Thickness (µm) Dep. from: C_3H_6	Density (g/cm^3)	Thickness (µm) Dep. from: CH_3SiCl_3	Density (g/cm^3)	Thickness (µm) Dep. from: C_3H_6	Density (g/cm^3)	Total Coating (µm)	Particle Diameter (µm)	Experiment	Capsule/Sphere	Time (fpd)	Temperature (°C)	Burnup (% FIMA)	Fluence 10^{21} cm^{-2} (E > 0.1 MeV)	Failure Mechanism	Particle Failure (%)	State
DO 760 t	BR2-P11 BR2-P12 FRJ2-P15	UO_2	9.5	10.56	591	B	82	<0.7	100	1.94	-	-	-	-	182	957	BR2-P11 BR2-P12 FRJ2-P15	2 1 2 + 4	366 541 444	1210-850 1100-1150 1250-850	24 19 20/19	9.9 1.5×10^{22} <2	Amoeba radial cracks in buffer & PyC. Annealing test indicates broken particles. All particles intact	69 98 31 98	Completed In progress In progress
DO 761 t	BR2-P12 FRJ2-P15	UO_2	9.5	10.56	590	B.	80	0.9	154	1.92	-	-	-	-	234	1050	BR2-P12 FRJ2-P15	1 + 2 3	541 444	1100-1150 1150-800	19 21	1.5×10^{22} <2	- Broken particles	-	In progress In progress
DO 765 t	BR2-P11	UO_2	9.5	10.56	603	B	160	<1.1	98	1.93	-	-	-	-	258	1102	BR2-P11	3	366	1200-950	18-22	6-8	Amoeba Amoeba Radial cracks Tangential cracks Tangential cracks Burst test	30 95 21 15 60 0	Completed
DO 767 t	BR2-P11	UO_2	9.5	10.56	591	B	40	<1.2	100	1.95	-	-	-	-	140	850	BR2-P11	1	366	1225-900	20-22	7-8	Amoeba Amoeba Radial cracks Damage Burst test	37 82 31 18 59	Completed
DO 787 t	BR2-P12 FFJ2-P15	UO_2	9.5	10.56	595	B	79	<0.7	52	1.99	-	-	-	-	131	868	BR2-P12 FRJ2-P15	1 + 2 1	541 444	1100-1150 1200-1000	19 16	1.5×10^{22} <2	Reaction kernel/coating Possibly some broken particles.	3 55 3	In progress In progress
EO 241/243/244 t	R2-K5 DR-S2 HFR-M5	UO_2	6.6	10.7	596	B	76	0.94	92	2.02	-	-	-	-	168	800-1000	R2-K5 DR-S2 HFR-M5	1 1 + 3	438 270 239	1000 1100 970/980	11.2 2-4 6.8/5.1	7.44 2.7 3.1/2.7	Particles intact	0 0	At USGAE Completed In progress
EO 249/250/251 t	BR2-P15 DR-S4	UO_2	9.49	10.3	616	T	67	-	42	-	34	3.19	36	1,935	174	800-1000	BR2-P15 DR-S4	1 + 2	375 656	1300/1150 920	11.2/8.2 5.8	10.7/6.4 4.1	Comp. 8 + 13 disintegration. T/C-corrosion Comp. 2 Comp. 5 Comp. 6 Comp. 7 Amoeba penetration 65 um. Tang. cracks in buffer. -	6 50-60 25-30 15-20 15 0	In progress At AERE
EO 391 t	DR-K5	UO_2	9.51	10.9	602	B	90	0.94	73	2.02	-	-	-	-	163	800-1250	DR-K5	1 - 27	334	1210	3.2-5.5	1.1-2.7	Particles intact		In progress
EO 403-405 t	DR-S3 DR-S6 HFR-M5	UO_2	6.65	10.47	615	T	86	-	46	-	29	0.21	38	1.94	199	900-1250 900-1250	DR-S3 DR-S6 HFR-M5	2	334 550 239	1100 1160 990	3-4 4-6 9.7	2.5 4.1 5.0	- - -	0	Harwell In progress
EO 414-428 t	AVR VI FRJ2-K8	UO_2	0.714 U_{nat}	10.57	608	B	89	1.05	77	1.97	-	-	-	-	n.b.	947	AVR VI FRJ2-K8	5 + 6	137	1200 1240-800	3.2 7.7/7.1	0.5-1.0 0.01	- -		In progress In progress
EO 431-441 t	AVR VI FRJ2-K8	UO_2	14.95	10.39	618	B	98	1.01	80	1.96	-	-	-	-	n.b.	944	AVR VI FRJ2-K8	5 + 6	137	1200 1240-800	3.7 7.7/7.1	0.5-1.0 0.01	Radial cracks in buffer -	0-25 0-10 0-25 -	In progress In progress

TABLE B-2

LEU FUEL PRODUCED AT KFA

Particle Batch	Experiment	Kernel: Composition	Kernel: Enrichment (%)	Kernel: Density (g/cm³)	Kernel: Diameter (µm)	Coating: BISO/TRISO	Coating: Buffer Thickness (µm)	Coating: Buffer Density (g/cm³) Dep. from: C_2H_2	Coating: Inner PyC Thickness (µm)	Coating: Inner PyC Density (g/cm³) Dep. from: C_3H_6	Coating: SiC Thickness (µ)	Coating: SiC Density (g/cm³) Dep. from CH_3SiCl_3	Coating: Outer PyC Thickness (µm)	Coating: Outer PyC Density (g/cm³) Dep. from: C_3H_6	Coating: Total Coating (µm)	Particle Diameter (µm)	Irradiation: Experiment	Irradiation: Capsule/Sphere	Irradiation: Time (fpd)	Irradiation: Temperature (°C)	Irradiation: Burnup (% FIMA)	Irradiation: Fluence 10^{21} cm^{-2} (E > 0.1 MeV)	Postirradiation Examination: Failure Mechanism	Postirradiation Examination: Particle Failure (%)	Postirradiation Examination: State
PAUOC 881	DR-P5/3 FRJ2-P16	UO_2 + 3% UC	11.01	10.1	604	B	83	-	101	1.952	-	-	-	-	184	966	DR-P5/3 FRJ2-P16		336 207	1390-1100 1600-960	3.1-7.8 10-12	1.1 0.34-0.46	- Amoeba	- 60-85	Completed Completed
PAUO 882	DR-P5/3 FRJ2-P16	UO_2	11.01	10.6	614	B	70	-	75	2.008	-	-	-	-	145	860	DR-P5/3 FRJ2-P16	22	336 207	1390-1100 1600-960	3.1-7.8 10-12	1.1 0.34-0.46	Slight amoeba -	- 50	Completed Completed
PAUC 883	DR-P5/3 FRJ2-P16	UC_2	11.01	n.b.	600	B	61	-	105	1.836	-	-	-	-	166	1037	DR-P/3 FRJ2-P16	1 - 4	336 207	1390-1100 1600-960	3.1-7.8 10-12	1.1 0.34-0.46	- Reaction with PyC layer	- -	Completed Completed
PSPAUO 1024	DR-P5/3 FRJ2-P16	UO_2	11.01	10.6	614	T	75	-	30	-	50	3.114	39	1.917	194	984	DR-P5/3 FRJ2-P16	1 - 4	336 207	1390-1100 1600-960	3.1-7.8 10-12	1.1 0.34-0.46	SiC corrosion on outer SiC surface. Amoeba	- -	Completed Completed
PSPAUC 1027	DR-P5/3 FRJ2-P16	UC_2	11.01	n.b.	580-610	T	n.d.	-	31	-	31	3.202	36	1.888	n.d.	970	DR-P5/3 FRJ2-P16	1 - 4	336 207	1390-1100 1600-960	3.1-7.8 10-12	1.1 0.34-0.46	Drastic SiC corrosion Amoeba	- -	Completed Completed
PSPAUOC 1042	DR-P5/3 FRJ2-P16	UO_2 + 3% UC	11.01	10.1	610	T	80	-	37	-	49	3.211	25	1.969	191	1069	DR-P5/3 FRJ2-P16	1 - 4	336 207	1390-1100 1600-960	3.1-7.8 10-12	1.1 0.34-0.46	Outer SiC surface (temp. dep.) Amoeba	- -	Completed Completed
PAUO 1260	FRJ2-P17	UO_2	15	10.91	684	B	60	-	120	2.01	-	-	-	-	180	1040	FRJ2-P17	2	114	1200	8.3	0.2	-	-	In progress
PAUASiO 1261	FRJ2-P17	UO_2 +10% $AlO_{1.5}$ +10% SiO_2	15	9.5	671	B	60	-	118	2.025	-	-	-	-	178	1040	FRJ2-P17	3	114	1140	7.9	0.2	-	-	In progress
PAUASiO 1262	FRJ2-P17	UO_2 +15% $AlO_{1.5}$ + 5% SiO_2	15	9.31	668	B	60	-	116	2.02	-	-	-	-	176	1000	FRJ2-P17	4	114	1140	8.2	0.2	-	-	In progress
PAUZO 1263	FRJ2-P17	UO_2 +20% ZrO_2	15	9.77	682	B	65	-	134	2.05	-	-	-	-	199	1040	FRJ2-P17	1	114	1180	7.1	0.2	-	-	In progress

B.1. EXPERIMENT BR2-P10

Objectives

1. Investigate the irradiation behavior of propene PyC with different parameters in comparison with methane PyC.

2. Determine the influence of different positions of the sealing layer.

3. Compare with particles irradiated in other experiments.

4. Compare loose and bonded particles.

5. Determine the dependence of kernel swelling on porosity and enrichment.

6. Determine the influence of CO pressure in carbide-doped oxide kernels.

7. Investigate the irradiation behavior of particles without inner pressure (graphite particles).

Loading

Thirty-six particle variants with different kernel compositions and coatings were tested, but only four of them were medium-enriched (20% and 40%) UO_2 kernels (M2AUO 411, 412, 427, and 431 produced at KFA). They were loaded in two magazines of the lower, uninstrumented capsule of the irradiation facility. The particles were irradiated in coupons (LEU) as well as loose in graphite magazines with annular grooves.

Irradiation Data (20% Enriched Fuel)

Irradiation time, fpd	258
Burnup, % FIMA	11-13

Fast fluence, 10^{21} cm^{-2} (E>0.1 MeV)	10-8.6
Temperature, °C	1150
In-pile R/B, (Kr-88)	$5x10^{-6}$ to $2x10^{-2}$

Postirradiation Examination

The PIE work on the MEU fuel, carried out only with respect to kernel swelling, produced the following results:

Enrichment (%)	Increase of Kernel Diameter (%)	Initial Kernel Porosity (%)
20	8-10	1
40	4-16	1
20	4.5-7.5	5-10

B.2. EXPERIMENT BR2-P11

Objectives

1. Determine particle endurance as a function of the thickness of the porous PyC layer and compare with stress model calculations.

2. Determine the influence of the outer HDI layer on the integrity of the particles at the HTR burnup dose.

3. Determine the incidence of particle failure as a function of free volume (in the buffer layer).

Loading

Three BISO particle variants with identical kernel geometry but different buffer layer thicknesses were used. The particles were pressed in monolayer coupons, and each variant was separately loaded in one capsule.

Capsule	Batch No. (HOBEG)	Buffer Layer Thickness (μm)
1	DO 767 t	40
2	DO 760 t	80
3	DO 765 t	160

Irradiation Data

	Capsule 1	Capsule 2	Capsule 3
Irradiation time, fpd	366	366	366
Burnup, % FIMA	20.2-22.6	24.2-24.5	18.6-22.2
Fast fluence, 10^{21} cm^{-2} (E>0.1 MeV)	7.37-8.75	9.75-9.90	6.68-8.65
Temperature, °C	1225-900	1210-850	1200-850
In-pile R/B, (Kr-88)	2×10^{-6}-2×10^{-3}	2×10^{-6}-7×10^{-3}	5×10^{-7}-3×10^{-5}

Postirradiation Examination

Capsule 1 (Buffer Layer 40 μm)

Only small amoeba migration was found, but it increased with higher fluence. In the upper part of the capsule, all particles were intact. The particles in the middle part showed radial cracks in the buffer layer. These cracks sometimes led to breakage of the whole coating. In the lower part, the cracks were smaller and amoeba migration was only detected within the buffer layer due to different temperatures and temperature gradients. The annealing test showed particle bursts at temperatures higher than 1000°C. A number of particles had released 35% to 55% of the total Kr-85 inventory. After disintegration, defective particles were found only in this variant (approximately 25%) depending on irradiation

temperature, fission gas pressure, and the interaction between the kernel and the buffer layer.

Capsule 2 (Buffer Layer 80 μm)

Because of high temperatures and fluences, a stronger amoeba effect was detected, sometimes up to 55 μm. Tangential cracks were found within the buffer layer as well as on the surface buffer/HDI, and gaps were found between the kernel and the buffer layer, but no failure caused fission product release. Particle burst during the annealing test began at 1200° to 1400°C. See Table B-3.

Capsule 3 (Buffer Layer 160 μm)

A smaller amoeba attack was noted, and tangential cracks within the buffer layer were found. In the upper part of the capsule, the kernels had large fission gas bubbles and gaps between the kernel and the buffer layer. In the lower part, all particles were intact. No particle failed during annealing of the coupons up to 1800°C, but when particles were annealed after disintegration the burst began 300° to 400°C. This may have been caused by a poor disintegration method. See Table B-4.

Conclusions

1. The large volume of the buffer layer improves the high-temperature behavior of coated particles.

2. Different failure behavior of particles from the same coupon indicates the buildup of cracks in the outer HDI layer was caused by neutron-induced embrittlement.

3. Fission gas pressure and accompanying mechanical stresses affect the permeability of the coating.

TABLE B-3
RESULTS FROM ANNEALING TESTS WITH 600-μm UO_2 PARTICLES
(9.5% ENRICHED) WITH 80-μm BUFFER LAYER (LTI BISO COATING)
IRRADIATED IN CAPSULE 2 OF BR2-P11

Sample Designation	Sample Designation	Irradiation Conditions		Annealing			
		Burnup (% FIMA)	Fluence ($10^{21}cm^{-2}$) (E>0.1 MeV)	Earliest Defect (°C)	Fracture of Coupon (°C)	Kr-85 Release From Coupon (%)	Broken Particles (%)
DO 760 t	1	24.3	9.8	1600	1500	20	100
	24	24.5	9.9	1230	1500	19	90
	23	24.5	9.9	1340	1600	23	100
	20	24.3	9.8	1170	1420	19	95

TABLE B-4
RESULTS FROM ANNEALING TESTS WITH 600-μm UO_2 PARTICLES WITH
160-μm BUFFER LAYER IRRADIATED IN CAPSULE 3 OF BR2-P11

Sample Designation	Sample Designation	Irradiation Conditions		Annealing	
		Burnup (% FIMA)	Fluence ($10^{21}cm^{-2}$) (E>0.1 MeV)	Temperature Reached Without Bursts (°C)	Temperature at which Particles Burst After Disintegration of Coupons (°C)
DO 765 t	5/11, 1,22	19-22	7 - 8.5	1800	400
	5/12, 21,17	20.5-22	7.8 - 8.5	1800	300

New microstructural investigations by small angle X-ray scattering (SAXS) and transmission electron microscopy (TEM) of the as-deposited OLTI coatings showed a high number of cracks indicating a subsequent irradiation performance (either failed coatings or cracks, leading to permeability).

B.3. EXPERIMENT BR2-P12

Objective

Test particles with different thicknesses of dense PyC (LTI) layer in connection with stress model calculations and correlation with burnup, temperature, and fast fluence.

Loading

In one swept capsule divided into three capsule units, 162 coupons with annularly arranged particles, each loaded with three particle variants, were tested. In a second uninstrumented capsule, loose particles were irradiated. The particle variants (all HOBEG) were DO 760 t (100 µm HDI), DO 761 t (154 µm), and DO 787 t (52 µm), all with BISO coatings.

Irradiation

It was planned first to irradiate the experiment up to a fast fluence of 9×10^{21} n/cm^{-2} (E > 0.1 MeV). After 311 fpd, the R/B values of 10^{-5} indicated 100% intact particles. Therefore, the irradiation was continued up to a fast fluence of 1.5×10^{22} to get a significant number of particles.

Irradiation Data

Irradiation time, fpd	541
Burnup, % FIMA	19
Fast fluence, 10^{21} cm^{-2} (E>0.1 MeV)	1.5×10^{22}
Temperature, °C	1100 - 1150
In-pile R/B, Kr-88	$3 \times 10^{-6} \rightarrow 5 \times 10^{-3}$

Postirradiation Examination

Capsule 1

The particles with the thinnest outer HDI layer had the highest failure rate (Table B-5), and the particles with thicker HDI layers showed large amoeba attack, depending on their position in the capsule. The buffer layer often had tangential cracks, which partly led to decoupling between the buffer and the HDI layer. The tendency to cracking in the HDI layer increased with fluence.

Capsule 2

Little amoeba migration occurred in all three variants, and tangential cracks in the buffer layer.

Capsule 3

The same effects were observed as in capsules 1 and 2, but more defined. In 14 particles, radial cracks had propagated through the whole coating.

The annealing test on batch DO 760 t (HDI layer 100 μm) showed a clear dependence of particle endurance on burnup and fast fluence (Table B-5). Table B-6 gives coupon annealing test results.

The particles in the capsule were positioned as follows:

Upper: bursts at temperatures higher than 1500°C
Middle: bursts at temperatures higher than 1300°C
Lower: no bursts up to 1800°C.

New SAXS and TEM studies showed pronounced differences in the LTI properties of these three coatings. The effect of LTI variation, therefore, may be added to the influence of coating thickness on irradiation performance. (P. Krautwasser, personal communication).

TABLE B-5
RESULTS FROM MICRORADIOGRAPHS

Particle Type	In Coupons		Loose	
	Number	Failure Fraction	Number	Failure Fraction
DO 787 t (50 μm HDI)	2530	6×10^{-3}	481	1.5×10^{-2}
DO 760 t (100 μm HDI)	2484	8×10^{-4}	402	2×10^{-3}
DO 761 t (150 μm HDI)	2438	8×10^{-4}	454	-

TABLE B-6
RESULTS FROM ANNEALING TESTS OF COUPONS

Particle Designation	Sample Designation	Irradiation Conditions		Annealing			
		Burnup (% FIMA)	Fluence (10^{21} cm^{-2}) (E>0.1 MeV)	Earliest Defect (°C)	Fracture of Coupon (°C)	Kr-85 Release From Coupon (%)	Broken Particles (%)
DO 760 t	0/13	14.9	13.4	-	-	0.35	0
	0/14	15.0	13.4	-	-	0.25	0
	0/15	15.0	13.4	-	-	0.44	0
	2-4	18.2	14.8	>1400		2.2	0
	2-5	18.2	14.8	>1400		10	0
	0/41	17.4	14.4	-		2.2	0
	0/30	16.0	13.4	1560	1560	7.3	55
	0/29	16.0	13.4	1550		1.8	0

B.4. EXPERIMENT BR2-P15

Objectives

1. Test TRISO LEU particles up to maximum power reactor conditions; i.e., burnup 12% FIMA, fast fluence 8×10^{21} cm^{-2} (E > 0.1 MeV), temperature 1300°C.

2. Compare the particles with SiC in propene-PyC and SiC in methane-PyC.

Loading

The particles were pressed in compacts with a fuel-free zone of 3 mm. Eight compacts at a time were loaded in instrumented capsules. The particle batch was EO 249/250/251 t (HOBEG).

Irradiation (Similar to BR2-P11)

Because parts of the loading failed after 18 months of irradiation time, the experiment was terminated.

Irradiation Data

	Capsule 1	Capsule 2
Irradiation time, fpd	375	375
Burnup, % FIMA	11.05	8.15
Fast fluence, $10^{21} cm^{-2}$ (E>0.1 MeV)	10.7	6.41
Temperature, °C	1300 - 800	1150
In-pile R/B, Kr-88	4×10^{-8}	1.6×10^{-2}

Postirradiation Examination

The particle damage in instrumented capsule 1, caused by corrosion of thermocouples (Cr-Ni), was between 5% and 60%. The thermocouples were mounted in the fuel-free zone of the compacts. The amoeba effect was detected mostly in the outer part of the compacts of capsule 1 (up to 65 μm), but no amoeba effect was found in capsule 2. After electrolytical disintegration of two compacts from 1000 particles, 60 from each were observed to be damaged.

B.5. EXPERIMENT FRJ2-P15

Objective

Determine the influence of burnup on the lifetime of particles with different outer PyC layer thicknesses.

Loading

Three particle variants pressed in coupons were loaded in four separately swept capsules, each containing 32 coupons. Particle batches (HOBEG) were as follows:

Capsule	Batch
1	DO 787 t
2	DO 760 t
3	DO 761 t
4	DO 760 t

Irradiation

The target values of this experiment - irradiation to 10-30% particle breakage - could not be reached because of particle failures in capsules 1 and 3.

Irradiation Data

	Capsule			
	1	2	3	4
Irradiation time, fpd	444	444	444	444
Burnup, % FIMA	16.58	20.37	20.63	19.18
Fast fluence, 10^{21} cm^{-2} (E>0.1 MeV)	1.5	1.5	1.5	1.5
Temperature, °C	1200-930	1200-850	1100-800	1250-870
In-pile R/B, Kr-88	first 300 fpd constant 10^{-5}, then continous increases to $1x10^{-2}$			

Postirradiation Examination

Postirradiation annealing showed that particles in capsules 2 and 4 (DO 760 t) were completely intact, while failures occurred in capsules 1 and 3. Kr-85 release from broken particles increased steadily from 25% at 1000°C to 50% at 2200°C.

B.6. EXPERIMENT FRJ2-P16

Objectives

1. Determine the influence of different kernel compositions and coatings under variable irradiation temperatures on the amoeba kinetics.

2. Determine the influence of carbide doping in the kernels.

3. Compare high- and low-enriched kernels.

Loading

The particles were partly pressed in coupons and partly put loose in graphite magazines with annular gaps. Into each of the four separately swept steel capsules, 24 coupons and 6 graphite magazines were loaded.

Particle batches (KFA) were: PSPAUO 1027, PSPAUOC 1042, PAUOC 881, PAUO 882, PAUO 883, and PSPAUO 1024.

Irradiation

Temperature was kept constant (He-N_2 mixture), independent fission gas measurement was possible in all four capsules.

Irradiation Data

	Capsule			
	1	2	3	4
Irradiation time, fpd	207	207	207	207
Burnup, % FIMA	10.0	11.9	12.0	11.5
Fast fluence, 10^{21} cm^{-2} (E>0.1 MeV)	0.34	0.41	0.46	0.36
Temperature, °C	1480-1020	1590-1190	1600-1130	1470-960
In-pile R/B, Kr-88	$5x10^{-5}$-$2x10^{-4}$	$2x10^{-4}$-$2x10^{-3}$	$3x10^{-4}$-$2x10^{-3}$	$3x10^{-5}$-10^{-4}

Postirradiation Examination

Carbide-doped and UC_2-BISO particles did not show any amoeba attack. Extremely large kernel migration was observed on UO_2 particles if there was a significant kernel/coating gap. This gap was more defined on particles with thicker buffer layers because of higher shrinkage of these layers. The TRISO variants showed less amoeba attack above 1500°C. Oxide kernels with added carbides did not show any improvement with respect to the amoeba effect above 1000°C. There was a stronger tendency to kernel migration in HEU $(U,Th)O_2$ kernels than in LEU oxide kernels.

CO measurements in TRISO particles at Seibersdorf demonstrated the effectiveness of the carbide additions in gettering oxygen:

O/F = 0.045 in UO_2 kernels
O/F = 0.001 in UO_2 + 3% UC kernels.

B.7. EXPERIMENT FRJ2-P17

Objective

Test fuel kernels with oxide additives Al_2O_3, ZrO_2, and SiO_2.

Loading

These additives should decrease the release of solid fission products like Sr, Ba, and Cs. The particles were designed to have the same geometry but different kernel compositions to get well-defined statements about the influence of kernel material on release of solid fission products.

Eight particle variants (four variants with low enriched fuel) were pressed in coupons. They were stacked into four separately swept capsules. Each capsule contained two particle variants separated by Mo plates (36 coupons/capsule).

LEU particles (KFA) in capsule 1, PAUZO 1263; 2, PAUO 1260; 3, PAUASiO 1261; and 4, PAUASiO 1262.

Particles with $(U,Th)O_2$ HEU kernels with and without chemical additives were also tested.

Irradiation

The increase of R/B values in capsules 1, 3, and 4 led to the termination of the experiment.

Irradiation Data

	Capsule			
	1	2	3	4
Irradiation time, fpd	114	114	114	114
Burnup, % FIMA	7.1	8.3	7.9	8.2
Fast fluence, 10^{21} cm^{-2} (E>0.1 MeV)	0.25	1.29	0.23	0.15
Temperature, °C	1180	1200	1140	1140
In-pile R/B, Kr-88	$6x10^{-8}$ to 10^{-6}	$2x10^{-7}$ (constant)	$8x10^{-8}$ to $5x10^{-6}$	$2x10^{-7}$ to $2x10^{-5}$

Postirradiation Examination

High concentrations of solid fission products could be detected in the ceramic phase formed by the kernel additives. Strong chemical interactions took place between the fission products Sr, Ba, and Cs and the alumina-silica inclusions, while the rare earths and the other metallic fission products were deposited in the fuel. In the porous buffer layer, in addition to solid fission products, Si and Al were found. These alumina-

silica precipitations in the coating with Si/Al ratios between 2.0 and 2.5 had equal fission product gettering properties by chemical reactions as the ceramic additives in the kernel.

Apart from local concentration peaks, the Cs concentration level in the porous PyC layer was measured to be lower by a factor of 10 or more, compared with coated particles without kernel additives. Data on the in-pile Cs-137 release from particles containing alumina-silica kernel additives are not available. The postirradiation annealing investigations, however, showed a considerable reduced release of Cs-137 by more than two orders of magnitude.

In spite of failure of 0.6% of the coatings on particles with Al_2O_3-SiO_2-doped kernels, the Cs release was one order of magnitude lower than on intact particles without kernel additives. The Ba release of intact particles was three orders of magnitude lower. The Ag release on all variants was observed to be 10% and not influenced by the kernel additives.

B.8. EXPERIMENT DR-P5 (MET V)

Objectives

Study fuel kernel migration and investigate methods for reducing this problem.

Loading

The high-temperature experiment was conducted jointly by five European partners under the sponsorship of the Dragon project.

The KFA particles varied in composition of the oxide kernels containing carbide additives acting as CO and CO_2 getter and also in different SiC layers. The experiment was conducted in three parts with identically loaded assemblies irradiated for 88, 152, and 336 EFPDs

(1, 2, and 3 cycles) in three Dragon center channels. Each partner specified his own loading.

The total assembly for each channel was comprised of 27 nut-and-bolt type graphite capsules, five of which were loaded with identical specimens by KFA. The particles were irradiated loose and in compacted monolayer coupons. Six of the 16 varieties of particles had LEU fuel kernels: KFA batch Nos. PSPAUC 1027, PSPAUO 1024, PSPAUOC 1-42, PAUC 883, PAUO 882, and PAUOC 881.

Irradiation Data

	Capsule		
	1	2	3
Irradiation time, fpd	90	152	336
Burnup, % FIMA	1.8-2.5	1.3-3.8	3.1-7.8
Max fluence (10^{21} cm^{-2}, E>0.1 MeV)	0.34	0.72	1.1
Max/Min temp, °C	1384-800	1530-1080	1090-1395

Postirradiation Examination

Met V/1

No amoeba attack was found at any variant, but most SiC layers were corroded, the reason for which is not fully understood. (In PSPAUC 1027, where the SiC layer was deposited at 2000°C, corrosion decreased with decreasing layer deposition temperature. PSPAUTO 1041 and PSPAUOC 1042, with a layer deposition temperature of 1900°C, had less severe damage, and little damage was found in batches where the layers were deposited at 1800°C.) But damage also depends on the irradiation temperature for compacted as well as losse particles; the latter showed higher failure fraction. Measurements of the CO pressure showed that fission product release depends on kernel composition and density as well as on irradiation temperature.

Met V/2

The examination did not provide any detailed results on amoeba behavior. In spite of the high irradiation temperature (up to 1500°C), none of the particule varieties exhibited any deterioration of the kernel. One batch (PSPAUO 1024) had little protuberances at the surface caused by corrosion of the outer SiC-layer surface. Beta autoradiographs showed that carbide-doped kernels UO_2 + 3% UC (initially) released more fission products than (U,Th)O_2 + 3% (U,Th)C kernels. In undoped UO_2 kernels, Ba and Sr are bound as zirconates.

Met V/3

No amoeba attack was observed in carbide-doped particles, but considerable corrosion of SiC occurred on the outer surface at the SiC-HDI interface.

B.9. AVR, RELOAD VI

Twenty-four hundred fuel spheres with 50% LEU-oxide and 50% U_{nat} particles (7500 resp. 8000/sphere) - so called GLE elements - were loaded in the AVR in 1973 and partly irradiated up to now. Spent fuel spheres of this variant reached a burnup of 8% FIMA at a fluence $\leq 2 \times 10^{21}$ cm^{-2} (E > 0.1 MeV).

Searching for reasons for the increase of coolant gas activity, numerous annealing tests were performed on different types of fuel elements, and the GLE variant was detected as the origin of this activity.

In postirradiation annealing tests below 1250°C, no particle failed. At annealing temperatures between 1250° and 1500°C, failure fractions $\leq 1\%$ were found, but they were increasing rapidly when the temperature reached 1500°C.

Ceramographic postirradiation examinations of these fuel spheres showed that frequent cracks in the buffer layer sometimes penetrated into the dense PyC layer (LT1) causing a failed particle fraction of about 2% (in one worst case 40%).

All the usual particle failure mechanisms were absent (pressure vessel failure, amoeba effect, PyC cracking at high fluence). Despite the fact that these were the fuel elements with the highest irradiation temperature, the failure mechanism is not understood. Detailed examinations are still in progress at KFA and ÖSGAE Seibersdorf.

B.10. EXPERIMENT FRJ2-K8

Objectives

1. Exploit relevant data on fission product transport in THTR fuel elements.

2. Study the irradiation behavior of methane- and propene-derived PyC coatings.

Loading

The irradiation rig consisted of two separately swept capsules. Each capsule was loaded with three spherical fuel elements in a graphite container. The upper capsule contained spheres of THTR specification, while the lower capsule was loaded with spheres from the AVR-reload VII/8 (ball 4) and VI/type 1 (spheres 5 and 6 with LEU particles) fuel elements. The particle batches were EO 431-441 t and EO 414-428 t (HOBEG).

Irradiation

Because of the higher U-235 content in the spheres with LEU particles (each 1.4 g instead of 1.0 g), the temperatures in capsule 2 were higher than planned.

Irradiation Data for Capsule 2

	Sphere No. 5		Sphere No. 6
Irradiation time, fpd	137		137
Burnup, % FIMA	7.7		7.1
Fast fluence, 10^{21} cm^{-2} (E>0.1 MeV)	0.01		0.01
Temperature, °C			
Surface	1240-800		1140-840
Fuel	1900-1300		1750-1280
In-pile R/B (Kr-88)		$5x10^{-7}$ to $5x10^{-5}$	

Postirradiation Examination

The postirradiation examinations carried out (using gamma spectrometry and disintegration) in connection with the R/B values during irradiation indicated a faultless behavior of the LEU particles. (Part of them were destroyed during disintegration because of a loosely controlled procedure.) Because of the high fuel element power at start of irradiation of the LEU fuel elements, initial temperatures were very high with resulting high release of solid fission products. The release of Ag-110m was determined up to 70% and Cs-137 up to 16%.

B.11. EXPERIMENT DR-K5

Objectives

1. Perform a long-term test of spherical fuel elements for the feed/breed cycle in the Dragon reactor.

2. Test fuel elements for the low-enriched cycle.

Loading

Twenty-seven spherical fuel elements with LTI BISO UO_2 particles with a heavy metal loading of 25 g/E were arranged as a stack in the inner tube of a D 15 type, directly cooled carrier in the Dragon reactor (length 1620 mm). The particle batch was EO 391 t (HOBEG).

Irradiation

The irradiation test was erroneously run at too-high temperatures resulting in high Cs release into the Dragon primary circuit. Therefore, it was necessary to stop the irradiation after 334 full-power days.

Irradiation Data

Irradiation time, fpd	334
Burnup, % FIMA	3.2-5.5
Fluence, $10^{21}cm^{-2}$ (E 0.1 MeV)	1.1-2.7
Initial temperature, °C	
Surface	1210
Center	1400
Particle	1400

No in-pile release data are available because it was directly cooled fuel.

Postirradiation Examination

The upper fuel elements showed heavy corrosion on the surface, cooling gas flow from bottom to top. The extent of the corrosion decreased from top to bottom of the stack as observed by visual examination. Below about the middle of the stack, no visible corrosion could be detected. Because the Cs-137 concentration in the surrounding graphite tube increased from the middle to the top, a catalytic influence of fission products on the

surface corrosion of the fuel spheres cannot be excluded. Annealing tests at 1500°C showed little Kr-85 release, indicating failure of only one or two particles out of 23,000.

Metallographic examinations showed no failure mechanisms, a surprising result in comparison to the AVR VI fuel elements.

B.12. EXPERIMENT R2-K5

Objectives

1. Test spherical fuel elements (breed-elements) for the Th-U-two-sphere cycle.

2. Test the one-sphere LEU cycle, which has a 10 mm fuel-free outer zone (instead of 5 mm normally) to demonstrate its mechanical integrity.

Loading

The rig contained four separately swept capsules, each loaded with one sphere. Sphere 1 contained the LEU particle batch EO 241/243/244 t (HOBEG).

Irradiation

The test conditions during the first 300 days were simulating the temperature sequence in a direct cycle HTR plant with continuous recycling. The fuel element surface temperatures were cycled between 650° and 1000°C. During the last 138 days an Otto-cycle was simulated with increasing temperature from 800° to 900°C in 3 hours.

Irradiation Data for Sphere 1

Irradiation time, fpd	438
Burnup, % FIMA	11.2
Fast fluence, $10^{21}cm^{-2}$ (E > 0.1 MeV)	7.44
Surface temperature, °C	1000-850
R/B (Xe-133 end of irradiation)	$8.4x10^{-7}$

Postirradiation Examination

The ceramographic postirradiation examination showed a faultless behavior during irradiation of the LEU particles. During irradiation, the buffer layer had shrunk 10% to 13%, and gaps between the particle/overcoating/matrix (as seen before irradiation) had closed. Detailed PIE at ÖSAGE Seibersdorf is in progress.

B.13. EXPERIMENTS DR-S2, S3, S4, S6

Objectives

1. Perform short- and long-term tests to investigate the influence of fluence and temperature on the mechanical stability of the compacts, including stress analysis and the interaction between matrix and graphite tube, under near-power reactor conditions.

2. Test the performance of different fuel varieties.

Loading

These experiments were carried out as a series of tests on directly cooled compacts (S2, 3, 6) and compacts of the tubular interacting type (S4).

All experiments contained fuel in the form of pressed annular compacts with a fuel-free shell. The matrix composition and fuel varieties were different in the tests. Besides testing particles with LEU oxide kernels,

feed and breed particles with $(U,Th)O_2$-, ThO_2 and UC_2 kernels, both with BISO and TRISO coatings and each in a short- and a long-term test, respectively, were tested. The LEU particles (all HOBEG) used were batches S2 (EO 241, 243, 244 t), S3/6 (EO 403 - 405 t), and S4 (EO 249, 250, 251 t).

Irradiation

The directly cooled compacts were stacked in block element carriers, and the compacts of the tubular interacting type were stacked in graphite pins with inner and outer tubes for the cooling gas flow. Both types were irradiated in center channels of Dragon elements type 16 and 21, respectively.

Irradiation Data

	DR-S2	DR-S3	DR-S4	DR-S6
Irradiation time, fpd	270	334	656	550
Burnup, % FIMA	2-4	3-4	5.8-7.7	4-6
Fast fluence, $10^{21}cm^{-2}$ (E > 0.1 MeV)	2.7	2.5	4.1	4.1
Temperature, °C				
Surface	1100	1100		1060
Fuel center	1250	1200	1200	1160

Postirradiation Examination

The main scope of the postirradiation examinations was to demonstrate the behavior of the compacts with respect to dimensional changes. Interactions between the different zones, fission product migration, and internal stresses will be studied to determine agreement with model stress calculations.

The particles in DR-S4 compacts 4 and 5, having achieved burnups of 7.6% and 7.8% FIMA, respectively, appear to have performed reasonably well. Although there are some indications of particles with cracked or broken

coatings being in one end of compact 4, it is thought that the damage was done during compaction. For the DR-S6 compacts examined, there are no indications of broken coated particles or detectable fission product release above the level of fuel contamination estimated to be about 10^{-4}, except for Ag-110m in compact 15 and possibly compact 7. After achieving about 6% FIMA, the general performance of the particles appear to be very good.

S6 Ceramography (Harwell)

About 40% (10) of the particles were irregular in shape, but all appear to have performed reasonably well. There was little or no indication of radial cracking of the buffer layer; the dense PyC layers, or SiC layers, and the UO_2 kernels had remained reasonably sound.

The principal characteristics to emerge from the examination were:

1. The buffer layer tended to densify at the surface in contact with the UO_2 kernel.

2. This densified layer tended to delaminate from the remainder of the buffer layer.

3. The buffer layer tended to decouple from the inner dense PyC layer.

In the rounder particles, this decoupling was fairly uniform, but in the irregularly shaped particles there tended to be a bias. In the microprobe analysis of the coating layers, only Cs was found in amounts greater than the limit of detection (0.3 wt %); Cs was not detected in SiC or the outer dense PyC layers.

B.14. EXPERIMENT DR-P4 (DRAGON MET IV EXPERIMENT)

The results of this experiment, which involved the irradiation of special coated particles with 40% and 20% enrichment and natural uranium are described in Dragon DPR 880 Parts I through VI edited by M. R. Everett of the Dragon Project.

B.15. EXPERIMENT HFR-M5

The irradiation experiment of UO_2 BISO and TRISO particles with 6.59% and 6.65% enriched U-235 and a fuel kernel diameter of 600 um was performed in the HFR Petten, Netherlands (Project E91-0). A summary of the results of this experiment is presented in Ref. B-1.*

*Conrad, R., Joint Nuclear Research Centre Petten Establishment, "Prototype Experiment of an Irradiation Facility for Large HTR Fuel Specimens in the HFR Petten (Project E91-0)," Commission of the European Communities Report EUR 5456e.

APPENDIX C

LEU FUEL PERFORMANCE DATA FROM THE ORNL PROGRAM

Irradiation testing of coated particle fuels under ORNL programs has been conducted in the Oak Ridge Research Reactor (ORR), the High Flux Isotope Reactor (HFIR), the Engineering Test Reactor (ETR) and the Peach Bottom Reactor. In addition, fuel has been fabricated for testing in the Fort St. Vrain Reactor, and some testing has been done in the Dragon Reactor. The vast majority of the Oak Ridge work has been done in support of fuel development for the high-enriched uranium (HEU) fuel cycle, although some work on low-enriched fuels has also been done, as described below.

C.1. ORR EXPERIMENTS (REF. 1)

Coated particle irradiations in the ORR can be divided into two categories: (1) experiments conducted in the 1960s, and (2) the OF experiments. The OF experiments were all conducted with fully enriched uranium and will not be discussed further. The early ORR experiments used mostly fully enriched uranium fuel as well, although some of these tests involved particles with uranium enrichments as low as 23%. However, these experiments are documented only in progress reports; the preirradiation characterization was very limited compared to the current capability, and postirradiation examination consisted only of visual examination and a small amount of metallography. Due to the lack of quantitative information on the performance of these particles they will not be discussed further in this report.

C.2. HFIR REMOVABLE BERYLLIUM EXPERIMENTS

The current HFIR Removable Beryllium (HRB) series began in August 1969 with HRB-1. These experiments have been conducted in support of the fuel development effort for the high-enriched uranium (HEU) cycle HTGR. Because of the high thermal flux in the HRB facilities, the early capsules (HRB-1 through HRB-5) contained low-enriched uranium (LEU) fissile particles. Higher enrichment in these fissile particles would have resulted in excessive particle power production rates at the beginning of irradiation and high risk of failing particles that might have survived under more typical HTGR power production rates. The HRB-6 experiment was the first test of fully enriched uranium in fissile particles, but the fissile particles were $(4Th,U)O_2$, which was the reference recycle fissile particle at the time of the test. Beginning with Capsule HRB-7, a preirradiation was conducted in the VXF-13 facility, where the thermal flux values are about half of that of the RB position. This type of operation permitted irradiation of fully enriched fissile particles containing only uranium. Approximately 80% of the U-235 burnup takes place during the preirradiation so that the particle power production rates are reduced to acceptable values during irradiation in the RB facilities.

Therefore, for purposes of the LEU cycle fuel evaluation, only capsules HRB-1 through HRB-5 are of interest. HRB-1 contained UO_2 and $(Th,U)O_2$ fissile particles, and a summary of this experience is contained in Table C-1. HRB-2 contained strong-acid-resin (SAR)-derived fissile particles with 10.16% enriched uranium. HRB-3 contained SAR-derived fissile particles with 7.35% enriched uranium. HRB-4 and -5 contained weak-acid resin (WAR) derived fissile particles with a 5.99% enriched uranium. It would appear that only the data from HRB-1 are relevant to the LEU cycle evaluation. However, postirradiation examination techniques improved with time, and the procedures used with HRB-4 and -5 yielded some information not obtained from HRB-1. This information is very pertinent to the performance evaluation of LEU fuel, even though the HRB-4 and -5 fissile particles did not contain dense kernels.

TABLE C-1
SUMMARY OF LEU UO_2 AND $(Th,U)O_2$ EXPERIMENTS IN CAPSULE HRB-1

Rod No.	Fuel	U Enr (%)	Burnup[a] (% FIMA)	Fast Fluence (F > 0.18 MeV) (x 10^{-21})	Max Fuel Temp (°C)	Remarks[b]
1A	$(Th,U)O_2$	36.0				
1B	$(Th,U)O_2$	36.0	9.8/	2.9		
1C	$(Th,U)O_2$	36.0			770	
2A	$(Th,U)O_2$	36.0	10.2/3.8	3.4		
2B	UO_2	7.07	16.6/4.6	4.0	1210	Metallographically examined
3A	$(Th,U)O_2$	36.0	12.7/5.9	4.8		
3B	$(Th,U)O_2$	36.0	12.7/5.9	4.8	1150	Metallographically examined
4A	$(Th,U)O_2$	36.0	13.8/7.1	5.3		Rods crumbled. No amoeba noted.
4B	UO_2	7.07	22.6/7.7	5.6	1230	Rods crumbled. Fuel swelling, amoeba noted.
5A	$(Th,U)O_2$	36.0	14.9/8.2	5.8	1130	Metallographically examined
5B	$(Th,U)O_2$	36.0	14.9/8.2	5.8		
6A	$(Th,U)O_2$	36.0	14.0/7.4	5.4		Metallographically examined
6B	$(Th,U)O_2$	36.0	14.0/7.4	5.4	1140	
8A	ZrO_2					Metallographically examined
8B	ZrO_2					

[a] Fissile/fertile

[b] Ref: ORNL/TM-3640

Capsule HRB-1 contained Sol-Gel UO_2 and Sol-Gel $(Th,U)O_2$ fissile particles, as shown in Table C-1. Only 7 of the 15 specimens were examined metallographically. Several conclusions were reached regarding the performance of matrix materials prepared with different recipes, and of coatings. The only conclusion drawn from this experiment that is of importance to the LEU evaluation is that thermal migration occurs at a faster rate in UO_2 than in $(Th,U)O_2$.

Capsules HRB-4 and -5 (Ref. 2) contained WAR-derived fissile particles with 5.99% enriched uranium. These kernels were nominally UC_2 and the fissile particles containing these kernels experienced the same type of chemical attack of the SiC layer by rare earth fission products that has been observed in other experiments (Refs. 3, 4).

What is of more interest from the HRB-4 and -5 experiments is the attack of the SiC layer by the fission product palladium. Palladium yields from Pu-239 fissions are about 10 times higher than yields fr m U-233 fissions and about 17 times higher than yields from U-233 fissions (Ref. 5). Palladium will not form oxides in oxide fuels, but will be present as metallic inclusions with Ru, Rh, and Mo. In carbide fuels, Pd will be present in the form $U_2(Ru,Rh,Pd)C_2$ or $U(Ru,Rh,Pd)_2C_x$ where $x < 0.7$. Although the HRB-4 and -5 fuel was nominally UC_2, the trends that have been identified are useful to the LEU/MEU development effort without respect to the composition of the LEU/MEU kernels.

There is considerable discussion in this appendix regarding the relative fission product yields from plutonium fissions compared with uranium fissions. Yield alone is a misleading indicator; it is the fission product concentrations that are important for such issues as attack of the SiC layer and diffusion out of the particle. As indicated, the yields of the fission product Pd from plutonium fissions is about 10 times the yield from uranium fissions. Using the well-characterized HRB experiments as an example, these relative yields can be translated into relative Pd concentrations for comparison.

The fissile fuel in HRB-4 and -5 was about 6% enriched, the U-235 burnup was 84%, and the U-238 burnup was 25% (maximum U-238 burnup at the HRB-4 horizontal midplane position). The overall burnup in the fissile particles can be computed from these numbers, and is about 29% FIMA. The fissile fuel in the HRB-7 and -8 capsules was 93% enriched, the U-235 burnup was 85%, and the maximum U-238 burnup was 25%. The overall fissile particle burnup was therefore 81% FIMA. The relative fission product yields can now be used to determine the relative concentration of Pd in the fissile particles from these two sets of experiments:

$$\text{U-235 burnup in HRB-4} = \frac{0.84 \text{ U-235 fissions}}{\text{U-235 atom}} \frac{0.06 \text{ U-235 atoms}}{\text{U atom}} = 5.04\%$$

$$\text{U-238 burnup in HRB-4} = \frac{0.25 \text{ U-238 fissions}}{\text{U-238 atom}} \frac{0.94 \text{ U-238 atoms}}{\text{U atom}} = 23.5\%$$

$$\text{U-235 burnup in HRB-8} = \frac{0.85 \text{ U-235 fissions}}{\text{U-235 atom}} \frac{0.93 \text{ U-235 atoms}}{\text{U atom}} = 79.05\%$$

$$\text{U-238 burnup in HRB-8} = \frac{0.25 \text{ U-238 fissions}}{\text{U-238 atom}} \frac{0.07 \text{ U-238 atoms}}{\text{U atom}} = 1.75\%$$

Relative Pd concentration for HRB-4 versus that for HRB-8

$$= \frac{(5.04\% \text{ U-235 FIMA}) \frac{1 \text{ Pd atom}}{\text{U-238 fissions}} + (23.5\% \text{ U-238 FIMA}) \frac{10 \text{ Pd atoms}}{\text{U-238 fissions}}}{(79.05\% \text{ U-235 FIMA}) \frac{1 \text{ Pd atom}}{\text{U-235 fissions}} + (1.75\% \text{ U-238 FIMA}) \frac{10 \text{ Pd atoms}}{\text{U-238 fissions}}}$$

$$\approx 2.5$$

Metallographic examination of the HRB-4 and -5 fuels showed evidence of chemical attack in the inner regions of the SiC layer in about one-third of the fissile particles appearing in the plane of polish. This attack appeared as localized regions and was not temperature-gradient dependent. The attack varied in degrees of severity from only slight to complete penetration of the SiC layer. A general degradation of the inner surface of

the SiC was also apparent in many of the coated particles. Analysis of the region of attack with the aid of an electron microprobe revealed the presence of the fission produce palladium. The results of this analysis are shown in Fig. C-1. The attacked regions appeared to have been molten. A Pd-Si phase diagram (Fig. C-2a) shows three eutectics with melting points below the surface temperature of the fuel rods (Ref. 6).

In order to understand the interaction between Pd and the SiC layer, it is probably necessary to consider more than the Si-Pd binary system. Figure C-2b shows the Pd-Si-C ternary phase diagram (Ref. 7). No temperatures are given on this phase diagram so it has been assumed that it is valid up to the liquidus temperature.

Some of the phase fields on the Pd-Si-C phase diagram have been numbered. The following materials are in equilibrium in the indicated areas:

Area 1: Pd_2Si, SiC, C
Area 2: Pd_2Si, Pd_3Si, C
Area 3: Pd, Pd_3Si, C

From the Pd-Si phase diagram, it can be seen that Pd_3Si melts incongruently; i.e., decomposes at 960°C. The results of Suzuki et al. (Ref. 8) confirm the Pd-Si-C phase diagram.

Thus, the interface between Pd and SiC may be pictured as: SiC-Area 1-Area 2-Area 3-Pd. As indicated earlier, the region of Pd attack in HRB-4 and -5 fissile fuels appears to have been molten. From the phases expected in this reaction, as given above, the melting was most likely brought about by the Pd-rich eutectic (760°C on Pd-Si phase diagram) and/or by the peritectic (960°C on Pd-Si phase diagram). The other two eutectics on the Pd-Si phase diagram involve phases not expected in this system. Thus, for example, the silicon-rich eutectic at 57 at. % Si requires excess Si and PdSi neither of which is expected. The conclusion, then, is that the

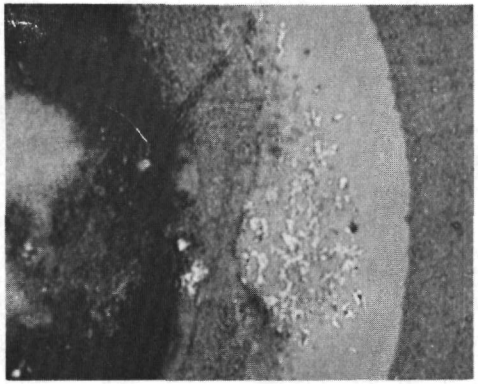

OPTICAL MICROGRAPH

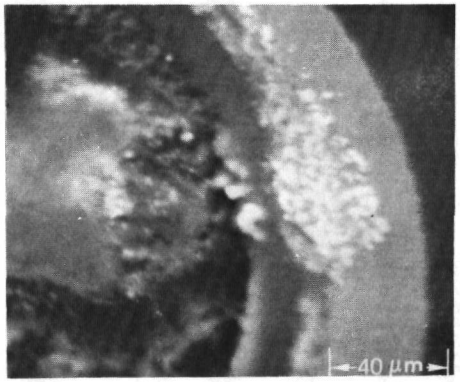

BACKSCATTERED ELECTRONS

UMβ

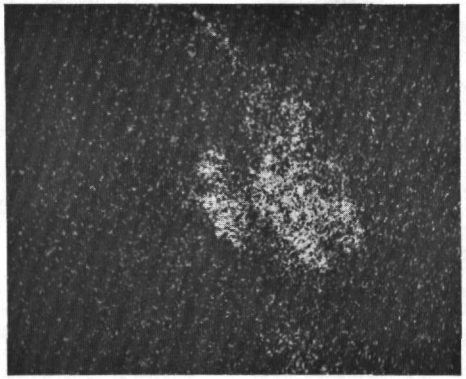

Pd L_a

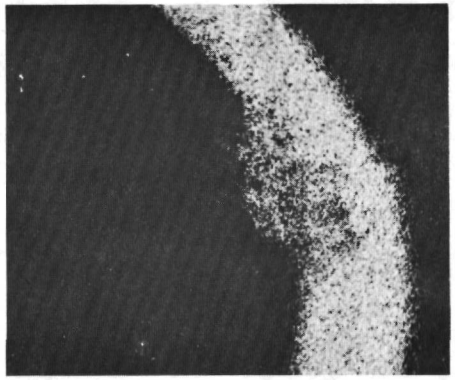

Si K_a

Fig. C-1. Palladium-SiC reaction in a TRISO coated WAR fissile particle contained in fuel rod 3A, HRB-4, as displayed by electron microprobe

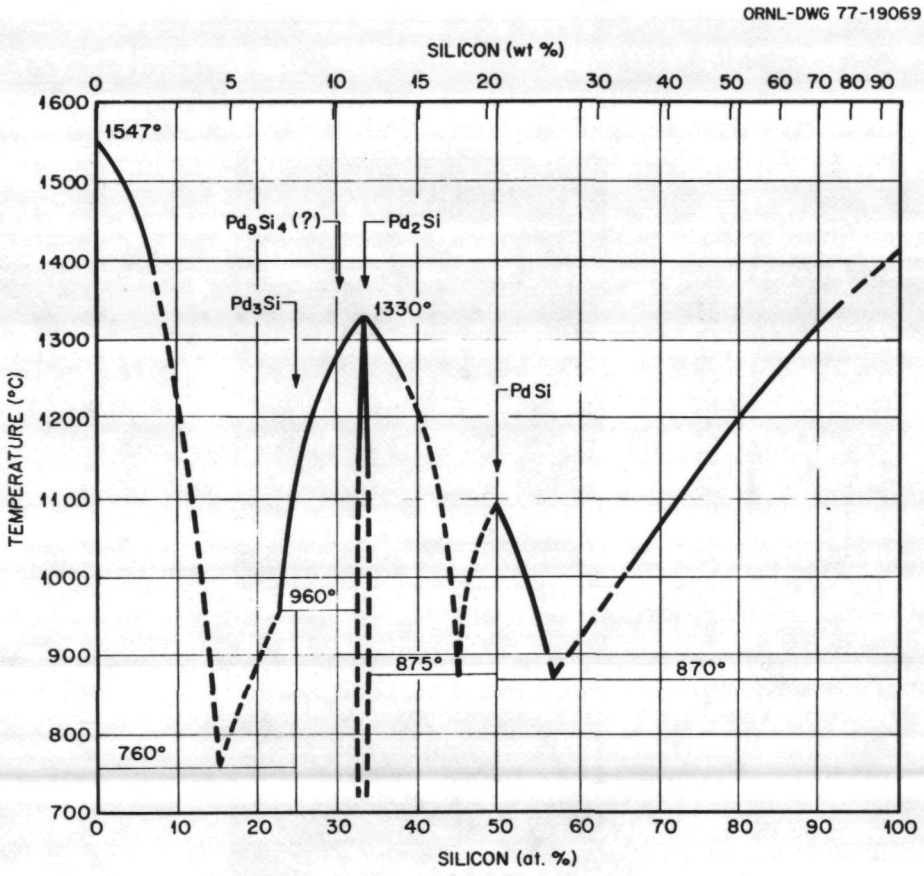

Fig. C-2a. Pd-Si phase diagram (from Ref. 6) shows three eutectics below 1000°C

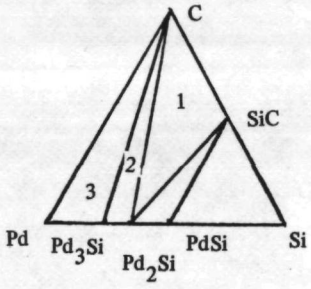

Fig. C-2b. Pd-Si-C Ternary Phase Diagram

melting occurs on the Pd-rich side of the Pd-SiC interface. This may be advantageous in an operating system since if melting were to occur in the SiC-rich area the failure rate would probably be more severe. On the other hand, melting on the Pd-rich area probably accelerates material transport via the liquid phase, and increases the rate of attack. If there is free silicon in the SiC (grain boundaries or small pores), melting caused by the silicon-rich eutectic may occur in these areas. Free silicon in grain boundaries may also lead to the formation of eutectic with Ag.

C.3. HFIR TARGET (HT) EXPERIMENTS

Low-enriched uranium particles (6% to 7% enrichment) are frequently used in HT capsules as driver fuel to produce heat for keeping the fertile particles being tested at the desired temperatures until sufficient U-233 is bred into these particles. The LEU driver particles are usually not examined. However, because of the recent interest in LEU and MEU cycles for the HTGR, the driver particles from capsules HT-31, -32, and -33 are now being examined metallographically and with the electron microprobe. Internal gas pressure measurements will be performed on these particles, as well as fission product inventory measurements with the irradiated microsphere gamma analyzer system (Ref. 9). In addition, particles from several of the driver batches will be evaluated in postirradiation heating tests at General Atomic.

Table C-2 is a summary of the irradiation conditions seen by the driver particles from Capsules HT-31 through -33. The conclusions drawn from metallographic and microprobe analysis of the WAR UCO particles examined to date are discussed and illustrated below.

Metallographic examination of the WAR UCO driver particles typically shows a densified buffer layer, and shrunken kernel, as shown in Fig. C-3. This type of behavior is normal for WAR particles and is typical of HEU fuel particles as well. Close examination of the SiC coatings reveals areas of localized corrosion due to Pd with visible penetration of about 10 microns, as shown in Fig. C-4.

TABLE C-2
SUMMARY OF LEU FUEL IRRADIATED IN HT CAPSULE DRIVER POSITIONS

Capsule	Batch	Fuel	% Conversion[b]	U-235 Enr (%)	No.	Fast Fluence ($n/cm \times 10^{-21}$)	%Burnup U-235	(% FIMA) U-235	Design Surface Temp (°C)	Remarks
HT-31	OR-2533H	UO_2 (T)	0	0.711	1	8.3	84	13	1250	
	OR-2511H	UO_2 (B)	0	0.711	1	8.4	84	12	1250	
	OR-2557H	WAR U • $C_{5.01}$ • $O_{1.26}$ (T)	37	6.36	1	8.65-9.00	84	18	1250	LASL rods
	OR-2248H	WAR U • $C_{4.86}$ • $O_{1.22}$ (T)	39	6.50	12	4-9	84	10-19	950 and 1250	
HT-32	OR-2576H	WAR U • $C_{4.04}$ • $O_{1.43}$ (T)	29	7.09	1		84	11.5		
	SC-375[a]	WAR U • $C_{4.04}$ • $O_{1.43}$ (SiC)	29	7.09	9		84	10.6-18.5		
HT-33	OR-2576H	WAR U • $C_{4.04}$ • $O_{1.43}$ (T)	29	7.09	16	5.56-11.6	84	10-23	950 and 1250	
	SC-375[a]	WAR U • $C_{4.04}$ • $O_{1.43}$ (SiC)	29	7.09	4	5.56-11.6	84	10-23	950 and 1250	

[a] Deleted outer LTI

[b] Conversion is from oxide to carbide. The % conversion is determined by the following formula: $\frac{2 - O/U}{2}$. Thus, batch OR-2557H is 37% UC_2, 63% UO_2.

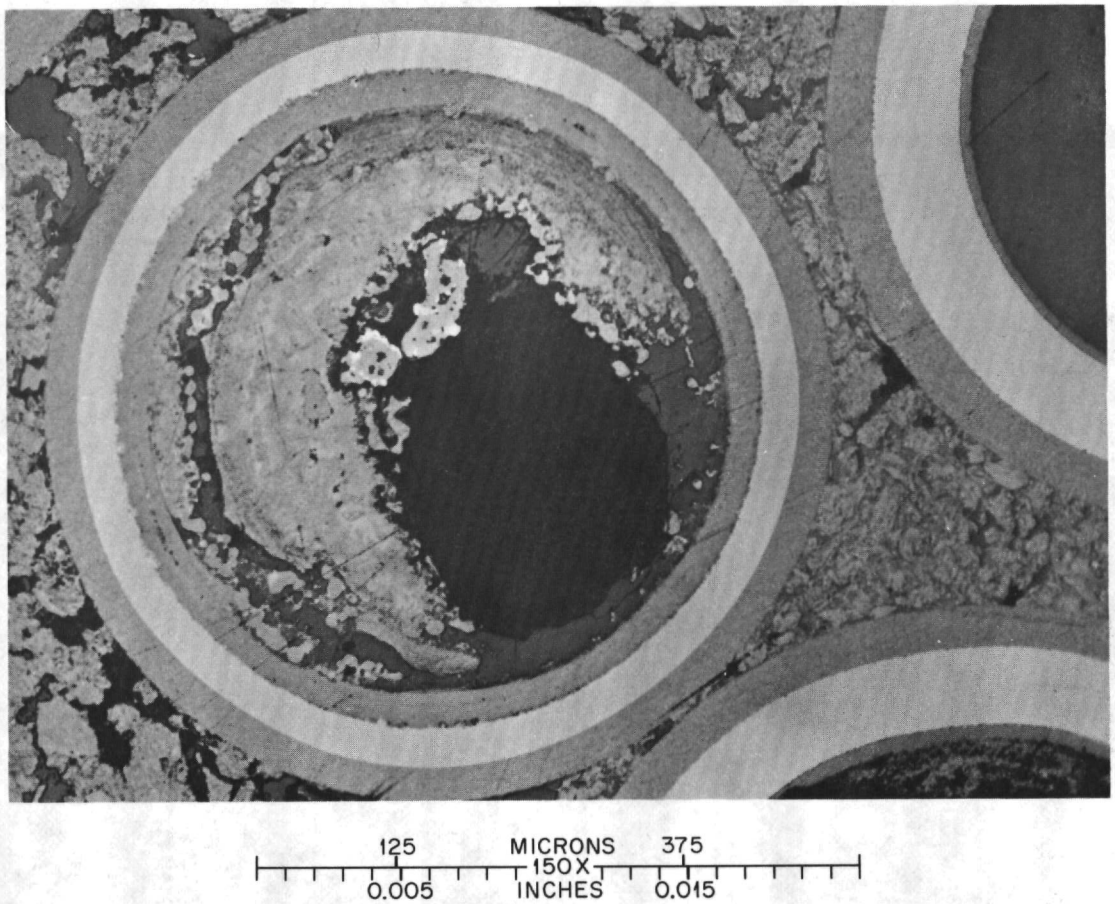

Fig. C-3. WAR $UC_{4.04}O_{1.43}$ particle, TRISO coated, irradiated in capsule HT-33. Kernel was 7.07% enriched, irradiated to a burnup of 84.7% FIMA (U-235) and 21.9% FIMA (U-238), and experienced a fast neutron fluence of 11.1×10^{21} ($E > 0.18$ MeV). Average operating temperature was 1329°C and average temperature gradient was 158°C/cm. There was no detectable chlorine (from microprobe analysis).

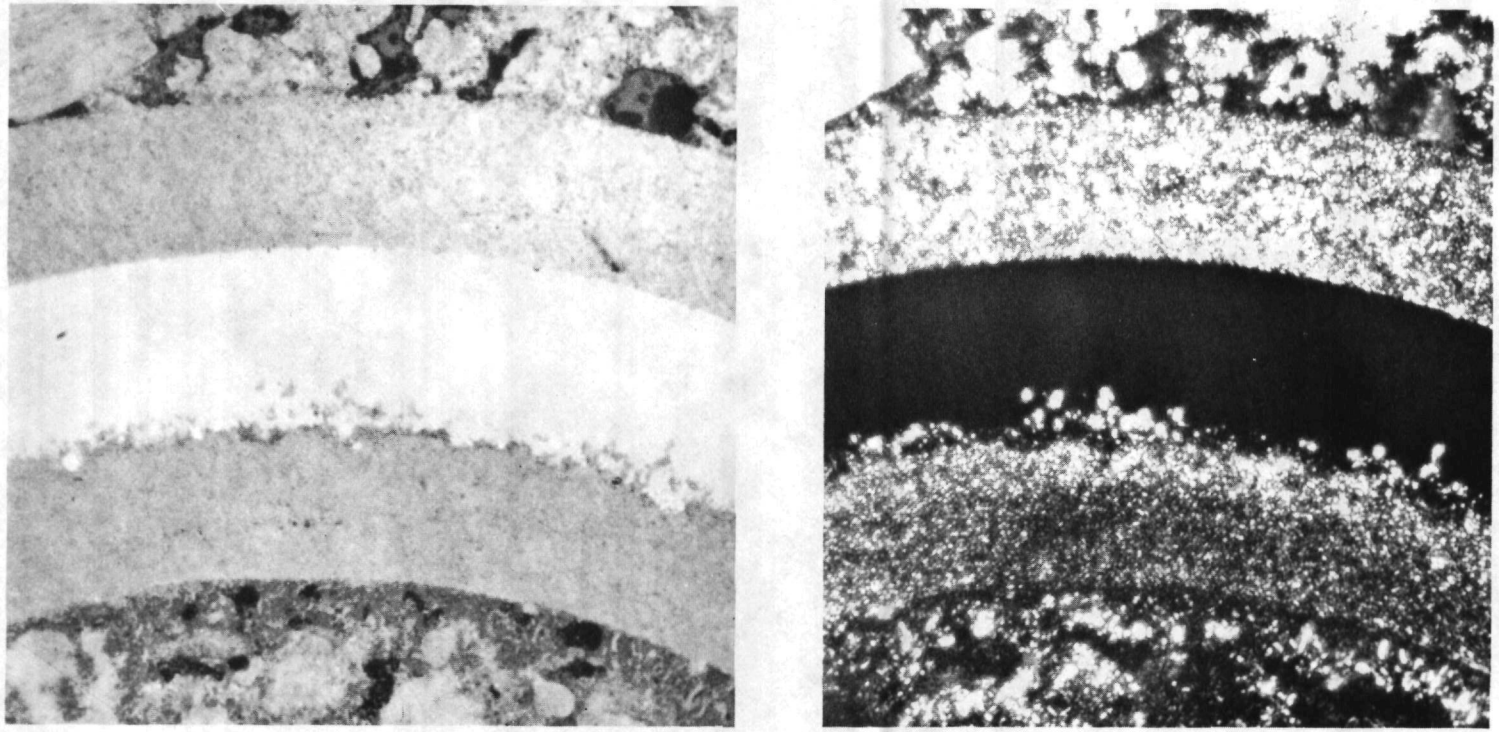

Fig. C-4. High magnification view of SiC coating from particle shown in Fig. C-3. Bright field illumination is shown on the left and polarized light on the right.

Microprobe examination of the WAR UCO driver particles from HT-33 shows that uranium and plutonium remain together in the kernel and densified buffer layer, as shown in Fig. C-5. The extent to which the uranium and plutonium move away from the kernel appears to be related to the amount of chlorine present in the kernel, as shown by the comparison of the amount of uranium and plutonium present at the inner surface of the SiC layer in Fig. C-5 (where there was no chlorine detected with the microprobe) with that shown in Fig. C-6 (where chlorine was detected). The influence of the presence of chlorine on actinide movement has also been observed by German workers (Ref. 10).

The fission product palladium is observed in large concentrations in LEU fuels. In all cases palladium was observed to have migrated from the kernel to the SiC layer, which indicates that Pd movement is not related to the presence of chlorine in the kernel or the kernel chemistry. Palladium will remain in the metallic state with high vapor pressure at the irradiation temperatures for these particles. Its high vapor pressure at these temperatures explains its easy movement to the SiC. Analysis by the electron microprobe showed that the corrosion of the SiC observed during metallographic examination is attributed to palladium (see Fig. C-7). As shown, palladium is observed all along the SiC, but penetration occurs in localized areas only. It is believed that Pd migration through the SiC takes place along grain boundaries.

Much more work is needed to quantify the relationships between chlorine concentration in the kernel and the movement of uranium, plutonium, and fission produces in the LEU fuel system. Attack rates and penetration rates of the SiC layer by the fission product palladium need to be studied and correlated with the SiC structure.

C.4. PEACH BOTTOM REACTOR EXPERIMENTS

ORNL experiments in the Peach Bottom reactor include the recycle test elements (RTEs) and the plutonium test element (FTE-13) FTE-13 was funded

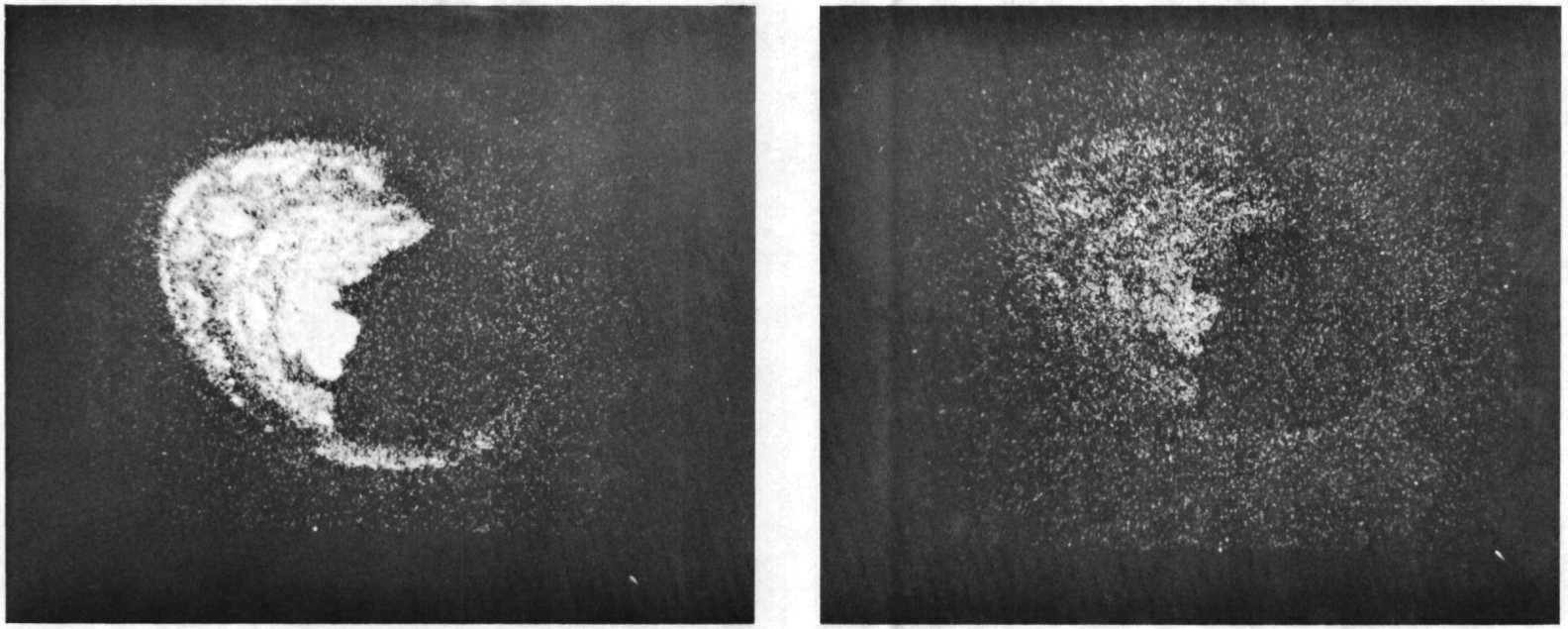

Fig. C-5. U (left) and Pu (right) microprobe displays for particle shown in Fig. C-3. Note presence of U and Pu in the densified buffer layer. The majority of the kernel from this particle fell out during metallographic preparation. The portion of the kernel that fell out is assumed to have had a high concentration of U and Pu as well. Note that no U and Pu have moved out to the SiC layer.

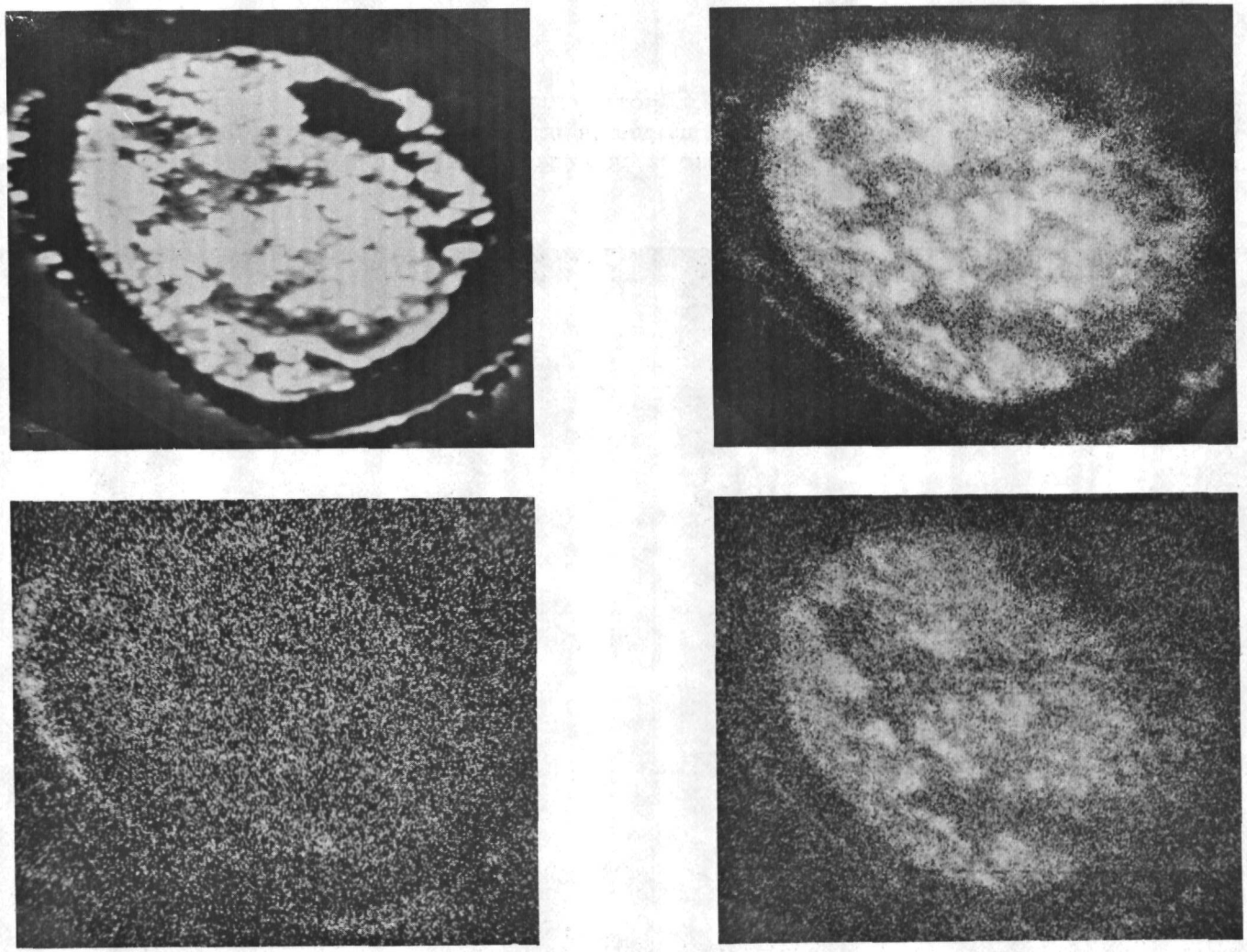

Fig. C-6. WAR $UC_{4.04}$ $O_{1.43}$ particle, TRISO coated, irradiated in capsule HT-33. Kernel was 7.07% enriched and irradiated to about 85% FIMA (U-235) and 21.9% FIMA (U-238) at a maximum temperature of 1430°C. Backscattered electron display is shown top left, uranium display top right, chlorine display lower left, and plutonium display lower right. Chlorine was detected in the particle U and Pu were observed at the SiC coating.

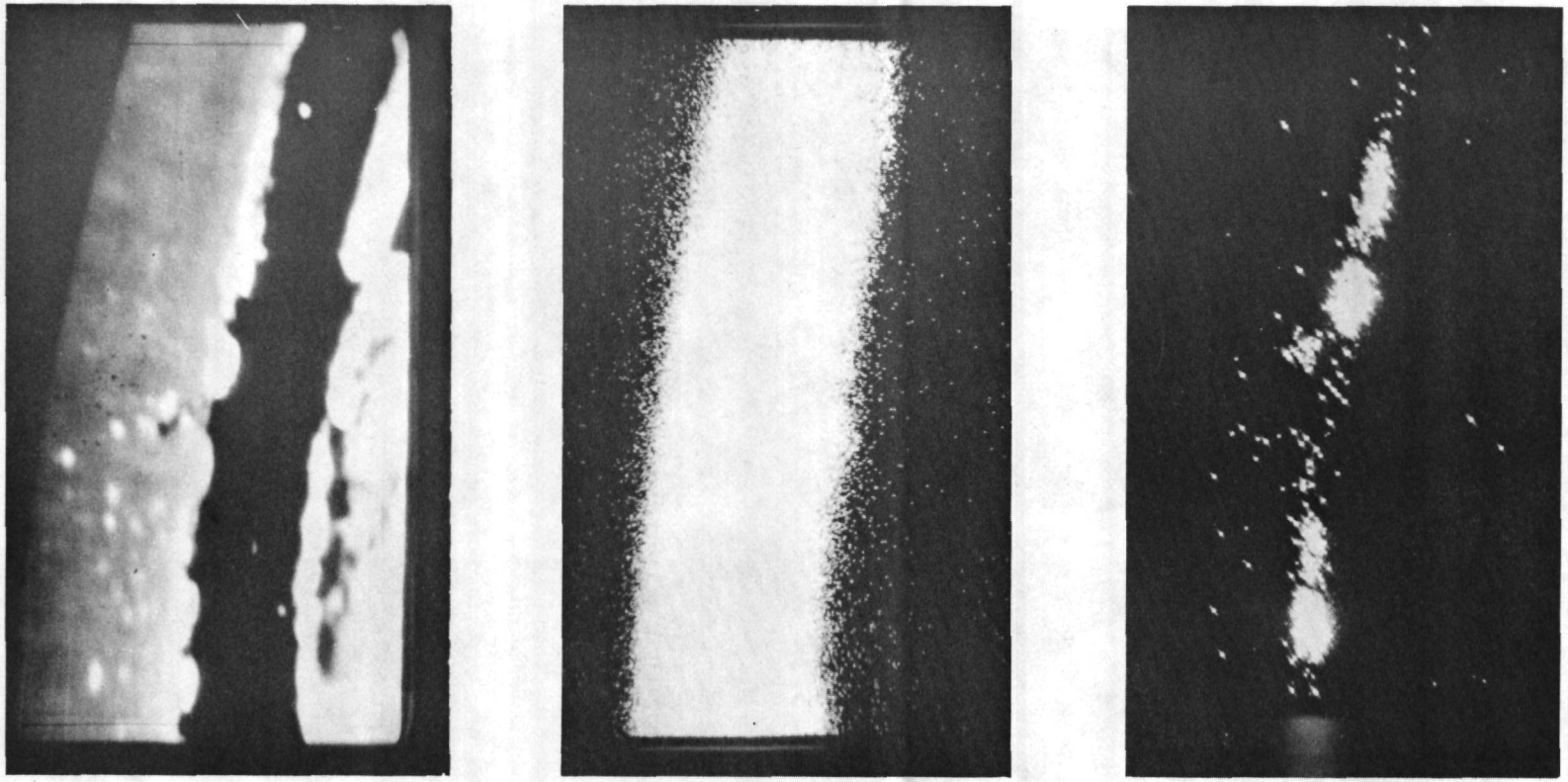

Fig. C-7. Backscatter electron display (left), Si microprobe display (middle), and Pd microprobe display taken using particle shown in Fig. C-3.

jointly by GA and EPRI. The fuel fabrication and postirradiation examination were done at ORNL. The RTEs contained HEU fuel and will not be discussed further. FTE-13 is the only definitive experiment on the performance of plutonium-bearing coated particle fuels, and is an important component of the LEU data base. Two performance problem areas have been identified for Pu-containing coated particle fuels, based on the FTE-13 experience. They are (1) thermal migration of the kernels, and (2) fission product attack of the SiC layer in TRISO coated particles. Thermal migration will be discussed later in this appendix. The fission product attack will be quantified more completely with microprobe analysis, but preliminary observations suggest palladium to be the major contributor to the attack. The appearance of areas of attack is very similar to those already described for HRB-4 and and -5, and the HT capsule driver particles.

A summary of the preliminary conclusions derived from the FTE-13 examinations completed to date is given below. Some introductory remarks concerning the thermal migration (amoeba) portions of the conclusions are in order. Migration in PuO_{2-x}-containing fuels cannot be stated by a simple KMC value or by "no migration" versus "migration observed" kinds of statements, even though these statements do appear in the conclusions given below. The O/Pu value is strongly dependent on burnup, and thus probably the KMC value is also strongly dependent on burnup. It is currently thought at ORNL that there is no migration of Pu-containing kernels until the O/Pu ratio reaches an unknown threshold value, then migration occurs at a rate more rapid than that indicated by the usually quoted "average KMC values" such as those in Ref. 11.

The plutonium oxide kernels showed a great deal of phase segregation. Metallic inclusions, ceramic inclusions, and fission gas bubbles were present. Many times the inclusions were at the surface of the fission gas bubbles. The kernels appeared to be extremely plastic during irradiation.

The mixed plutonium-thorium-oxide kernels appeared very much like uranium-thorium mixed oxides. Metallic inclusions, fission gas bubbles,

and some intermittent plastic flow through the fission-recoil zone were observed.

In every metallographic section examined, metallic-appearing inclusions were observed at the SiC-inner pyrocarbon coating interface. The distribution of these inclusions did not appear to be influenced by any thermal gradient. Many times localized attack of the SiC was associated with these inclusions. From previous experience, it is believed that the inclusions and subsequent SiC attack are attributable to Pd.

Kernels with O/Pu ratios less than 1.69 had no detectable amoeba migration. Kernels with O/Pu ratios greater than 1.81 showed appreciable amoeba migration. No amoeba migration was observed in any of the ThO_2 particles.

C.4.1. $PuO_{1.81}$ (Kernel Diameter = 100 μm)

Gross amoeba migration (<100 μm) was observed in practically every particle in all temperature regions. SiC attack was present at the amoeba head in most particles. Complete penetration was observed in many cases. In addition, some chemical attack of the particles, presumably by iron contamination, was observed.

C.4.2. $PuO_{1.84}$ (Kernel Diameter = 200 μm)

Gross amoeba migration (<90 μm) was observed in particles from the high-temperature regions. Particles from low-temperature regions showed less amoeba migration. The cross section from the lowest temperature region had no migration readily apparent.

C.4.3. $PuO_{1.68}$ (Kernel Diameter = 200 μm)

No amoeba migration was readily apparent. Kernels behaved extremely well, even at the higher temperatures and temperature gradients.

C.4.4. $(3Th,PU)O_{1.84}$ (Kernel Diameter = 350 μm)

Amoeba migration (<25 μm) was observed in many particles with the greater migrations at the higher temperatures. A number of failed buffer coatings were observed in one metallographic cross section. Parts of the kernels were observed to be extruding into the cracks, proving the failures did occur during irradiation.

C.4.5. $(3Th,Pu)O_{1.69}$ (Kernel Diameter = 350 μm)

No amoeba migration was readily apparent. Kernels behaved extremely well, even at the higher temperatures and temperature gradients.

C.5. THERMAL MIGRATION

A significant contribution to the quantification and understanding of thermal migration (amoeba) in coated particle fuels has been made by T. B. Lindemer and others at ORNL. Numerous topical reports and open literature reports have been written on the subject. A summary paper (Ref. 11) contains the highlights of Lindemer's work on HEU fuel, and several of the conclusions from this paper are relevant to LEU and MEU fuel as well:

1. The kernel migration rate for UO_2 + fission product oxides is controlled by a solid-state diffusion mechanism operating across the kernel.

2. In-reactor migration of $Th_{0.8}U_{0.2}O_2$ appears to be controlled by a solid-state diffusion mechanism.

3. The ThO_2 kernel migration rate does not appear to be controlled by the rate of carbon transport resulting from in-particle $CO-CO_2$ diffusion. Circumstantial evidence suggests that solid-state diffusion is the controlling mechanism.

4. Kernel migration in UO_2, ThO_2 mixed uranium-thorium oxides does not seem to be dependent upon burnup, the fissile isotope present (U-233 or U-235), or the coating design (BISO or TRISO).

5. Kernel migration in $(Th_{1-x}U_xO_2)$ appears to be independent of composition in the range $0.11 \leq x \leq 0.50$.

6. Kernel migration rates for irradiated $PuO_{1.84}$ are about equivalent to those for irradiated UO_2. Kernel migration rates for irradiated 75% ThO_2 - 25% $PuO_{1.84}$ are about equivalent to those for irradiated $Th_{1-x}U_xO_2$.

7. Reduction of the O/Pu ratio to 1.60 in plutonia or thoria-plutonia kernels prevents migration. Since significant changes in the O/Pu values are calculated to occur with burnup in all Pu-containing fuels, the kernel migration characteristics of such fuels may be time dependent.

While direct measurements of thermal migration characteristics of LEU or MEU fuels have not been made at ORNL, some comparisons have been made between ORNL measurements on HEU fuels, with Dragon data on LEU fuels (Refs. 12, 13). The results of these comparisons are shown in Figs. C-8 through C-12.

Figures C-8 and C-9 show comparisons between the kernel migration coefficients computed for low-enriched UO_2 kernels irradiated in the Dragon reactor, with curve fits for U.S. data for HEU fuel. The data upon which the curve fits shown in Figs. C-8 and C-9 are based are plotted in Figs. C-10 and C-11. Figure C-12 is another comparison between LEU and HEU migration coefficients, but the Dragon data (LEU) is at somewhat higher temperatures in this comparison.

From the data shown in Figs. C-8 through C-12 it can be concluded that the HEU curvefits are conservative (i.e. showing more migration) with

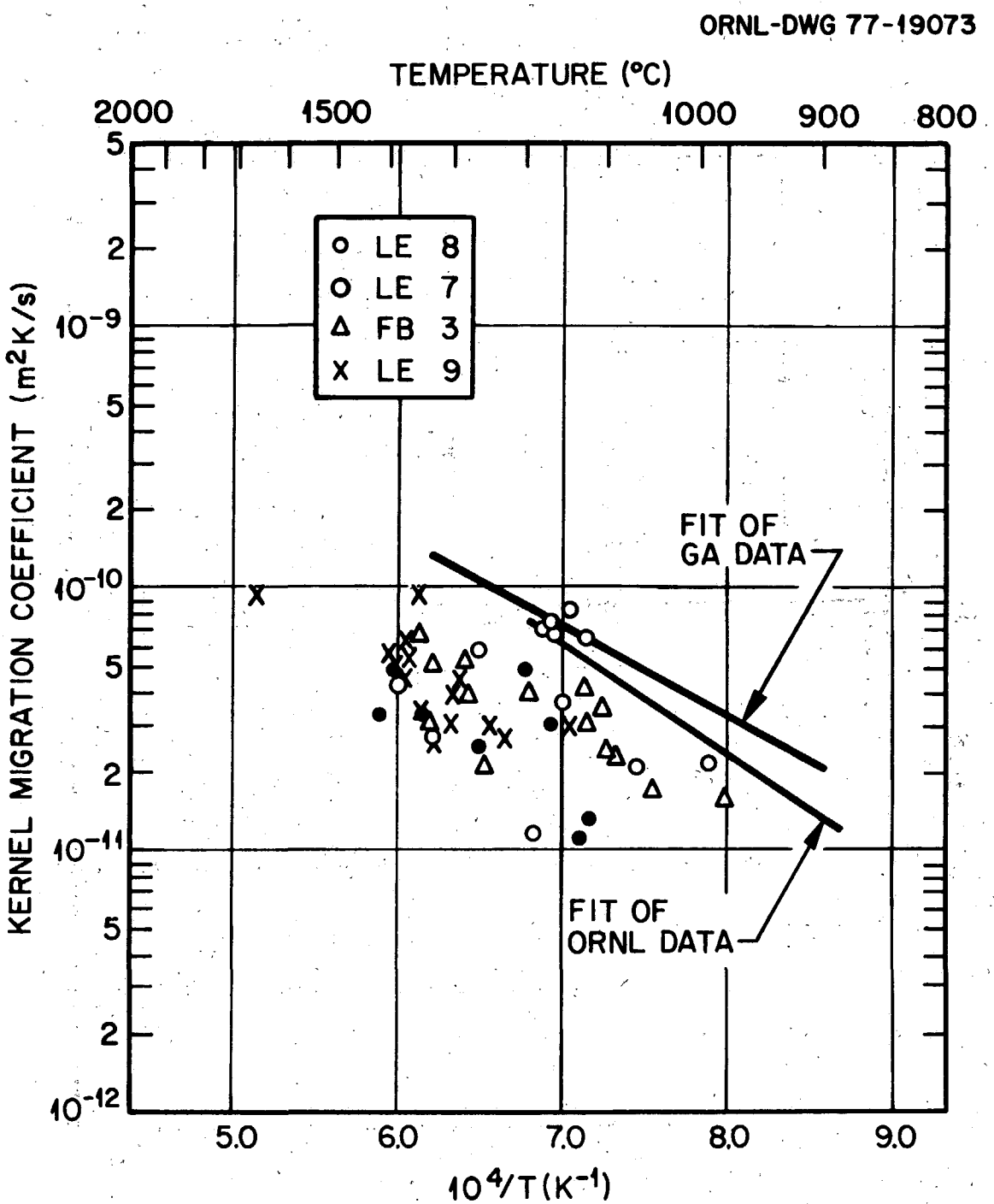

Fig. C-8. Comparison of ORNL and GA data on kernel migration of UO_2 kernels containing high-enriched uranium with Dragon Project data on low-enriched uranium UO_2 kernels. Solid curves are fits of GA and ORNL data.

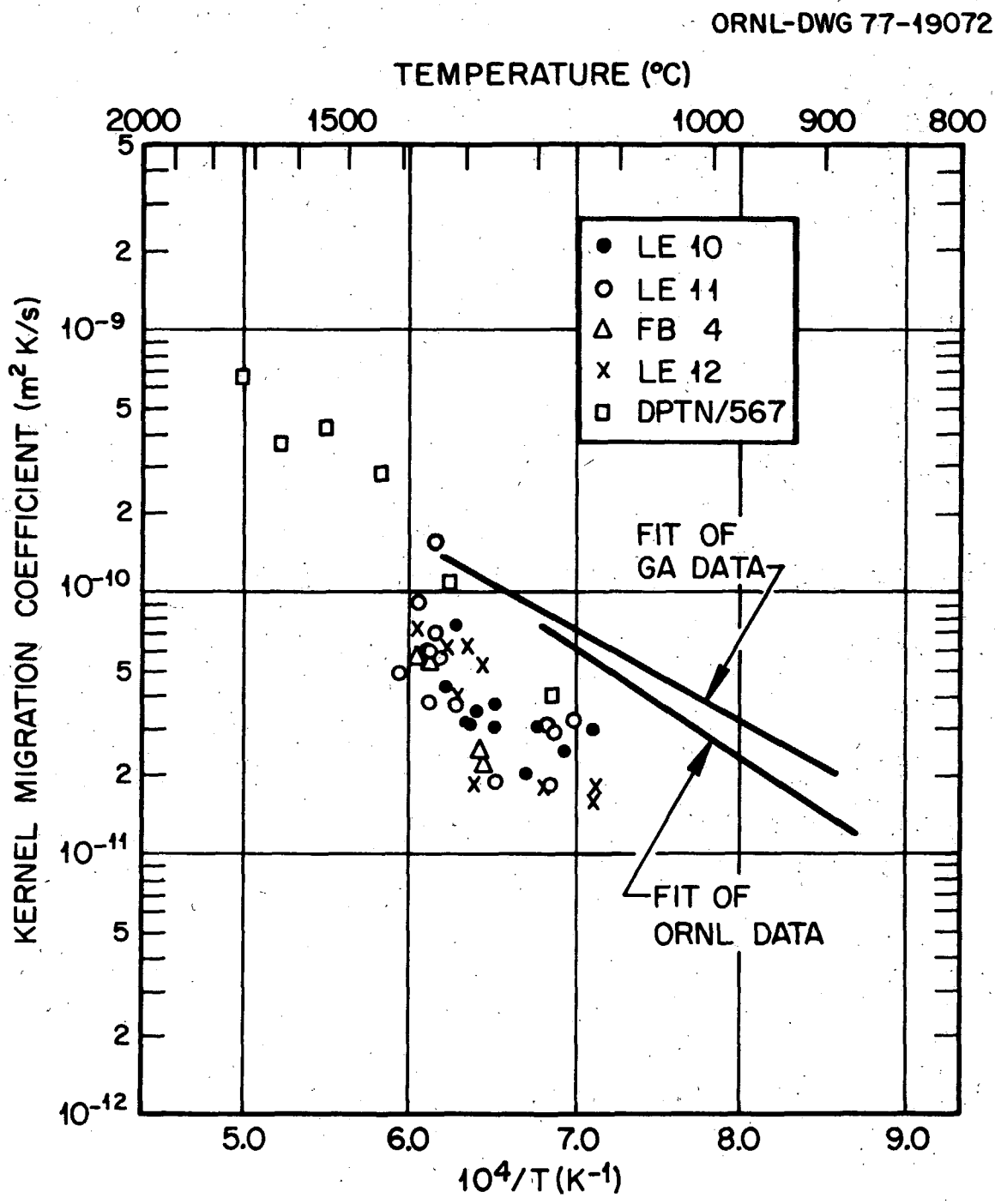

Fig. C-9. Comparison of ORNL and GA data on kernel migration of UO_2 kernels containing high-enriched uranium with Dragon Project data on low-enriched uranium UO_2 kernels. Solid curves are fits of ORNL and GA data.

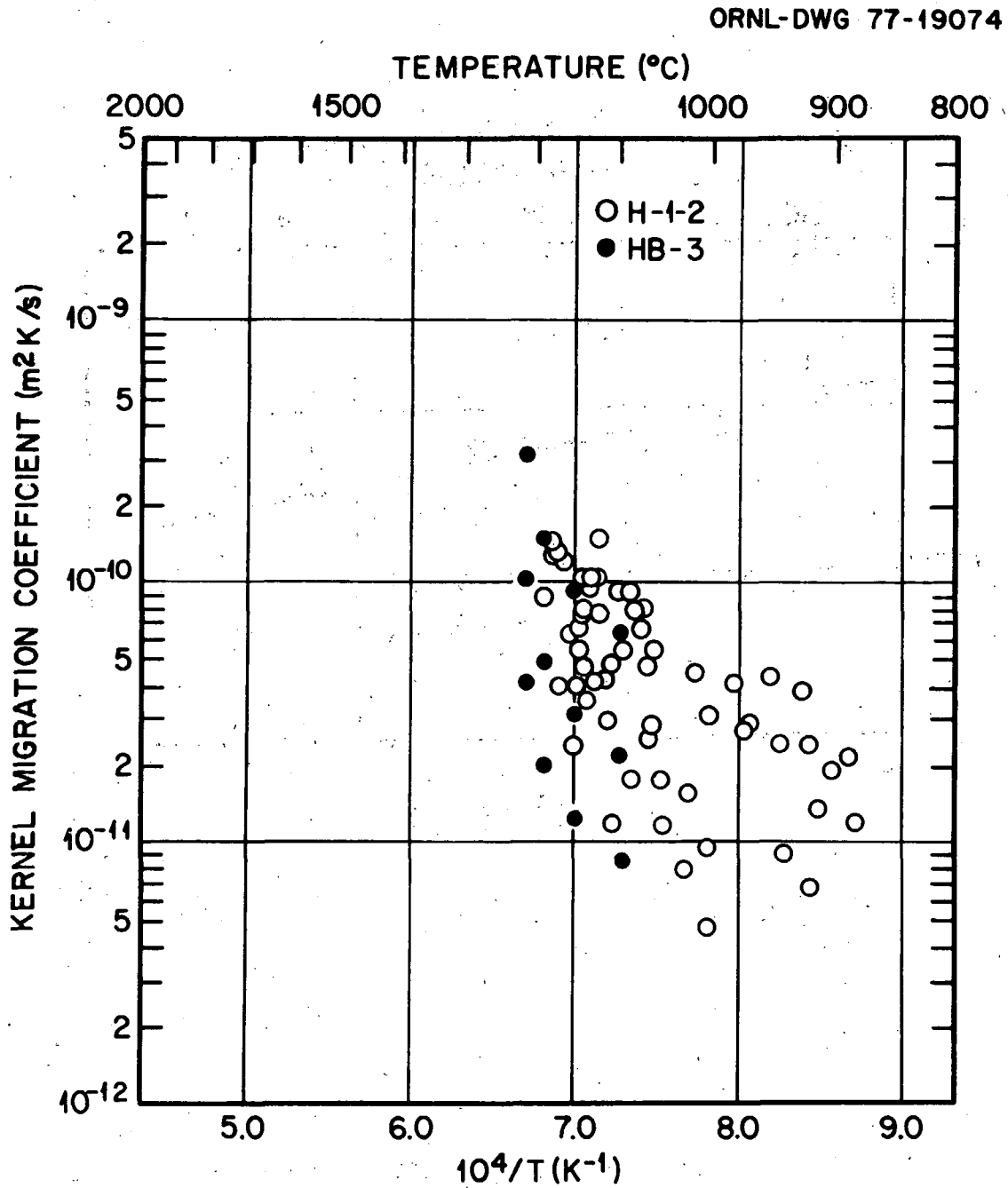

Fig. C-10. ORNL kernel migration data for HEU UO_2 kernels from which the fits shown in Figs. C-8 and C-9 were developed

ORNL-DWG 77-19070

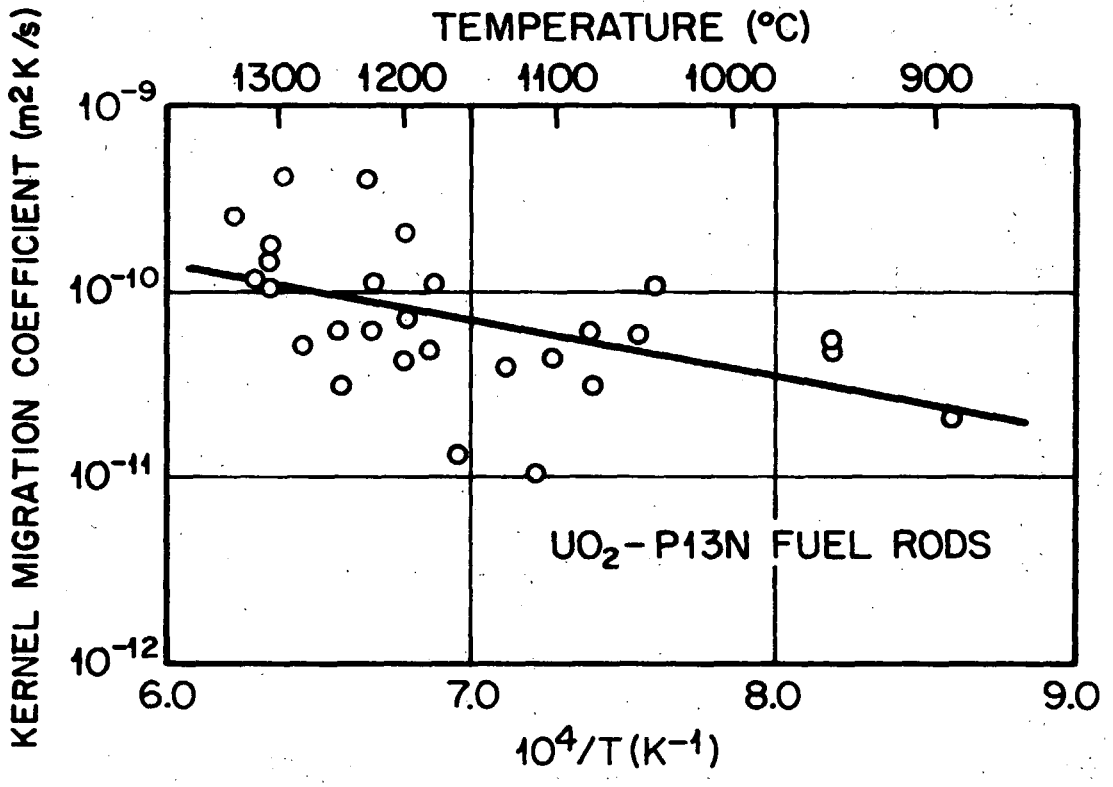

Fig. C-11. GA kernel migration data for HEU UO_2 kernels from which the fits shown in Figs. C-8 and C-9 were developed. These data were taken from TRISO coated UO_2 particles irradiated in capsule P13N in rods 2D-16, 2A-10, 4D-9, and 5A-19

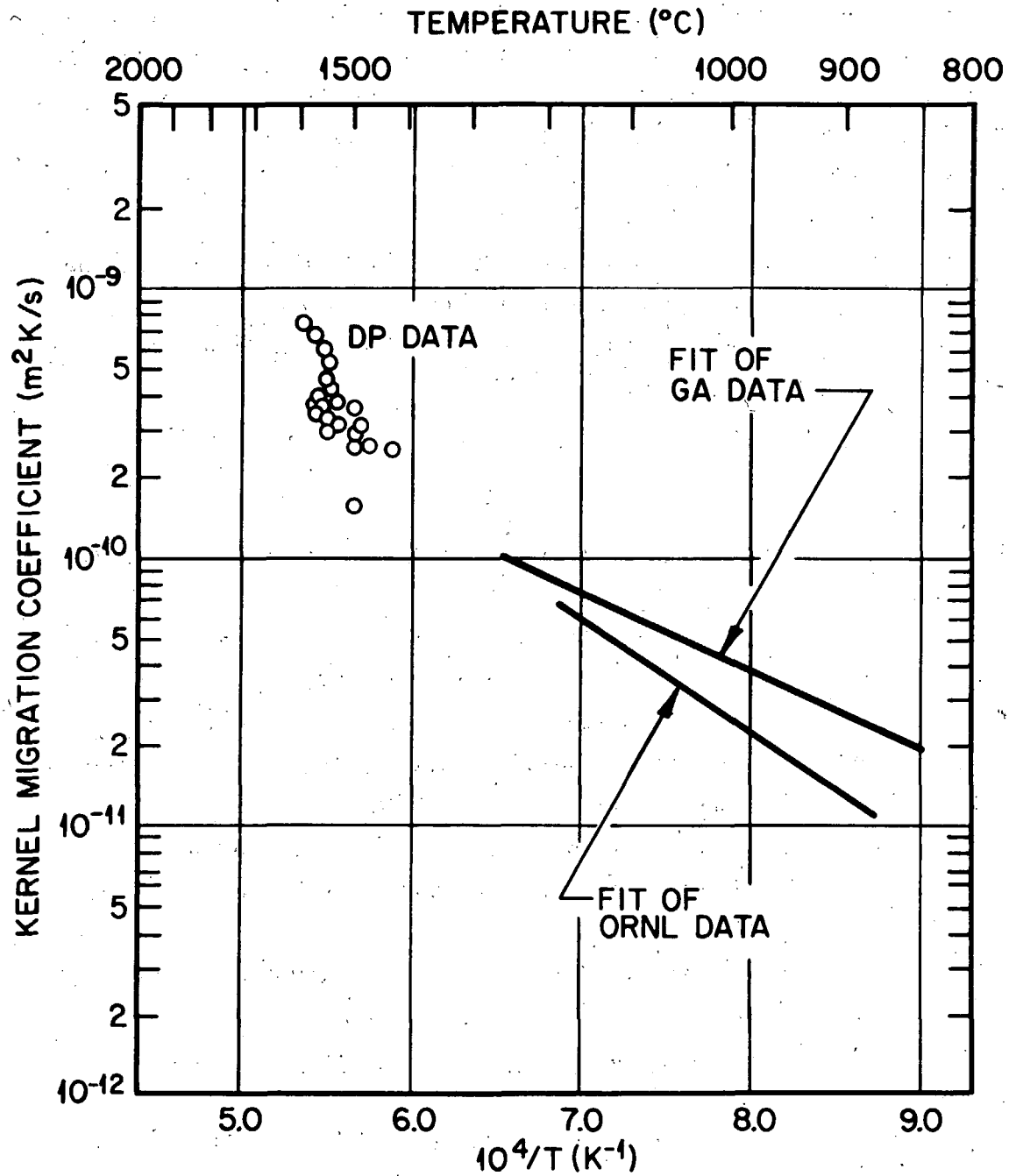

Fig. C-12. Comparison of ORNL and GA data on kernel migration of UO_2 kernels containing high-enriched uranium with Dragon Project data on low-enriched uranium UO_2 kernels. Solid curves are fits of GA and ORNL data.

respect to LEU kernel migration behavior in the temperature range below 1400°C. Above 1400°C, a linear extrapolation of the U. S. curve fits yields results that are nonconservative (i.e., showing less migration) relative to the LEU data. However, the great scatter in both the HEU and LEU data makes it difficult to make a statement about the relative stability of HEU and LEU UO_2 with a high level of confidence.

An important, unpublished opinion of Lindemer's is that there will be no migration in UPuCO fuels containing sufficient UC_2 or $(U,Pu)C_{1.5}$ initially. This is an important point, and it will be experimentally verified in the next capsule irradiation series.

REFERENCES

1. "Gas-Cooled Reactor Programs, Annual Progress Report for Period Ending December 31, 1973," ORNL-4975, pp. 92-95.
2. Homan, F. J., et al., "Irradiation Performance of HTGR Fuel Rods in HFIR Experiments HRB-4 and -5," ORNL-5115, June 1976.
3. Long, E. L., et al., "Fabrication of ORNL Fuel Irradiated in the Peach Bottom Reactor and Postirradiation Examination of Recycle Test Elements 7 and 4," ORNL-TM-4477, September 1974.
4. Homan, F. J., et al., "Stoichiometric Effects on Performance of High-Temperature Gas-Cooled Reactor Fuels from the U-C-O System," Nucl. Tech. (35) 2, pp. 428-442.
5. Meek, M. E., and B. F. Rider, "Compilation of Fission Product Yields," NEDO-12154-2, July 1977.
6. Elliott, R. P., Constitution of Binary Alloys, First Supplement, McGraw-Hill, New York, 1965.
7. Searcy, Alan W., and Lies N. Finnie, "Stability of Solid Phases in the Ternary Systems of Silicon and Carbon with Rhenium and the Six Plutonium Metals," J. Am. Ceram. Soc. 45(6), 268-273 (1962).
8. Suzuki et al., J. Nucl. Sci. Tech. 14(6), 44, (1967).
9. Valentine, K. H., "Irradiated Microsphere Gamma Analyzer System, Gas-Cooled Reactor Programs, High-Temperature Gas-Cooled Reactor

Base-Technology Program Progress Report for Period January 1, 1974 through June 30, 1975," ORNL-5108, pp. 446-456.

10. Grubmeier, H., A. Naoumidis, and B. A. Thiele, "Silicon Carbide Corrosion in High-Temperature Gas-Cooled Reactor Fuel Particles," Nuclear Technology, (35)2, pp. 413-427, September 1977.
11. Lindemer, T. B., and R. L. Pearson, "Kernel Migration for HTGR Fuels from the System Th-U-Pu-C-O-N," J. Am. Cer. Soc. (60) pp. 5-14, Jan-Feb 1977.
12. Memo from T. B. Lindemer (ORNL) to P. R. Kasten (ORNL) dated 15 March 1974. Subject: Analysis of Dragon Project UO_2 Migration Data.
13. Letter from T. B. Lindemer (ORNL) to L. W. Graham (Dragon) dated 21 May 1974.

APPENDIX D

BELGONUCLEAIRE PROGRAM FOR DEVELOPMENT OF COATED PARTICLE FUELS CONTAINING PLUTONIUM AND LOW-ENRICHED URANIUM

The fuel development program in Belgium was a joint effort between Belgonucleaire and the Belgian Nuclear Research Center (SCK/CEN). The development work on fuels, which was directed toward steam cycle HTR application, began in 1959 with the development of manufacturing procedures for microspheres using the powder agglomeration method. This program lasted through 1977. The initial work was directed at the thorium fuel cycle and plutonium utilization. Later, the program moved toward the low-enriched uranium cycle then in favor with European reactor designers and customers.

The information in this appendix has been compiled from documents provided by Belgonucleaire (Refs. 1-21). Although numerous additional references given in these reports undoubtedly contain significant additional data, the conclusions reached in Refs. 1 through 21 and stated in this appendix are representative of the broader program and therefore serve the purpose of this report.

The particle designs developed in the Belgian program are summarized in Fig. D-1. The low-enriched particle is essentially the same design as the Dragon low-enriched particle. Of particular interest to this report is the Pu-containing particle, which will be discussed in some depth.

D.1. IRRADIATION PROGRAM

The Belgian experiments containing LEU fuel are described in the burnup-vs-fast fluence plot shown in Fig. D-2. A similar plot for the HEU fuel and Pu-containing fuel irradiations is shown in Fig. D-3. A summary of some of the pertinent irradiation conditions and operating parameters for these experiments is included in Table D-1.

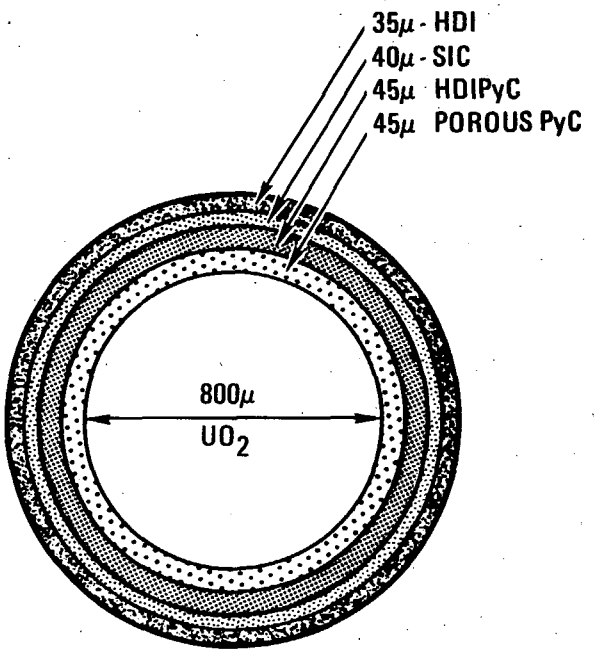

800μ LOW ENRICHED UO_2 PARTICLES

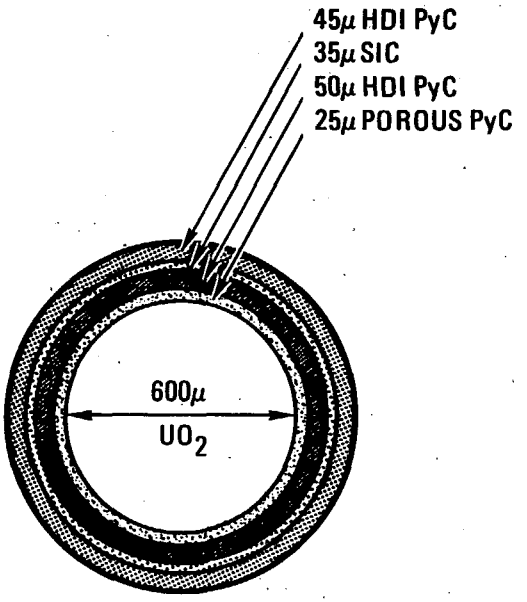

600μ HIGHLY ENRICHED UO_2 PARTICLES

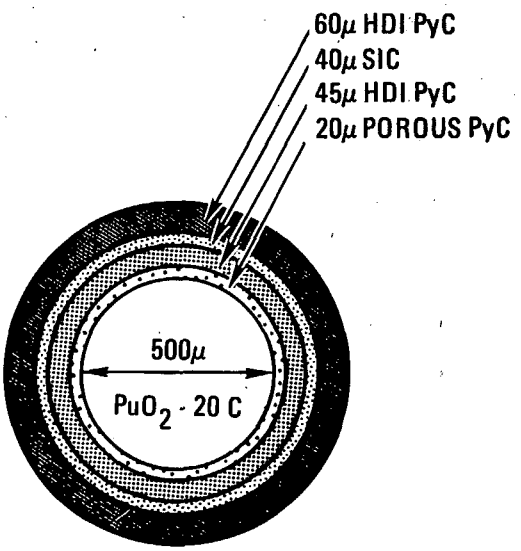

500μ $PuUO_2$ - 20 C PARTICLES

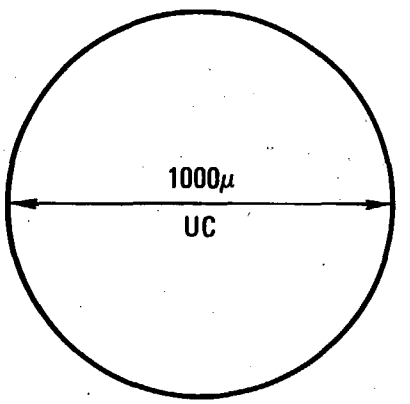

UC PARTICLES

Fig. D-1. Particle types developed in Belgonucleaire program

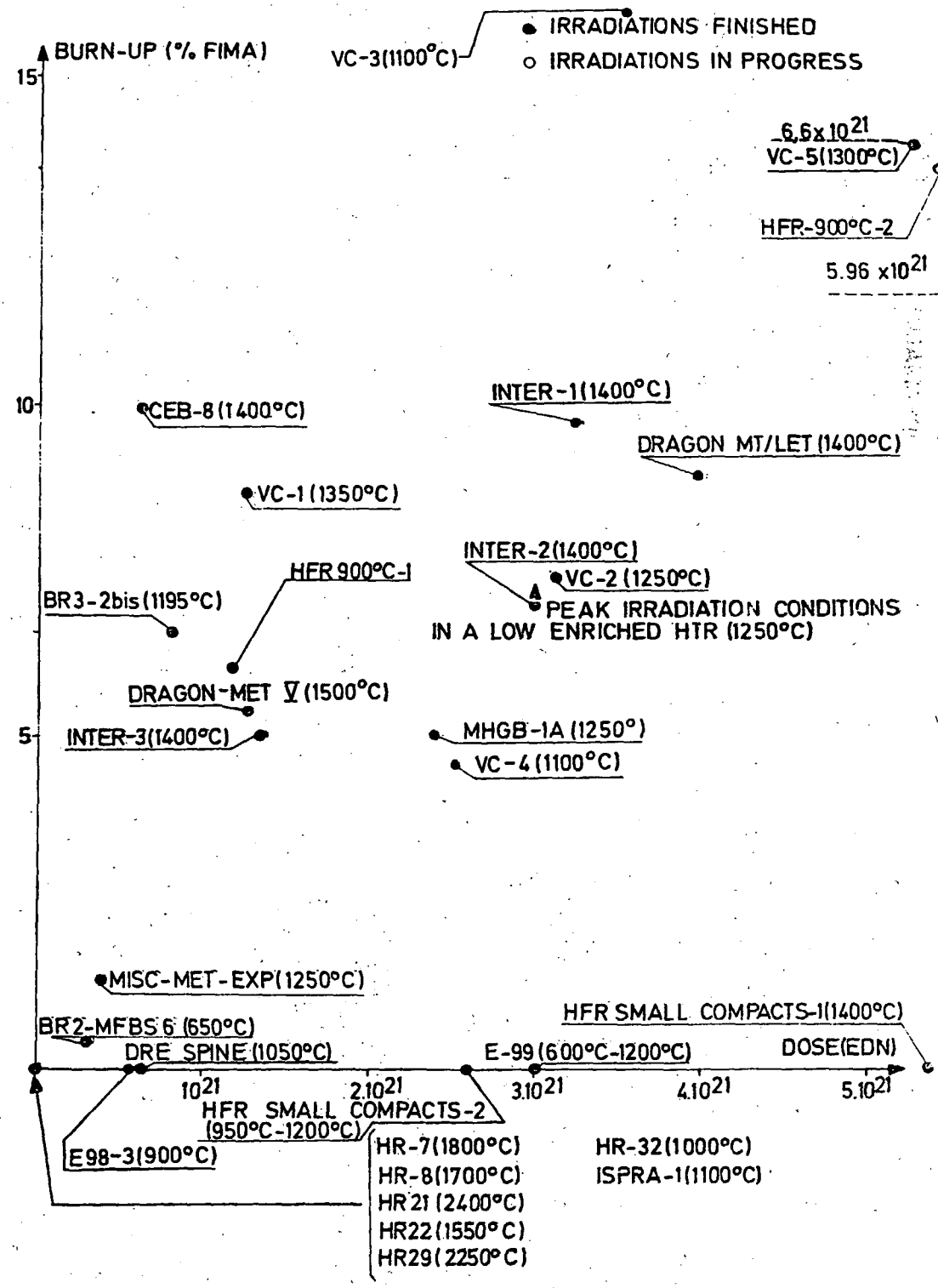

Fig. D-2. Doses and burnup reached by HTR low-enriched fuel at end of 1976

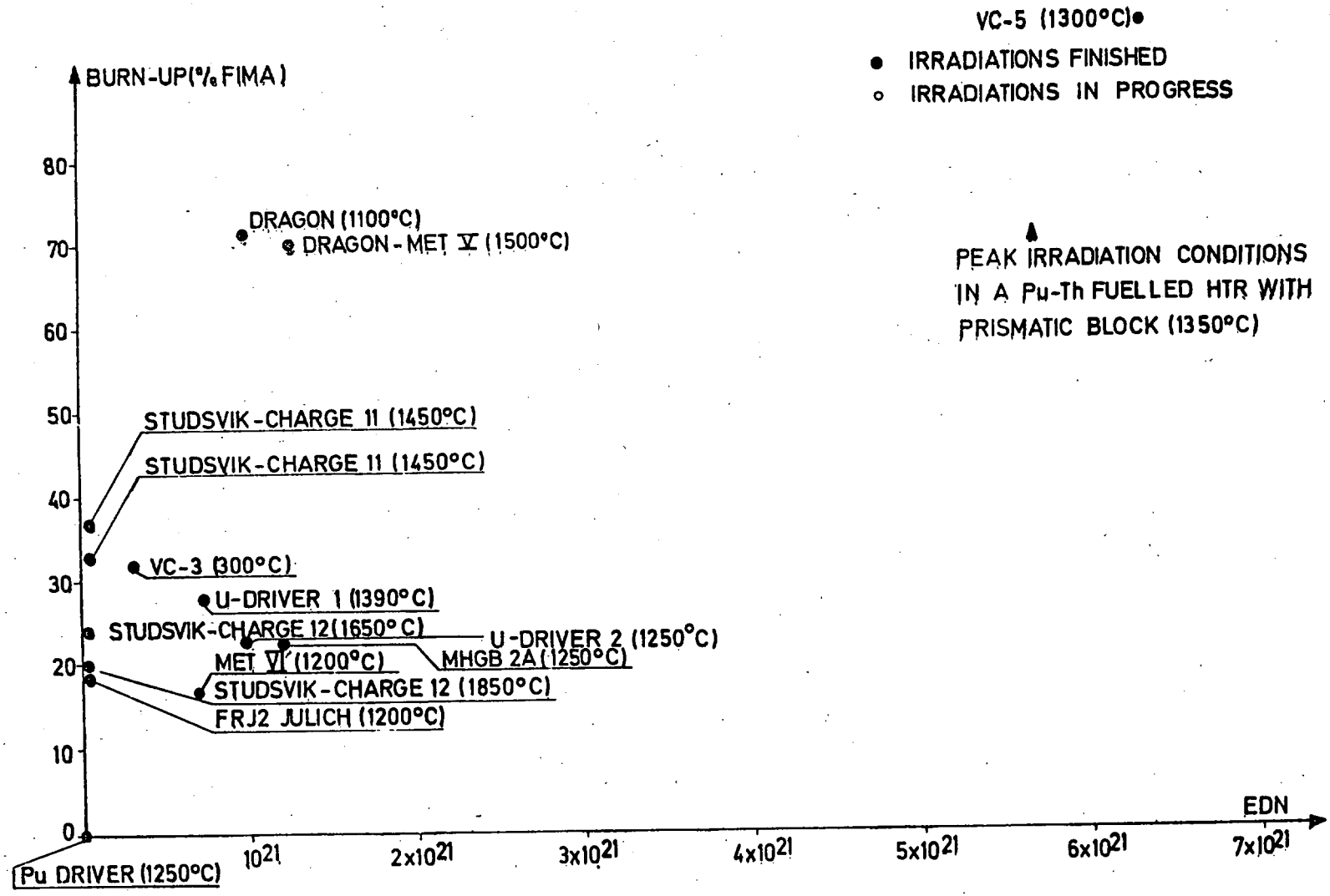

Fig. D-3. Doses and burnup reached by high-enriched and Pu HTR fuel at end of 1976

TABLE D-1

SUMMARY OF BELGONUCLEAIRE IRRADIATIONS OF LEU AND Pu CONTAINING HTR FUEL

Expt.	Reactor	Ref.	Number of Spec.	Max. Enrichment (%)	Peak Temp. (oC)	Peak Fast Fluence (EDN)	Fuel	Kernel (DIA) (μm)	Peak Burnup FIFA	Peak Burnup FIMA	EOL[e] Fission Gas R/B	EOL Internal Gas Pressure (ATM)
MT[f]	Dragon	BN-7608-04	16	3-6	711-1225	22.6×10^{20}	UO_2	766-781	34	1.2		
LET[f]			42		720-1239	26.3×10^{20}	UO_2		47	2.8		
MET V	Dragon	BN-7607-04	80[a]	48[b]	1520	1.25×10^{21}	$PuO_{1.92}$ + 20C	550		86		
			160[a]	89[b]	1520	1.25×10^{21}	$PuO_{1.91}$	270		86		
			80[a]	90[b]	1520	1.25×10^{21}	$PuO_{1.70}$	270		86		
			208[a]	3	1520	1.25×10^{21}	UO_2	750-780		~2.2		
			208[a]	9	1520	1.25×10^{21}	UO_2	780		4.3		
BR-2/VC-3		BN-7602-07		9	1100	3.55×10^{21}		800		16.8	5×10^{-4} (Kr^{85m})	
BR-2/VC-5		BN-7602-07		5	1300	6.60×10^{21}		500		13.9	5×10^{-4} (Kr^{85m})	
BR-2/VC-4		BN-7404-01										
HFR 900°C C-2		BN-7602-07										
E 96-1	HFR	BN-7602-07		.4, 3, 9	900	6.00×10^{21}		800		13.6	1×10^{-3} (Kr^{85m})	
E 96-2	HFR	BN-7602-07										
c	FRJ-2				1200	1.00×10^{20}				18	4×10^{-7} (Xe^{133})	
MHGB-1A												
MHGB-21	Dragon	BN-7702-04		8						6.2		
MOPS-CO2 (VC-2)	BR2	BN-7410-03	9	4.7 9.0	~1250*	3.12×10^{21}	UO_2	760		7.4		450 700
MOPS-CO2 (VC-1)	BR2	BN-7410-02	12	9.0	1350	1.27×10^{21}	UO_2	800		8.7	$<10^{-4}$	811 at 1250°C
INTER 1		BN-7410-02					UO_2					
INTER 2		BN-7410-02					UO_2	746				
INTER 3		BN-7410-02	64		1400	1.3×10^{21}	UO_2	780		4.9		
LV4/JK4	FRJ2	EUR 5066e	8		1450	5.3×10^{19}	D[d] PuO_2	600-890		17.0		
					1200	5.3×10^{19}	T PuO_2	790		18.7	4.2×10^{-7}	
					1300	5.3×10^{19}	C PuO_2	850		18.3		

*No thermocouples in BN portion of capsule.

[a] Particles in trays

[b] % Pu

[c] MET V particles

[d] D=Diluted Kernel prepared by powder agglomeration
T=Sol Gel fabricated kernel
C=SNAM fabricated Kernel

[e] EOL=end of life

[f] Fractional Silver release was 4×10^{-2} for MT and 5×10^{-3} for LET.

D.2. RESULTS AND CONCLUSIONS FROM BELGIAN PROGRAM

1. In the Studsvik experiment (Charges 11 and 12), particles with diluted plutonium kernels were irradiated successfully to 37% FIMA in the temperature range of 1200° to 1450°C and to 20% FIMA at temperatures of up to 1850°C. For fuel temperatures of 1450°C, the measured fission gas (Xe-133 and Kr-85m) release to birth (R/B) values were about 5×10^{-6}. For fuel temperatures of 1850°C, the R/B values were in the range of 10^{-2}, and the solid fission product release fractions were in the range of 10^{-4}. There was no evidence of plutonium release from these particles, although there was some evidence of chemical attack in the buffer layer. In some particles, the attack extended into the inner PyC layer. In general, this experiment demonstrated that this type of plutonium-coated particle can operate safely at 1450°C during a limited period, and that excursions to 1850°C lasting several weeks would not result in catastrophic failures. It should be noted from Fig. D-3 that the fast neutron exposure for these particles was very low.

2. In the FRJ 2 and Met V experiments, thermal migration of the Pu-containing kernels through the buffer layer and inner PyC layers was noted for both the diluted and concentrated particles. The difference between the diluted and concentrated particles will be covered later in this appendix. In the Met V experiment, the behavior of the Pu-containing particles was strongly dependent on the irradiation temperature and neutron exposure. This dependence is shown in Table D-2. Particles irradiated at temperatures of 1500°C to neutron exposures of 1.25×10^{21} n/cm^2 (EDN) experienced about 40% failure. The source of failure has been identified as liberation of Pu from plutonium oxide of low stoichiometry during high temperature operation. The Pu penetrates the buffer layer and damages and ultimately fails the inner PyC by modifying its structure. The Pu then reacts with

TABLE D-2
INFLUENCE OF IRRADIATION TEMPERATURE AND NEUTRON FLUENCE ON PARTICLE FAILURE FRACTION FOR PU-CONTAINING PARTICLES IRRADIATED IN MET V EXPERIMENT

		Temperatures					
		1200°C		1350°C		1500°C	
Dose (DNE)	Fraction of broken particles	1.5×10^{20} n cm^{-2}	0%	2.5×10^{20} n cm^{-2}	0%	3.1×10^{20} n cm^{-2}	0%
Dose (DNE)	Fraction of broken particles	3×10^{20} n cm^{-2}	0%	4.5×10^{20} n cm^{-2}	1.5%	6×10^{20} n cm^{-2}	20%
Dose (DNE)	Fraction of broken	5.5×10^{20} n cm^{-2}	1%	9×10^{20} n cm^{-2}	10%	1.25×10^{21} n cm^{-2}	40%

the SiC and provokes a catastrophic failure of the particle. From this experiment it was concluded that 1300°C was the maximum operating temperature for plutonium oxide kernels of low stoichiometry.

3. Low-enriched uranium fuel (9% enriched UO_2 - TRISO coated) was irradiated to temperatures of up to 1500°C, 3% FIMA, and 1.25×10^{21} fast fluence (EDN), and temperatures of up to 1350°C to 8.5% FIMA. The typical failure mechanisms observed were pressure vessel failures, irradiation induced PyC failures, and thermal migration failures. Interestingly, higher irradiation temperatures did not seem to enhance the failure fraction. The VC-5 experiment was run at temperatures up to 1400°C to 14% FIMA and neutron exposures up to 6×10^{21} (EDN), and the results of the lower fluence experiments were confirmed. An interesting comparison of the U-containing and Pu-containing particle performance is shown in Table D-3. For particles irradiated in the Dragon Met V experiment, very high failure fractions were observed for Pu-containing particles under conditions where no failures were observed for U-containing particles of 3% and 9% enrichment.

D.3. DISCUSSION

Data from the Belgian program do not deal significantly with any of the major issues identified in the body of this report as performance limiting for LEU or MEU fuels. Only the 21 references cited in this appendix have been reviewed for data on the Belgian program, but it is likely that major conclusion from the Belgian program would have been mentioned somewhere in these references. The limited amount of data pertaining to LEU/MEU performance is summarized below.

TABLE D-3
MET V (3) EXPERIMENT
FRACTION OF BROKEN PARTICLES IN THE TRAYS (%)
(Determination Based on the Visual Examination)

Tray No. (Particle Type)[a] \ Spine Assembly No. (Irrad. Temperature)	B3-6 (1300°C)	B3-11 (1400°C)	B3-16 (1500°C)	B3-21 (1350°C)	B3-26 (1200°C)
1 (Pu-D)	17.5	72	77.5	12.5	2.5
2 (Pu-D)	12.5	27.5	65	20	2.5
3 (Pu-T)	12.5	10	23	7.5	0
4 (Pu-T)	0	12.5	27.5	9.09	0
5 (Pu-T)	7.5	10	12.82	5.26	0
6 (Pu-T)	10	15	17.5	2.5	0
7 (Pu-C)	50	60	74.36	10	0
8 (Pu-C)	42.5	60	62.5	17.5	2.5
9 (U - 3% PyC)	0	0	2	0	0
10 (U - 3% PyC)	0	0	0	0	0
11 (U - 3% no PyC)	0	0	0	0	0
12 (U - 3% no PyC)	0	0	0	0	0
13 (U - 9% PyC)	0	0	0	0	0
14 (U - 9% PyC)	0	0	0	0	0
15 (U - 9% no PyC)	0	0	0	0	0
16 (U - 9% no PyC)	0	0	0	0	0

[a] Type D plutonium oxide kernels were prepared by powder agglomeration and contained significant porosity (diluted kernel).
Type T plutonium oxide kernels were prepared by sol-gel process.
Type C plutonium oxide kernels were prepared by the SNAM process.

D.3.1. Plutonium Migration

Reference 17 discusses Pu "displacement" during particle fabrication and after irradiation. The Pu was noted to migrate during application of the buffer and inner PyC coatings to the extent that the buffer layer was completely impregnated with Pu. Migration during irradiation was observed to be small compared with the migration during coating. Migration of about 20 microns was found in the T type kernels (fabricated using the sol-gel route). In all cases, the migration was stopped by the SiC layer. It is noted that these irradiations were rather short-term.

D.3.2. Silver Diffusion

Silver release data were published for the MT and LET experiments, which are summarized in Table D-1. The release fractions were in the range of 10^{-4} to 10^{-2}. Very little is said about the release mechanism.

D.3.3. CO Pressures

CO pressures have been investigated both with the COCONUT model (Ref. 1) and postirradiation internal gas pressure measurements (see Table D-1). CO pressures were of most interest in the Belgian program for Pu-containing fuels. The CO pressures were described as being highest for particles containing plutonium oxide kernels with high O/Pu ratios at the beginning of life (of the three types of Pu-containing kernels tested in the Belgian program, the type T particle, fabricated using the sol-gel technique, had the highest O/Pu ratios). The O/Pu ratio for this particle was calculated to increase from about 1.91 at 0% FIMA to about 2.007 at 19% FIMA. The CO pressure is calculated to remain relatively constant until about 12% FIMA, and then increase linearly by about a factor of 9 (to about 9 kg/cm^2) between 12% and 18% FIMA. While these data are not directly applicable to the LEU/MEU fuel performance problems, they are indicative of the high CO pressures that are developed in Pu fuel systems.

A calculation (Ref. 22) of the internal gas pressure in particles irradiated in the VC-1 and VC-2 experiments is presented in Table D-4. From this table the contribution of CO pressure to total pressure can be determined for UO_2 fuels of different enrichments and burnups.

D.3.4. Thermal Migration (Amoeba)

While the Belgian program discusses observations of thermal migration, there is very little quantitative treatment such as presented in the Dragon, KFA, and ORNL programs. The only quantitative treatment found in the 21 references cited is shown in Fig. D-4. It should be noted that this treatment is somewhat simpler than the kernel migration coefficient treatment used by Dragon, GA, ORNL, and KFA.

REFERENCES

1. Thomson, J. M., "Assessment with the Code COCONUT of the Behaviour of HTR Coated Particles in Different Irradiation Experiments," Vol I, September 1973.
2. Gaube, M., et al., "Operation Capability of Standard HTR Fuel at High Temperature," reprinted from Nuclear Energy Maturity (1975).
3. Thomson, J. M., "Study of the Chemical Failure of UO_2 Low Enriched Particles."
4. Everett, M. R., et al., "Joint Programme of Uni-Axial Creep Measurements of HTR Compacts and Matrix Material Under Tensile Load at 900°C," J Nucl Mater 65 (1977).
5. Everett, M. R., and M. Gaube, "The Creep Strain Limit Experiment," J Nucl Mater 65 (1976).
6. Gauge, M., and C. Van Loon, "Metallurgical V Experiment Final Report," BN7607-04, July 1976.
7. Thomson, J. M., "MT and LET Series Experiment Final Report," BN7608-04, August 1976.
8. Thomson, J. M., "Small Compacts 2 Experiment Final Report," BN7606-01, June 1976.
9. Gaube, M., "Rapport Final de l'Irradiation of de Combustible HTR Dans l'Appendice de l'Experience MFBS-6," BN7402-04, January 1974.

TABLE D-4
RESULTS OF THE GAS PRESSURE MEASUREMENTS (MEAN VALUES)

Experiment	VC-1	VC-2	VC-2	VC-2
Kernel diameter, mm	762	762	760	760
Fuel	UO_2	UO_2	UO_2	UO_2
Enrichment, % U-235	9	9	4.7	4.7
Burnup (Cs-137), % FIMA	8.7	7.0	4.5	4.5
Full-power days	142	247	247	247
Buffer thickness, µm	36	36	32	32
Buffer porosity, %	50	50	50	50
Free volume, X 10^{-5} cm^3	3.6	3.6	3.15	3.15
Gas Determ. Temp., °C	1250	1250	1250	1250
Xe release, %	73.9	83.4	76.9	55.6
Xe amount, X 10^{-3} cm^3	3.42	3.03	1.86	1.37
Xe pressure, atm	615	536	364	263
Kr release, %	59.8	74.2	70.6	53.8
Kr amount, X 10^{-3} cm^3	0.313	0.303	0.169	0.131
Kr pressure, atm	51	49	31	24
CO release, %	2.69	2.64	1.66	1.53
CO amount, X 10^{-3} cm^3	0.88	0.679	0.278	0.270
CO pressure, atm	145.8	111.0	51.0	50.0
Total pressure, atm	811	696	446	337

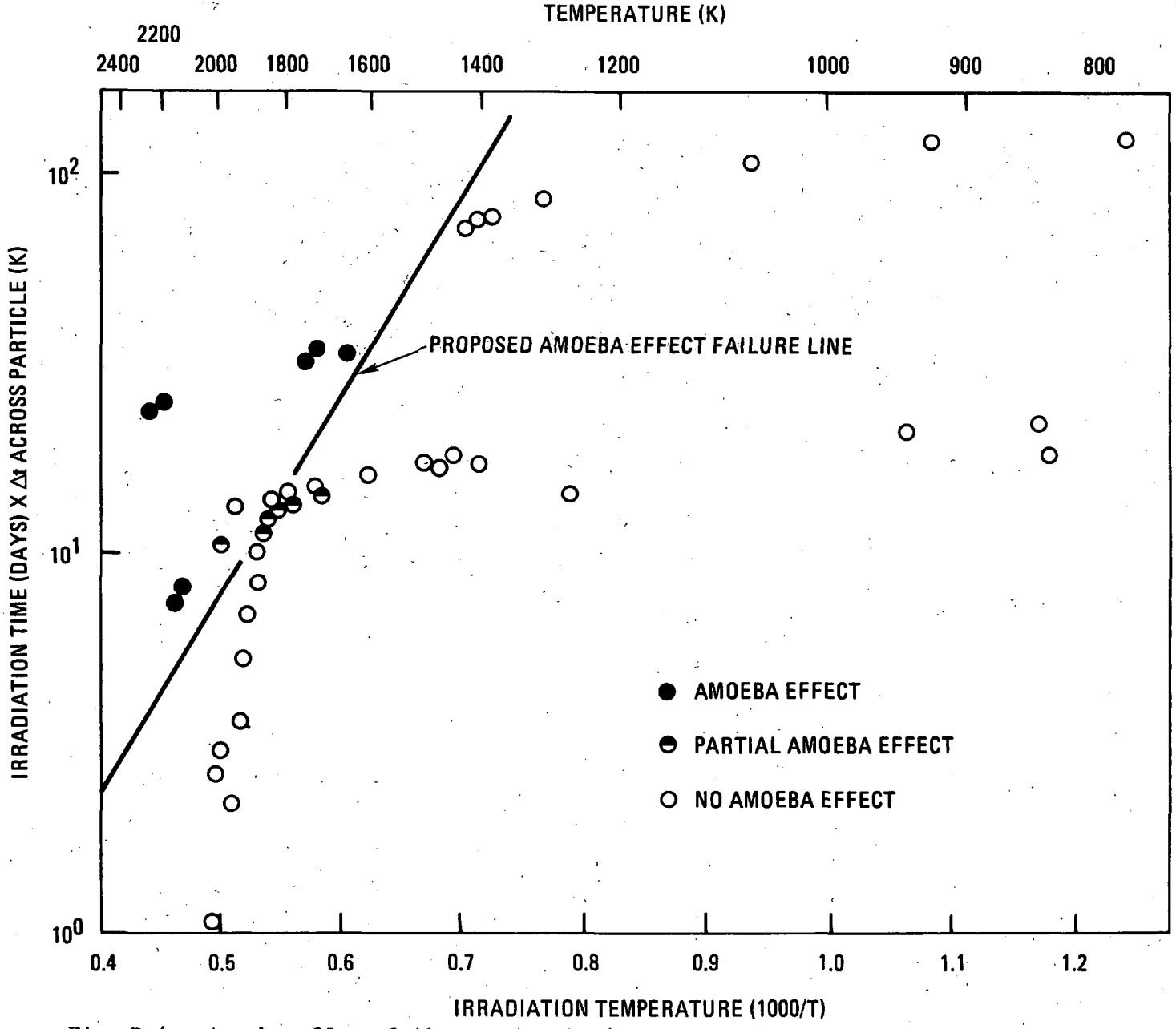

Fig. D-4. Amoeba effect failure criteria (based on 7-8 and 22 HR experiments

10. Gaube, M., B. van Outryve d'Ydewalle, and A. Lhost, "Rapport Final de l'Experience CEB-8," BN7307-01, July 1973.
11. Gaube, M., and J. M. Thomson, "Rapport Final de l'Irradiation de Combustible HTR Dans La Cellule N° 80 DU COEUR BR 3/2 bis," BN7312-05, December 1973.
12. SCK/CEN, "Belgian Five-Year Programme (1973-1977) for Nuclear Research and Development, Item D.1. High Temperature Gas Cooled Reactor Fuel (work performed from 1 January to 31 December 1974)," BN7503-03, March 1975.
13. SCK/CEN, "Belgian Five-Year Programme (1973-1977) for Nuclear Research and Development, Item D.1. High Temperature Gas Cooled Reactor Fuel (work performed from 1 January to 31 December 1975)," BN7602-07, February 1976.
14. SCK/CEN, CCR-Ispra, AGIP Nuclear, Dragon Project, "Fuel Development for High Temperature Gas Cooled Reactors," BN7303-10.
15. SCK/CEN, "Belgian Five-Year Program (1973-1977) for Nuclear Research and Development, Item D.1. High Temperature Gas Cooled Reactor Fuel (work performed from 1 January to 31 December 1973)," BN7404-01, April 1974.
16. CEN/SCK, "Belgian Five-Year Program (1973-1977) for Nuclear Research and Development, Item D.1. High Temperature Gas Cooled Reactor Fuel (work performed from 1 January to 31 December 1976)," BN7702-04, February 1977.
17. Baier, J., et al., "Irradiation of Plutonium Fuelled Coated Particles in FRJ2," EUR5066e, 1974.
18. Gaube, M., "Rapport Final de l'Experience d'Irradiation Small Compacts 1," BN7401-04, January 1974.
19. Gaube, M., "Internuclear 3 (TI51) Tubular Interacting Experiment Final Report," BN7408-02, August 1974.
20. Trauwaert, E., et al., "Utilization of Low Enriched Uranium in High Temperature Gas Reactors," BN7206-02, paper presented at the 18th Annual Meeting of the American Nuclear Society, Las Vegas, June 18-22, 1972.
21. Gaube, M., and J. M. Thomson, "MOPS-CO1 (VC-1) Experiment Final Report," BN7410-02, October 1974.

22. Letter dated November 2, 1977, from J. M. Thomson and M. Gaube (BN) to H. Nabielek (KFA) - Subject: Fission and CO Gas Pressure Measurements in the VC-1 and VC-2 Experiments.